NASA/CR—2001-210613

Experimental Assessment of the Emissions Control Potential of a Rich/Quench/Lean Combustor for High Speed Civil Transport Aircraft Engines

T.J. Rosfjord and F.C. Padget
United Technologies Research Center, East Hartford, Connecticut

January 2001

The NASA STI Program Office . . . in Profile

Since its founding, NASA has been dedicated to the advancement of aeronautics and space science. The NASA Scientific and Technical Information (STI) Program Office plays a key part in helping NASA maintain this important role.

The NASA STI Program Office is operated by Langley Research Center, the Lead Center for NASA's scientific and technical information. The NASA STI Program Office provides access to the NASA STI Database, the largest collection of aeronautical and space science STI in the world. The Program Office is also NASA's institutional mechanism for disseminating the results of its research and development activities. These results are published by NASA in the NASA STI Report Series, which includes the following report types:

- TECHNICAL PUBLICATION. Reports of completed research or a major significant phase of research that present the results of NASA programs and include extensive data or theoretical analysis. Includes compilations of significant scientific and technical data and information deemed to be of continuing reference value. NASA's counterpart of peer-reviewed formal professional papers but has less stringent limitations on manuscript length and extent of graphic presentations.

- TECHNICAL MEMORANDUM. Scientific and technical findings that are preliminary or of specialized interest, e.g., quick release reports, working papers, and bibliographies that contain minimal annotation. Does not contain extensive analysis.

- CONTRACTOR REPORT. Scientific and technical findings by NASA-sponsored contractors and grantees.

- CONFERENCE PUBLICATION. Collected papers from scientific and technical conferences, symposia, seminars, or other meetings sponsored or cosponsored by NASA.

- SPECIAL PUBLICATION. Scientific, technical, or historical information from NASA programs, projects, and missions, often concerned with subjects having substantial public interest.

- TECHNICAL TRANSLATION. English-language translations of foreign scientific and technical material pertinent to NASA's mission.

Specialized services that complement the STI Program Office's diverse offerings include creating custom thesauri, building customized data bases, organizing and publishing research results . . . even providing videos.

For more information about the NASA STI Program Office, see the following:

- Access the NASA STI Program Home Page at ***http://www.sti.nasa.gov***

- E-mail your question via the Internet to help@sti.nasa.gov

- Fax your question to the NASA Access Help Desk at 301–621–0134

- Telephone the NASA Access Help Desk at 301–621–0390

- Write to:
  NASA Access Help Desk
  NASA Center for AeroSpace Information
  7121 Standard Drive
  Hanover, MD 21076

NASA/CR—2001-210613

Experimental Assessment of the Emissions Control Potential of a Rich/Quench/Lean Combustor for High Speed Civil Transport Aircraft Engines

T.J. Rosfjord and F.C. Padget
United Technologies Research Center, East Hartford, Connecticut

National Aeronautics and
Space Administration

Glenn Research Center

January 2001

Acknowledgments

This report describes a study of the Rich/Quench/Lean (RQL) combustor, and an assessment of its applicability to a HSCT engine cycle. The study was performed at the United Technologies Research Center (UTRC) in support of a Pratt & Whitney (P & W) contract with the NASA Glenn Research Center, NAS3–25952. The UTRC Principal Investigator was Dr. T. Rosfjord who was greatly supported by Mr. F. Padget in the combustor design, fabrication, and test efforts. The NASA Program Manager was Mr. R. Tacina. Dr. R. Lohmann and Mr. D. Kwoka from P&W provided excellent technical guidance during the course of these studies to assure that the information critical to the development of a RQL combustor was acquired. As reported, this study contained many aspects and the contributions of Mr. T. Snyder to the waterflow visualization and Mr. J. Kennedy and Mr. L. Chiappetta to the CFD analyses were greatly appreciated. The test efforts were ably supported by the Jet Burner Test Stand technician staff, with particular acknowledgment of Mr. Paul Hamel. The efforts of Mr. Graham Fulton to provide timely data processing were also greatly appreciated.

Document Availability Change Notice

This document was published in January 2001 with an EAR restriction.
It was changed March 28, 2003 to Unclassified/Unlimited per DAA modified February 10, 2003.

Per the STI Program Office and Code I at Headquarters, you may modify copies in your possession. The restriction notice on the cover, title page, and report documentation page, should be boldly crossed out and the above statement printed clearly above or below it.

Note that at the time of research, the NASA Lewis Research Center was undergoing a name change to the NASA John H. Glenn Research Center at Lewis Field. Both names may appear in this report.

Available from

NASA Center for Aerospace Information
7121 Standard Drive
Hanover, MD 21076

National Technical Information Service
5285 Port Royal Road
Springfield, VA 22100

Available electronically at http://gltrs.grc.nasa.gov

TABLE OF CONTENTS

LIST OF TABLES

LIST OF FIGURES

LIST OF SYMBOLS

A_{cf}	area of quench crossflow not blocked by quench jets
A_{cf0}	geometric area available to quench crossflow ($A_{cf0} = \pi \times DQ^2$)
A_j	area of quench crossflow blocked by quench jets ($A_j = A_{cf0} - A_{cf}$)
B	fractional area of quench crossflow blocked by quench jets penetrating into a confined flow
B_0	apparent fractional area of quench blocked by quench jets penetrating into an unconfined flow
Cd	quench orifice discharge coefficient
d	diameter of quench jet
DL	diameter of lean combustor
DQ	diameter of quench crossflow
DR	diameter of rich combustor
DPQ	pressure loss of airflow through quench orifices
DPR	pressure loss of airflow entering the rich combustor
DP/P-NS	air pressure drop percentage across the fuel nozzle/swirler
DP/P-Q	air pressure drop percentage across quench orifices
EI_i	emissions index of specie i expressed as gm i per kgm fuel [$EI_i = 10^{-3} \times PPM_i \times (1 + f/a)/f/a \times MW_i/MW_m$]
EINOx	emission index of NOx using molecular weight of NO_2
EICO	emissions index of CO
exp	exponential function
F/AOA	overall combustor fuel-air ratio (F/AOA = WF/WAT)
f/a	local, emissions-based fuel-air ratio
FN	net thrust of engine
J	quench jet-to-crossflow momentum flux ratio for unconfined flow (J = MOMJ/MOMQ)
J_b	quench jet-to-crossflow momentum flux ratio for confined flow
LL	length of lean combustor
LR	length of rich combustor
MOMJ	momentum flux of quench jet
MOMQ	momentum flux of quench crossflow
MOMR	momentum flux of rich combustor gasflow
MW_i	molecular weight of specie i
MW_m	molecular weight of the f/a mixture
N	number of quench jets
PL	pressure in the lean combustor
PPM_i	concentration of specie i in parts-per-million
PQ	pressure in the quench crossflow
PR	pressure in the rich combustor
P3	general combustor inlet air pressure

P3Q	pressure of airflow to quench section
P3R	pressure of airflow to rich combustor
S	airflow split, fraction of the total airflow to the rich combustor (S = WAR/WAT = ØL/ØR)
T	time at cycle condition for EPAP calculation
TAU	general combustor hot residence time
TAUL	hot residence time in lean combustor (TAUL = LL/UL)
TAUR	hot residence time in rich combustor (TAUR = LR/UR)
TF	flame temperature
TL	temperature in lean combustor
TR	temperature in rich combustor
T3	general combustor inlet air temperature
T3Q	temperature of airflow to quench section
T3R	temperature of airflow to rich combustor
UL	1D velocity in lean combustor based on WAT, PL, TL, and DL
UR	1D velocity in rich combustor based on WAR, PR, TR, and DR
UREF	combustor reference velocity based on WAT, P3, T3, and DL
WAA	fuel nozzle air-assist flowrate
WAQ	air flowrate to quench section
WAR	air flowrate to rich combustor
WAT	total combustor air flowrate (WAT = WAR + WAQ)
WF	total combustor fuel flowrate
x	downstream coordinate for quench-jet penetration analysis
y	transverse penetration of quench jet into a confined crossflow
y_0	transverse penetration of quench jet into an unconfined crossflow
Ø	general mixture equivalence ratio
ØL	equivalence ratio in lean combustor
ØR	equivalence ratio in rich combustor
SLTO	Sea-Level Takeoff condition
SSC	Supersonic Cruise condition
S-SSC	Scaled Supersonic Cruise condition
SSCl	Supersonic Climb condition
SuC	Subsonic Cruise condition
SuCl	Subsonic Climb condition

SECTION I SUMMARY

Two combustor concepts are being studied by P&W and GE in NASA-sponsored HSR programs to define a burner which achieves goal level NOx control at the supersonic cruise operating condition of a HSCT engine. Such a burner must also preserve high efficiency, broad operability, and low emissions at all operating conditions. These two concepts are the Lean, Premixed, Prevaporized (LPP) combustor and the Rich-Quench-Lean (RQL) combustor. In support of P&W efforts to define the RQL combustor for the HSCT aircraft engine, UTRC conducted a flametube-scale study of the RQL concept. The overall objective of this study was to evaluate the suitability of applying the RQL combustor concept to the HSCT cycle. Specific technical objectives were to:

- determine whether the RQL combustor concept offered sufficient emissions control to achieve a nitric oxides emission index (EINOx) of 5 while retaining high combustion efficiency at the Supersonic Cruise (SSC) operating condition; and

- assess the sensitivities of the combustor performance and emissions to variations in the RQL design or operating condition.

Waterflow visualization and CFD studies were performed to support the definition of components of the flametube-scale RQL combustor, and to anticipate the combusting flow features that would be achieved. The waterflow visualization study illustrated the key flow structures in the rich combustor, and their response to changes in the swirl strength of the fuel nozzle. Both low and high swirl strength nozzles produced steady vortical regions suitable to stabilize the combusting flow. These regions existed for either a shorter (4-in.) or longer (8-in.) rich combustor length, persisted for a wide variation in the flow split, S, and were independent of the specific configuration of the quench jets. CFD predictions replicated the observed rich combustor flow features when an algebraic-stress turbulence model was used. Combusting flow predictions indicated that a stabilizing flowfield and a near-uniform temperature profile would enter the quench section for 4-in. to 8-in. long combustors.

Combustion tests were performed using a flametube-scale RQL combustor to assess its performance and emissions control characteristics. Tests were performed at HSCT engine cycle operating conditions and at parametric variations from them. The test variables also included geometrical variations to achieve different residence times in the rich and lean combustors, and variations in the quench-jet configuration. The primary data were analyses of emissions samples extracted from the exit of the lean combustor; limited

analyses of samples from the exit of the rich combustor or the quench section were also performed.

Extensive combustor testing was performed at the Supersonic Cruise (SSC) condition of a HSCT engine cycle. Data obtained with a slanted-slot quench configuration were correlated to described the NOx emission response to changes in inlet air pressure or temperature, and lean-combustor equivalence ratio and residence time. The dependence determined for pressure was typical for thermal NOx, while the dependence on stoichiometry was best represented by a combination of the inlet temperature and lean equivalence ratio; this combination was not equal to the lean combustor temperature. This hybrid representation was interpreted to reflect a combination of diffusion combustion during the transition from fuel-rich to fuel-lean conditions in the quench, and premixed combustion in the high-temperature lean combustor downstream of the quench. The residence time in the lean combustor influenced the NOx emissions, but the effectiveness of the quench process was the dominant influence on the level of NOx at the combustor exit. Neither the rich-combustor equivalence ratio (ØR) nor its residence time was a direct contributor to the exit NOx; near-equilibrium specie concentrations exit the rich combustor. The CO and smoke emissions were very low at SSC, even for a short lean-combustor residence time, with combustor efficiencies typically exceeding 99.9 pct.

Test results with alternative quench configurations demonstrated the importance of the quench-jet penetration in controlling the combustor emissions. Circular-hole quench configurations, which produced rapidly-, highly-penetrating jets, were more effective at limiting NOx. NOx data acquired at the SSC condition with an eight, circular-hole quench were at the HSCT program goal of EINOx = 5.

Data obtained from probe traverses near the quench exit confirmed that the quench section was the critical component in controlling combustor emissions. At the SSC condition, 60 to 70 pct of the exit NOx was formed in the quench; 99 pct of the CO entering the quench was oxidized by its exit. The spatial profiles of NOx and CO at the quench exit were not directly interpretable using a simple flow model based on quench-jet penetration, and a greater understanding of the flow and chemical processes in this section are required to optimize it.

Combustion tests were performed at selected part-power operating conditions of a HSCT engine cycle following a candidate schedule to control ØR. In particular, data were acquired to assess the performance and emissions for this candidate schedule and alternatives to it which imposed ØR values more favorable for emissions control, combustor durability, and combustor air redistribution. At lower power conditions, it was determined that the desirable combustor mode was lean-lean, with a rich-lean mode at higher

power. The lean-lean mode was required because the lean combustor was ineffective at oxidizing CO frozen in the quench section; unacceptable combustion inefficiencies were achieved at low power in the rich-lean mode. Quench configurations which demonstrated enhanced emissions control at SSC also performed better at part-power conditions. Data from quench exit traverses reflected the expected quench-jet behavior for off-design quench-jet to crossflow momentum ratios.

Based on these studies, it was concluded that:

1. A RQL combustor can achieve the emissions goal of EINOx = 5 at the Supersonic Cruise operating condition for a HSCT engine.

2. While NOx formation in both the quench section and the lean combustor contribute to the overall emission, the NOx formation in the quench section dominates. Negligible NOx exits the rich combustor.

3. Quench section designs based on discrete quench jets are more effective at controlling NOx formation when rapidly-, highly-penetrating jets are produced.

4. A stable rich combustor flowfield structure, consisting of an axial vortex core surrounded by larger recirculation zones as produced by the swirling inlet flow, exists for combustor length-to-diameter ratios as low as 0.8. The ability of CFD to predict this structure strongly depends on the turbulence model.

5. The gas composition exiting the rich combustor can be reasonably represented by the equilibrium composition corresponding to the rich combustor operating condition defined by P3, T3, and ØR.

6. At the SSC condition, the oxidation processes occurring in the quench section consume 99 pct of the CO exiting the rich combustor. Soot formed in the rich combustor is also highly oxidized, with combustor exit SAE Smoke Number < 3.

7. A RQL combustor can achieve stable, robust, and efficient combustion at all operating conditions of a representative HSCT engine cycle.

8. Low power operating conditions require that the RQL combustor operate as a lean-lean combustor to achieve low CO and high efficiency.

SECTION II INTRODUCTION

HSCT Technology Program

In 1990, Pratt & Whitney (P&W) and the General Electric Aircraft Engine Company (GE) announced the formation of a partnership to develop the propulsion system for a U. S. High Speed Civil Transport (HSCT) aircraft under the sponsorship of the National Aeronautics and Space Administration (NASA). Such a vehicle was targeted to carry 250 to 350 passengers over a distance of 6000 to 7000 nautical miles, at speeds ranging from Mach 1.5 to 3.5 (Ref. II-1).

The agreement between P&W and GE was to proceed with the engine development in a series of steps. First, the technical feasibility of developing a HSCT engine would be assessed, including a forecast of the environmental barriers such as engine noise and nitric oxide (NOx) exhaust emissions. With a favorable assessment, technology studies would be performed both to demonstrate that the performance and environmental goals could be achieved, and to establish effective strategies for engine component design. Engine component development would follow, including large-scale validation and demonstration.

The P&W/GE partnership plan paralleled a two-phase NASA plan, with Phase I focused on technology readiness and Phase II targeted at critical component development. These programs represented a part of the NASA High Speed Research (HSR) Program. Complementing HSR was the multi-year, NASA-sponsored Enabling Propulsion Materials (EPM) Program which was formulated to develop the high temperature materials necessary for a successful HSCT engine. The development of ceramic matrix composite (CMC) materials to withstand the steady-state and transient mechanical and thermal loads in either the combustor or the exhaust nozzle was a target of EPM. Again, P&W and GE joined in a partnership for EPM. Together, the HSR and EPM programs formed the backbone for NASA-sponsored technology acqusition for a HSCT engine.

Low and High Altitude Emissions

One of the potential barriers impeding the development of a HSCT engine is the effect of exhaust emissions on the environment of the upper atmosphere. In order to maximize fuel efficiency, subsonic aircraft cruise in the upper troposphere, the atmospheric layer adjacent to the earth. This region is thermally unstable, which results in gross mixing patterns throughout the layer; these motions are responsible for the earth's weather patterns. Pollutants emitted into this layer are both diluted by the mixing process and

scrubbed from it by the weather. In contrast, the optimal cruise altitude for supersonic aircraft is in the lower stratosphere, the atmospheric layer above the troposphere. The separation between these layer is not precise, however, because of both seasonal and latitudinal variations. Generally, the stratosphere is isothermal and consequently void of convective currents. Pollutants emitted into the stratosphere tend to remain stratified, and because of minimal interaction with the troposphere, they are not removed from the stratosphere.

Subsonic aircraft engine emissions have long been a public concern. They are regulated in the vicinity of airports by the Environmental Protection Agency according to the value of an EPA Parameter (EPAP). This parameter combines the emissions produced by an engine at each of four low-altitude operating conditions for a specified landing-take-off (LTO) cycle. The cycle points include take-off, climb, approach, and taxi/idle, with specified operating times (T) of 0.7, 2.2, 4.0, and 26.0 minutes, respectively; cruise emissions are not a factor in this evaluation. The cycle emission of a pollutant is the sum of its production at each LTO condition. This total is normalized by the rated thrust of the engine (FN) to calculate the EPAP in units of grams of pollutant per kilonewton of thrust.

$$EPAP = \frac{\sum_{Cycle} WF * T * EI}{FN}$$

The numerator of this parameter is the product of fuel consumption (i.e. product of fuel flowrate, WF, and time, T) and Emissions Index (EI) for any pollutant, where EI represents the grams of pollutant formed per kilogram of fuel burned. The EPAP then reflects the combination of the engine emission control technology as represented by the EI, and the engine fuel efficiency as represented by the fuel consumption per rated thrust. Regulations set the maximum permitted EPAP values for NOx, carbon monoxide (CO) and unburned hydrocarbons (UHC) to achieve engine certification.

A similar EPAP has been defined for aircraft engines intended for propulsion at supersonic speeds. In this case, the parameter is based on the five operating conditions of take-off, climb, descent, approach, and taxi/idle with specified operating times of 1.2, 2.0, 1.2, 2.3, and 26.0 minutes, respectively. Again, cruise emissions are not a factor in this evaluation. However, the effect of exhaust emissions at cruise are a concern for a HSCT engine.

During cruise operation, emissions from subsonic aircraft are emitted into the troposphere where they are dispersed and scrubbed. As stated above, however, cruise emissions from supersonic aircraft will be emitted into and retained within the stratosphere because it is relatively stagnant. This

stagnation has also resulted in the accumulation of ozone (O3) in the stratosphere. In this layer, oxygen molecules (O2) photodissociate by the absorption of ultraviolet (UV) radiation from the sun. The oxygen atoms (O) combine with other O2 molecules to form O3. These processes form a dynamic equilibrium with O3 photodissociation to produce small, but significant, steady-state concentrations of O3 in the stratosphere. These O3 concentrations absorb most of the UV-B radiation from the sun directed toward the earth, reducing the occurrence of UV-induced skin cancers. An atmospheric chemistry concern affecting the development of an engine for a HSCT is for the role of NOx emissions in depleting the stratospheric ozone concentration.

The chemistry of the upper atmosphere has been studied for decades. Despite this period, a considerable uncertainty exists about reaction mechanisms, and their rates, involving NOx. For example, it is known that nitric oxide (NO) and ozone react to form nitrogen dioxide (NO2) and oxygen (O2):

$$NO + O3 = NO2 + O2$$

This reaction is the basis of many NO concentration analyzers, where the NO2 is initially formed in an excited state, which then spontaneously decays and emits a chemiluminescence radiation. Since the radiation intensity is proportional to the number of decaying NO molecules, measuring the radiation quantifies the NO concentration. While other reactions accompany the above step to form an overall dynamic equilibrium for the influence of NOx on ozone, this step illustrates how NO molecules can react with the stratospheric O3 to deplete it. However, the chemistry is more complicated. Even a more comprehensive reaction mechanism which includes O3 formation by photodissociation of O2, NO2 photodissociation to NO to produce a catalytic effect, O and O3 interactions, etc., neglects the potential influences of water, particulates, or UHC on the ozone balance. Despite many advances in modeling the effect of NOx on stratospheric ozone depletion, there are still many uncertainties for the effects of mixing and dilution, uncertainties in rate constants, and uncertainties in heterogeneous chemistry.

Cruise NOx Goal and Combustor Strategies

The uncertainties surrounding both atmospheric chemistry and the mixing in and between atmospheric layers made it difficult to establish a long-term goal for HSCT cruise NOx emissions. Based on the available data and predictive capability, NASA established an emissions goal believed to be sufficiently conservative that a fleet of HSCT aircraft which would have a negligible effect on the stratospheric ozone concentration. It was also recognized that the goal might have to be altered as additional data and atmospheric analysis capability became available.

The supersonic-cruise NOx emissions goal was set to be:

EINOx = 5 gm NOx/kg fuel

with PW and GE agreeing that the combustor operating condition at supersonic cruise was thermodynamically defined to be:

Combustor inlet air pressure (P3)	150 psia
Combustor inlet air temperature (T3)	1200 F
Overall fuel-air ratio (F/AOA)	0.030

This NOx goal represented a significant challenge for the HSCT engine combustor design. The goal is approximately 25 pct of the level achieved by subsonic aircraft engines despite the fact that both T3 and F/AOA are notably higher for supersonic cruise conditions. As a consequence, new aircraft combustor strategies had to be studied to both demonstrate that the HSCT cruise NOx goal was achievable in a high performance combustor, and to develop the technology strategies required for engine component designs.

Two combustor concepts are being studied by P&W and GE in the NASA-sponsored HSR programs to define a burner which achieves the goal level NOx control at the supersonic cruise operating condition. Such a burner must also preserve high efficiency, broad operability, and low emissions at all operating conditions. These two concepts are the Lean, Premixed, Prevaporized (LPP) combustor and the Rich-Quench-Lean (RQL) combustor. At high power, the LPP combustor strives to achieve a uniform mixture of vaporized fuel and air before injecting it into the combustor. This composition produces the lowest flame temperature, and consequently promotes the lowest thermal NOx formation. However, special measures must be taken, such as piloting or fuel-staging, to sustain combustor operation at part power conditions. The RQL combustor strives for NOx control by first establishing a fuel-rich zone of combustion to preserve combustor stability for all conditions, and then rapidly transitioning to the overall fuel-lean stoichiometry. The NOx control strategy for both of these combustor concepts relies upon achieving a rapid mixing process.

However, since each concept attempts to optimize this process differently, the design, attributes and challenges of each burner are not the same. Specific features of these two combustor concepts are discussed and contrasted in Section III of this report. By agreement, P&W is developing technology for the RQL concept and GE is developing technology for the LPP concept. After sufficient data are acquired for each concept, and comprehensive ground-rules are established, P&W, GE, and NASA will participate in a selection process to identify the preferred HSCT engine combustor.

Program Objective and Scope

In support of P&W efforts to define a RQL combustor for the HSCT aircraft engine, the United Technologies Research Center (UTRC) conducted a flametube-scale study of the RQL concept at HSCT cycle conditions. This study was performed as Task 3, HSR Low NOx Combustor, of NASA Lewis Research Center contract NAS3-25952, Aero-Propulsion Technology Research Program, with Pratt & Whitney of the United Technologies Corporation.

The overall objective of this study was to evaluate the suitability of applying the RQL combustor concept to the HSCT cycle. Specific objectives were to:

- define and acquire a flametube-scale RQL combustor test capability which could achieve the full range of HSCT cycle conditions, particularly the high combustor inlet air temperature of supersonic cruise (SSC) design condition;

- perform combustion tests at cycle design points and variations from them, and with purposeful variations in the combustor components, to assess the sensitivities of the combustor performance and emissions to RQL design and operating conditions; and

- specifically, perform combustion tests at the SSC design condition to determine whether the RQL combustor concept offered sufficient emissions control to achieve a nitric oxides emission index (EINOx) of 5 while retaining high combustion efficiency.

The activities performed in this program were consistent with the above objectives. A high inlet air temperature, RQL combustor test facility was assembled and used to acquire emissions data at the combustor exit, in the rich combustor, and at the quench mixer exit to assess combustor performance and sensitivities.

A RQL combustor test facility was specified, designed, fabricated, and installed in Cell 1E of the UTRC Jet Burner Test Stand. This facility permitted combustion testing at combustor pressures of 200 psia, and combustor inlet air temperatures of 1400 F, and contained airflow control features to alter the airflow rates delivered the rich combustor and the quench mixer. The facility contained a modular, 5-in dia RQL combustor which allowed variations of either the rich or lean combustor length, the quench mixer configuration, or the fuel nozzle design.

In support of the combustor definition, a combined water flow visualization and computational fluid dynamic (CFD) study was performed to assess the

flow in the rich combustor. In particular, this study related the principle flow structures in the rich combustor and the flow quality entering the quench section to the swirl characteristics of the fuel nozzle.

The RQL test facility was used to perform combustion tests at conditions representing the HSCT cycle. Tests were also performed at variations from the design conditions, and with alternative combustor components, to assess the sensitivity of the combustor performance and emissions to them. Combustor exit emissions were used to perform these assessments. Emissions data were also acquired in the rich combustor to characterize the major species concentrations, and at the exit of the quench mixer to evaluate the development of the mixing process during combustor operation.

Report Organization

This report details the activities and results of the UTRC study of a HSR Low NOx Combustor. Section I provides a Program Summary, while Section II outlines the basis of the combustor strategies. Section III compares the primary combustor concepts being considered by P&W and GE for supersonic-cruise NOx control, and outlines the study conducted for the RQL combustor concept. Section IV provides a detailed description of the RQL combustor facility at UTRC, including the flametube-scale combustor, the airflow control system, and the emissions sampling techniques. The water flow visualization and CFD studies which supported the combustor definition are described in Section V. The results from the combustion test program are presented and discussed in Section VI. Conclusions and Recommendations are presented in Sections VII and VIII, respectively.

SECTION III LPP AND RQL COMBUSTOR STRATEGIES

The Lean, Premixed, Prevaporized (LPP) combustor and the Rich-Quench-Lean (RQL) combustor are the primary concepts being developed for use in a HSCT engine. Both strategies rely upon a rapid mixing process to achieve NOx emissions control. However, since each concept attempts to optimize this process differently, the design, attributes, and challenges of each burner are not the same. This section of the report describes each of these two primary combustor concepts, discusses a primary challenge to achieve a high level of NOx emissions control, and identifies strengths and weaknesses in implementing the concept. The discussion of the RQL combustor forms the basis of the flametube-scale technology program conducted by UTRC.

Lean, Premixed, Prevaporized Combustor

Concept

The LPP combustor concept strives to premix all of the combustor fuelflow with all combustor airflow not required for combustor liner cooling before these flows enter a single zone of fuel-lean combustion. Further, the strategy attempts to process the liquid fuel in a manner to achieve complete vaporization of it during the fuel preparation. Two versions of the LPP concept are depicted in Fig. III-1. In the first, fuel atomization, vaporization, and fuel-air mixing are separated from combustion stabilization. In the second LPP layout, all of these processes are integrated by use of premix tubes attached to the stabilizer. For either version, if both premixing and prevaporizing goals are achieved, only a homogeneous mixture of fuel vapor and air is admitted into the combustor.

When combusted, a LPP mixture produces the most favorable flame temperature to achieve NOx emission control at a high-power operating condition. The flame temperature will be uniform and at a level below that achievable if the mixture is non-uniform. The fully-mixed combustor exit temperature at the HSCT supersonic cruise condition approaches 2900 F, after experiencing an approximately 1700 F temperature rise above the combustor inlet. Flame temperatures associated with non-uniform mixtures will exceed the 2900 F level and enter a regime of rapid NOx production. For example, a local fuel-air mixture 10 pct above the average would result in a flame temperature of approximately 3070 F. The LPP flametube-scale combustor study performed at GASL using gaseous propane fuel (Ref. III-1) can be used to estimate the impact of this temperature deviation. Among the results from that study was a correlation of NOx emissions per millisecond of combustor residence time, expressed as EINOx/TAU, with flame temperature:

$$Log_{10}(EINOx/TAU) = -30.83 + 1.2 \times TF^{0.5} - 0.0113 \times TF$$

where TF = flame temperature (K). For a 2 msec residence time, EINOx = 1.7 is predicted for the uniform f/a case, whereas EINOx = 2.8 is predicted for the non-uniform mixture case. Both of these NOx emission levels are low because an idealized LPP combustor was studied. More importantly, the NOx emissions were 65 pct higher for only a 10 pct non-uniformity. This result illustrates the sensitivity of NOx emission control to the quality of premixing. It should be recognized that the fuel-air non-uniformity could arise from either fluid flow, and that diffuser flow profiles may be critical to achieving an acceptable airflow distribution.

Challenge for NOx Control

Achieving a high degree of fuel-air premixing is the most significant challenge to the LPP combustor fuel nozzle design. Since the fuel originates in the dense liquid state and represents approximately 3 pct of the airflow, the duct required to deliver the entire combustor fuelflow is relatively small. Generally, small passages are desirable to finely-atomize the fuel and produce a rapidly-vaporizing spray. However, it also results in the difficult mixing problem of homogenizing a minute flow into a large one. The solution is often to geometrically subdivide the flows into numerous smaller units. In essence, the airflow is divided into modules which better match the smallest practical fuel passage in order to maximize fuel vaporization. As a consequence, many small fuel delivery and injection passages are required. This strategy has been successfully executed by other researchers, as summarized by Tacina (Ref. III-2), to achieve low NOx emissions from a LPP combustor. It is not clear, however, that the use of numerous small fuel passages represents a practical fuel preparation design because of thermal stability concerns.

The fuel-air premixing challenge for the LPP combustor is greatly aggravated for HSCT applications because of the high combustor inlet air temperatures, and the associated tendency to promote autoignition of the fuel-air mixture prior to achieving the LPP conditions. If such an autoignition occurs, both the NOx control strategy will be severely compromised and often the LPP nozzle will be destroyed. Hence, the LPP conditions must be achieved in a device offering a residence time which is short compared to the autoignition time. Further, the device must manage the flowfield to avoid both separated flow regions which would sustain long residence times and regions of low flow velocity which would permit upstream flame propagation (i.e. flashback) from the combustor. The former requirement is usually met by avoiding rapid expansions or high swirl which promote flow separation. Flashback avoidance is sought by applying the airflow pressure drop across the entire length of the fuel preparation device, and not at one station (e.g. orifice plate), in order to preserve high flow velocities throughout the mixer. Special care

must be taken to prohibit the development of thick, fuel-enriched boundary layers. The layout shown in Fig. III-1b reflects this strategy.

The autoignition character of aviation fuels has been studied by several researchers; the NASA report by Spadaccini and TeVelde (Ref. III-3) provides a summary of prior and their current work. Figure III-2 is from that report, and displays the dependence of the product of autoignition time (Tau) and pressure (P) on the mixture temperature (T) for several aviation fuels. For HSCT cycles, T=1200 F and P=150 psia (approximately) at supersonic cruise. Unfortunately, the data are sparse for this temperature and the trends of neighboring temperature regimes are not continuous. For the data plotted, the time-pressure product is near 10 msec-atm, which implies an autoignition time of 1 msec at supersonic cruise. This time can be converted to an equivalent length assuming a fuel preparation Mach number of 0.2 (i.e. a nominal pressure loss of 3 pct). For this case, the autoignition length is 5 in. However, a correlation of the Jet A data obtained up to T=1000 F extrapolates to an autoignition time of 0.2 msec, or an autoignition length of 1 in. It appears that a considerable uncertainty exists on the residence time guideline to avoid autoignition, and that conservative values would require extremely rapid fuel mixing to avoid its occurrence.

Design/Operation Strength

The LPP combustor liner layout is relatively simple. While the need to package many fuel preparation devices on the dome may result in a large dome height, the liner contains a single combustion zone which always operates fuel-lean. This stoichiometry permits the consideration of many alternatives for the liner cooling technique. Effusive cooling by means of louvers or high-density arrays of orifices could be used if high cooling effectivenesses were achieved. Low cooling effectiveness designs would require larger coolant flowrates which would both elevate thermal NOx production because of reduced combustion-zone airflow (i.e. higher core fuel-air ratio), and promote inefficiencies because of CO quenching by the wall coolant. Alternatively, backside cooling by impingement and convective techniques could be used for the liner. Again, high cooling effectiveness is necessary to avoid excessive NOx production, although CO wall quenching should not be experienced. The relative simplicity of the LPP liner layout may facilitate the use of non-metallic liner materials such as being developed under the EPM program, further reducing coolant flowrate requirements.

Design/Operation Weakness

Achieving an ideal LPP mixture at high power conditions is not a favorable situation for low-power operation. The fully premixed fuel-air mixture does not provide the combustor stability required for the range from low to high

power; the LPP combustor will blowout at low power. Hence, either a pilot burner or extensive fuel staging must be used to cover the range. In the former approach, the pilot must be integrated with the LPP devices to preserve low-emission operation throughout the cycle. If the pilot remains active at all times, its emissions must not compromise the low emissions characteristic of the LPP devices. Fuel staging could be used to span the operating range but low emissions will be preserved only if the active zones are sufficiently shielded from inactive zones. That is, the airflow of non-combusting regions can quench the boundaries of the combusting regions and result in high CO emissions.

The use of a fuel staging strategy exaggerates the LPP fuel thermal stability problems. Generally, LPP combustor designs include numerous fuel injection points; hence, numerous fuel delivery passages must be insulated to avoid excessive heat transfer to wetted fuel surfaces. If fuel staging is use, some of these passages will be void of fuel at various operating conditions. Since flowing fuel is the heatsink for energy transferred through the fuel duct, it will get hot and internal fuel films may degrade and form deposits. The fuel system design must prevent this occurrence by purging all fuel film or actively cooling the duct. Since numerous passages are involved, these techniques will likely require very complex fuel management systems.

LPP Summary

In summary, the LPP combustor concept has been successfully executed at inlet air temperatures up to approximately 1000 F to achieve excellent NOx emission control. The challenges for a HSCT engine application are to achieve homogeneous vapor fuel-air mixtures while avoiding autoignition at the supersonic cruise condition, develop a practical fuel preparation device which avoids fuel deposition, and demonstrate a turndown strategy which preserves high combustion efficiency and broad operability.

Rich-Quench-Lean Combustor

Concept

The RQL combustor concept strives to achieve separated zones of combustion to preserve combustor stability while achieving emission control. The combustor pursues these goals by establishing a fuel-rich combustion zone ($\varnothing > 1$) and a fuel-lean combustion zone ($\varnothing < 1$), with a rapid transition between them (Fig. III-3). The rich zone provides the combustor stability, while the lean zone, which reflects the overall fuel-air ratio of the combustor, achieves low CO and UHC. Low NOx emissions will be achieved only if the transition between the zones is sufficiently vigorous to avoid significant flow residence time near stoichiometric mixtures. This combustor concept has

been identified by several different names including Rich-Quench-Lean (RQL), Rich-Burn Quick-Quench (RBQQ), and Rich-Burn Quick-Mix (RBQM). All of these names refer to the same concept.

The rich and lean combustion zones of an RQL combustor are established by dividing the total combustor airflow. Since all of the fuel is injected into the first combustion zone, the rich and lean zone equivalence ratios (ØR and ØL, respectively) are related by the airflow split (S) defined to be the ratio of the rich zone airflow (WAR) to the total combustor airflow (WAT):

$$S = WAR/WAT = ØL/ØR$$

At high power conditions, with a nominal value of ØL = 0.4, 23 pct of the total combustor airflow is admitted to the rich zone to achieve ØR = 1.8. At this equivalence ratio, there is sufficient oxygen to convert all carbon in the fuel to CO or CO2, and avoid soot. Hydrogen and water are other major products of fuel-rich combustion. However, the equilibrium level of NOx is negligible because of the low free oxygen concentration.

The airflow not admitted into the rich combustor is termed the quench airflow (WAQ), and is rapidly mixed into the rich combustor effluent to achieve the overall lean combustor equivalence ratio. Since values for S are typically 20 to 30 pct, the quench airflow represents the majority of the combustor airflow. The potential energy available to mix the quench airflow into the rich combustor exhaust is the liner pressure loss. This energy must be used efficiently since the effectiveness of the quench mixing process is critical to achieving the RQL combustor NOx emissions control. If a rapid transition from the rich to lean conditions is not achieved, near-stoichiometric mixtures will exist for unacceptably long times; high temperatures and high NOx formation rates will be experienced.

The lean combustor is the simplest component of the RQL combustor. If the quench mixer is effective for NOx control, its exit flow will be homogeneous and the lean combustor can be sized to complete the oxidation of CO and soot. Such sizing must be performed at the condition yielding off-design operation of the quench mixer, since this condition will likely deliver the greatest CO carryover from the rich to the lean combustor.

Challenge for NOx Control

The critical role of the RQL quench process in achieving NOx emission control has been recognized, resulting in the performance of numerous studies of the scalar mixing of flows in the proportions experienced in a RQL combustor (Ref. III-4 through III-18). These studies have included both experimental and analytical studies, for cylindrical and rectangular combustor geometries, of configurations consisting of quench airflow jets penetrating

into a rich combustor crossflow. The quench jet geometry has included radiused-end slot orifices of differing length/width aspect ratio (including aspect ratio = 1 which is a circle), and at different angular orientations of the slot axis to the flow axis. The earlier studies focused on arrays of slot orifices inclined to the flow ("slanted slots") while more recent studies have evaluated the mixture uniformity achieved with circular orifice arrays. The mixing capabilities of alternative configurations have been compared by evaluating the scalar homogeneity in a plane one-half of a duct height downstream from the orifice centerline. Highly uniform flows have been achieved. However, only one study (Ref. III-9) has attempted to integrate the scalar mixing results with chemical kinetics to predict the associated NOx control potential. Data have not been acquired to confirm the predictive capability of that model. Hence, while studies of quench mixing indicate that a rapid transition from the rich to the lean combustor may be possible for HSCT cycle flowrates, corresponding NOx control data do not exist. Also, since the flow in the mixer is multidimensional and reacting, reliable NOx control predictions have not been produced.

A significant RQL combustor data base exists from its application to industrial gas turbine emission control (Ref. III-19 through. III-23). These studies were performed using standard distillate fuels (e.g. Jet A) and synthetic distillate fuels (e.g. coal derived liquids) for combustor inlet air temperatures ranging from 750 F to 850 F. In these studies, NOx emissions control depended on the rich combustor equivalence ratio as illustrated in Fig. III-4. As ØR increased above stoichiometric, the exhaust NOx concentration minimized at EINOx = 3 near ØR = 1.5. This "bucket" characteristic has been explained as a competition between diminishing NO formation and increasing formation of other nitrogen compounds (XN) as ØR increases. The total NOx from the combustor will be the sum of these two sources since the XN species will be readily oxidized in the lean combustor. However, equilibrium thermochemistry indicates that this trade-off should minimize near ØR = 2. Possibly other chemistry or quench-mixing effects are controlling the optimal ØR. The RQL was particularly effective at suppressing the conversion of fuel bound nitrogen contained in synthetic distillate fuels to exhaust NOx emissions. This attribute is not likely to be important in controlling NOx with use of aircraft fuel, however, because of its low fuel nitrogen content. The challenge is to extend these RQL NOx control experiences to the high combustor inlet temperature conditions accompanying a HSCT engine cycle.

The quench mixer configurations being considered for the RQL combustor are fixed geometry devices and may achieve optimal performance only at the design condition. One parameter of importance to the mixer performance is the momentum flux ratio of the quench jets to the crossflow (J). Often, an optimal value of J exists which maximizes the mixing. Reduced mixing occurs for either higher or lower J values, which is often interpreted as achieving either over- or under-penetration of the quench jets, respectively.

For a fixed geometry jet mixer, J depends primarily on the temperature and flowrate of the two flows:

$$J = C1 \times T3Q/TR \times (WAQ/WAR)^2$$

where C1 = constant, and T3Q, TR are the quench airflow and rich combustor temperatures, respectively. Assuming T3Q and T3 are equal, an approximate, linear relationship between TR and T3Q would be:

$$TR = T3Q + C2 - C3 \times ØR$$

where C2, C3 = constant. Then with the definition of S:

$$J = C1/(1 + C2/T3Q - C3 \times ØR/T32) \times (1/S - 1)^2$$

If the RQL control strategy holds S constant, then J varies as the quotient ØR/T3Q. Since both increase (or decrease) together through the HSCT cycle, J variation is minimal However, if the airflow split changes, the momentum ratio is substantially affected and off-design mixing performance might be experienced. This feature must be considered in developing the turndown strategy for a RQL combustor.

Design/Operation Strength

The existence of the fuel-rich combustor provides excellent operational stability for the RQL combustor; it does not operate near a blowout limit. Since only a small fraction of the total burner flow is processed by the rich combustor, it provides a relatively long residence time and achieves at least a near-equilibrium product mixture at its exit. There is no need to premix the fuel with the rich combustor airflow. Since this flow is small, it is often admitted to the combustor as a non-premixed component of an aerating fuel nozzle. A high degree of mixing within the combustor is desirable to promote the formation of equilibrium products in minimal combustor length.

Design/Operation Weakness

The rich combustor presents a special liner requirement with the RQL combustor concept. Since a fuel-rich environment must be maintained, no cooling airflow may pass through the liner; convective, backside cooling techniques must be used. As a consequence, the liner is directly exposed to the hot, fuel-rich combustion gases; no protective cooling air film is permitted. Furthermore, the liner coolant flow originates at a higher temperature than for subsonic engines. Both the high temperature and composition of the combustion gases, and the higher coolant temperature,

represent challenges that could exceed the long-term capability of currently available liner metals. Therefore, the successful development of the RQL combustor concept would benefit from high-temperature material advances such as are being sought in programs like EPM.

At low power operation, the lean combustor equivalence ratio may be reduced to a level such that, for the same airflow split, the rich zone would also operate as a lean combustor. That is, using the above high power setpoints and S, if ØL = 0.2, then ØR = 0.9. While this may be the desired operating condition to achieve high efficiency at low power, the ØR value will promote NOx formation. As discussed above, the rich zone temperature may also exceed an acceptable operating level for the combustor liner design. Such an undesirable operating condition will be encountered during turndown for any cycle unless a discontinuous control feature, such as an abrupt change in S, is employed. Fuel staging could maintain a rich value for ØR over the cycle, however, at low ØL values, that region would likely achieve high carbon monoxide emissions and poor efficiency. Operating the rich combustor in a lean mode also requires that the fuel nozzle produce a spray suitable to achieve NOx control and stability at these conditions.

Summary

In summary, the RQL combustor concept has demonstrated excellent emission control at aeroderivative, industrial gas turbine conditions with broad operability. The challenges for a HSCT engine application are to identify the quench mixing strategy that controls NOx emissions at the supersonic cruise condition, develop a rich combustor liner design capable of long life, and specify a workable combustor control strategy for low-to-high power operation.

Program Objective

As stated in Section II, the overall objective of this study was to evaluate the suitability of applying the RQL combustor concept to the HSCT engine cycle. In particular, the objective was to assess the sensitivities of the combustor performance and emissions to variations in the RQL design or operating condition, with special emphasis on determining whether the RQL combustor concept offered sufficient emissions control to achieve a nitric oxides emission index (EINOx) of 5 at SSC.

This program, then, addressed aspects of the first challenge cited above for developing the RQL concept. The development of a long-life, rich combustor liner is being addressed in the EPM program. Aspects of the combustor control strategy are being studied in a task of the NASA-sponsored Large Engine Technology contract with P&W.

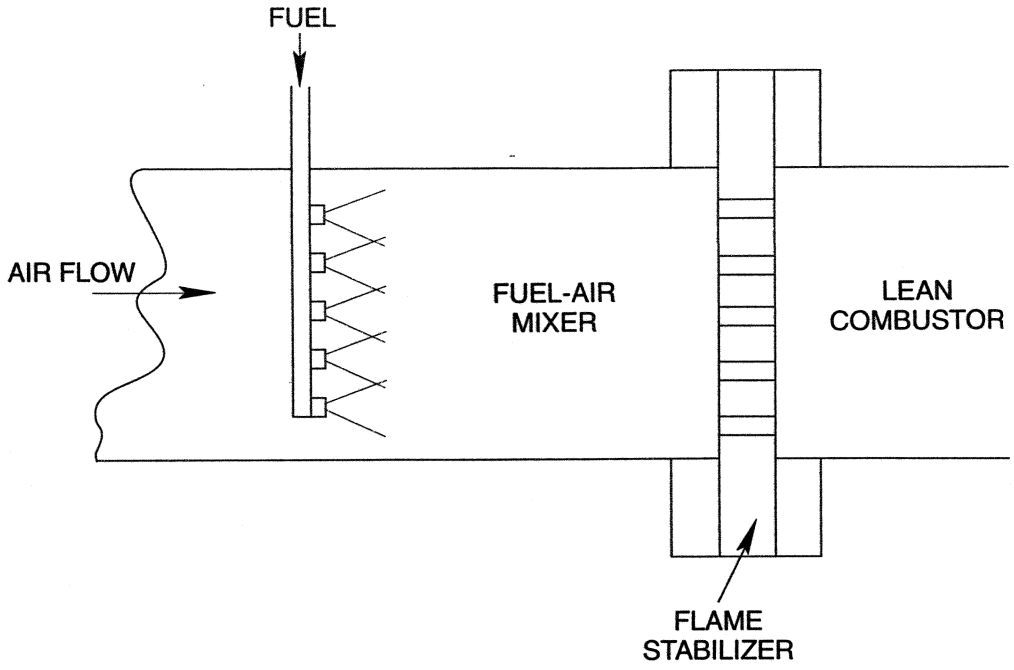

a) SEPARATED FUEL PREPARATION

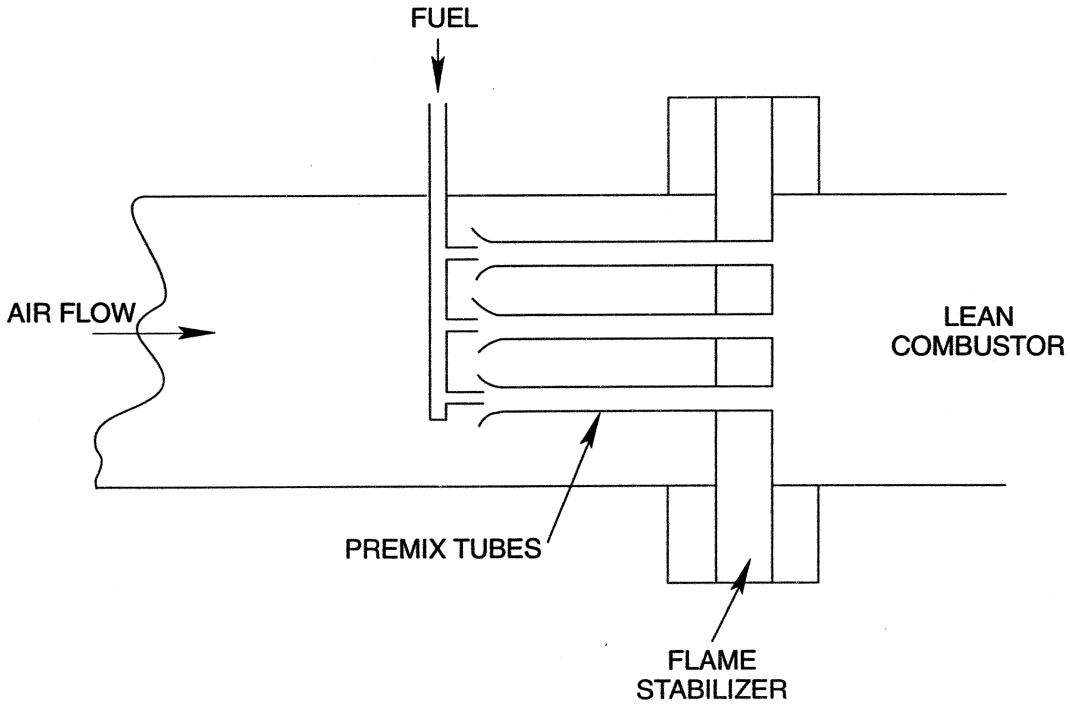

b) INTEGRAL FUEL PREPARATION

Figure III-1 Lean-Premixed-Prevaporized Combustor Concepts

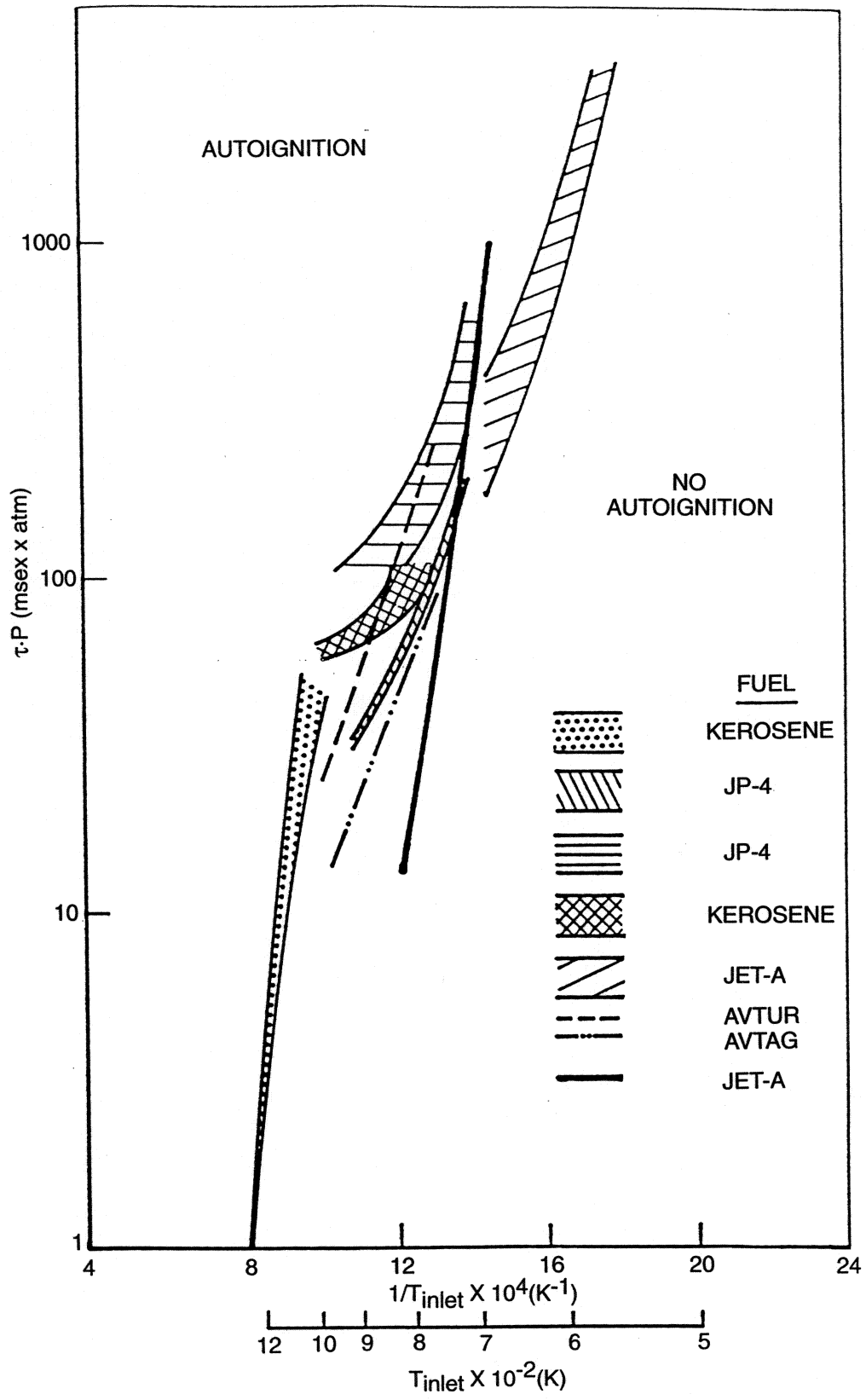

Figure III-2 Autoignition of Liquid Hydrocarbon Fuel Sprays in Air (Ref III-3)

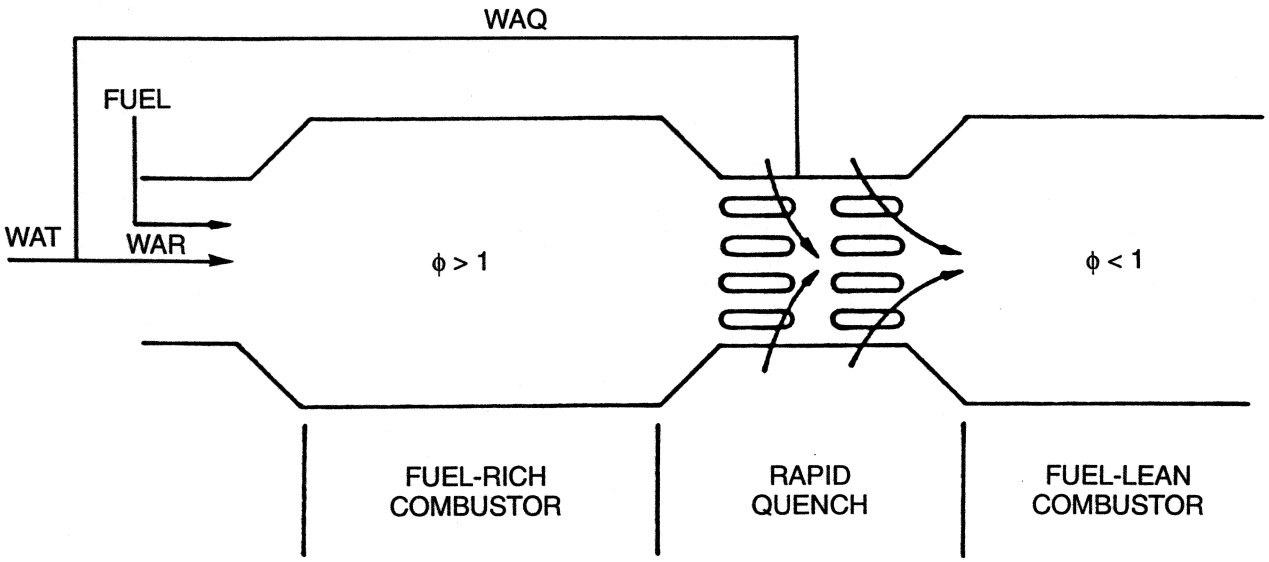

Figure III-3 Elements of Rich-Quench-Lean Combustor

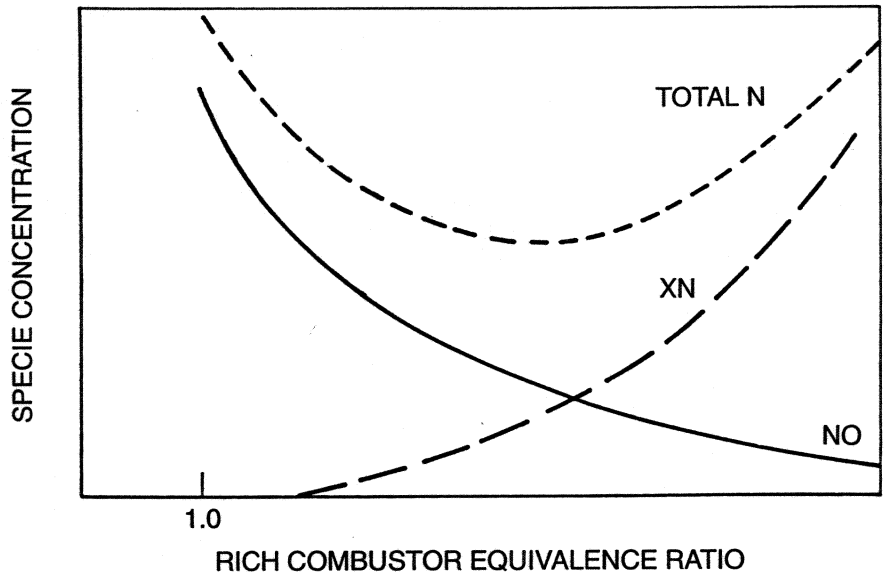

Figure III-4 Nitrogen Compound Evolution in Rich Combustion

SECTION IV RQL COMBUSTOR AND TEST FACILITY

The RQL combustor contains physically separated zones of fuel-rich and fuel-lean combustion. At the design condition, approximately 25 pct of the total combustor airflow, and all of the fuelflow, are combusted at an equivalence ratio above 1.5 in the rich combustor. The balance of the airflow, termed the quench airflow, is rapidly mixed into the rich-combustor effluent during the transition to a lean combustion zone operating at the combustor overall equivalence ratio. The performance and emissions control achieved by the RQL combustor will depend on the equivalence ratio and residence time established in each combustor, the fuel preparation quality, the quench mixer effectiveness, and the nominal operating condition. The UTRC flametube-scale RQL combustor, and the facility which supported it, were specified to allow investigations of these issues. The combustor was modular to permit efficient changes to alternative configurations to evaluate fuel preparation, residence time, and quench design influences. The test facility supplied controlled airflow rates to simulate a wide range of operating conditions from idle to very-high inlet temperature, supersonic cruise. Further, the airflow control permitted independent variation of the rich combustor and quench airflows to alter the equivalence ratios. This section of the report describes the flametube-scale RQL combustor and the facility used to support it.

Flametube-Scale RQL System Design

The flametube-scale RQL combustor and the supporting facility airflow system were specified by performing a system flow analysis. The analysis modeled the airflow delivery and control system and the combustor to assess the range of test conditions that could be achieved, and the flow control and metering device requirements. The system analysis was performed using a personal computer spreadsheet and therefore used one-dimensional fluid dynamic representations of the flows and correlations for thermochemistry calculations.

The system modeled is depicted in Fig. IV-1, which also indicates the parameter symbols for the model. The model first used a specified combustor geometry and reference test condition to calculate the pressure and temperatures in the rich, quench, and lean zones of the RQL; other flow parameters (e.g. residence time, momentum ratio) were also calculated. These properties were then used to size the supply airflow metering and control devices for the reference condition. Using the same metering and control devices, the flow parameters were calculated for other test conditions to determine the achievable range of variation.

Iterations of the metering and control device specifications led to the selection of airflow devices with maximum range while retaining acceptable sensitivity. Venturi diameters and control valve sizes were set. The analysis also established the flametube-scale RQL combustor geometry, including diameters and lengths, and quench-jet area.

The reference test condition was HSCT supersonic cruise (SSC) which is defined for the RQL combustor in Table IV-1.

Table IV-1 RQL SSC Test Condition

Parameter	Symbol	Units	Value
Combustor Inlet Air Pressure	P3	psia	150
Combustor Inlet Air Temperature	T3	F	1200
Combustor Overall Fuel-air Ratio	F/AOA	---	0.030
Combustor Reference Velocity	UREF	ft/s	90
Rich Combustor Equivalence Ratio	ØR	---	1.8

The value for ØR was set based on both prior applications of the RQL concept and the expected rich combustor temperature. That is, studies of industrial gas turbine combustors suggested a ØR value near 1.5, but at this level the rich combustor temperature would exceed 3800 F. The selection of ØR = 1.8 set the combustor temperature at 3400 F, still a challenge for rich liner materials, while retaining a stoichiometry believed suitable for both NOx and soot control.

This definition of SSC permitted the direct calculation of:

Combustor overall equivalence ratio (ØL)	0.438
Rich combustor airflow split (S)	0.243

where the value of S denoted the fraction of the total combustor airflow admitted directly into the rich combustor.

The steps performed in this system analysis were:

1. Specify the combustor geometry, including the combustor diameters (DR and DL) and lengths, quench diameter (DQ), quench orifice number (N),

diameter (d) and discharge coefficient, and rich combustor effective inlet airflow area.

2. Calculate the combustor total airflow (WAT) to achieve UREF.

3. Calculate the combustor fuel flowrate (WF) from WAT and F/AOA.

4. Calculate the rich combustor airflow (WAR) and quench airflow (WAQ) from WAT and S.

5. Calculate the pressure loss across the rich combustor inlet airflow area (DPR) and the rich combustor pressure (PR) using P3 and DPR.

6. Calculate the rich combustor temperature (TR) using:

$$TR(R) = 5227 - 1342 \times \text{ØR} + 0.634 \times T3(R)$$

7. Calculate the rich combustor mean velocity (UR) and residence time (TAUR) using the rich combustor dimensions.

8. Calculate the rich combustor momentum flux (MOMR), including WF in the total combustor massflow.

9. Calculate the quench section pressure (PQ) based on the acceleration of the rich combustor flow in the contracted quench crossflow area.

10. Calculate the quench section crossflow momentum flux (MOMQ) using MOMR, PQ, and the quench contraction.

11. Calculate the effective quench-jet area from the quench jet geometry and the discharge coefficient.

12. Calculate the quench-jet momentum flux (MOMJ) using WAQ, T3, and PQ.

13. Calculate the quench-jet-to-crossflow momentum flux ratio (J) as:

$$J = MOMJ / MOMQ$$

14. Calculate the pressure loss across the quench jets (DPQ) and the quench supply pressure (PQ3) using PQ and DPQ.

15. Calculate the lean combustor pressure (PL) assuming the loss of the quench section dynamic pressure from PQ.

16. Calculate the lean combustor temperature (TL) using:

$$TL(R) = T3(R) + 10395 \times \text{ØL}^{0.889} \times T3(R)^{-0.148}$$

17. Calculate the lean combustor mean velocity (UL) and residence time (TAUL) using the lean combustor dimensions.

18. Specify the rich combustor airflow venturi throat diameter (DVR).

19. Calculate the choked-flow, venturi upstream pressure (PARVUP*) required to pass WAR through DVR, and the overall venturi pressure ratio: RVPR = PARVUP* / P3. If RVPR < 1.2, specify a smaller value for DVR.

20. Specify the flow coefficient for a control valve in the rich combustor airflow (CVR).

21. Calculate the pressure upstream of the control valve (PCVR) to pass WAR.

22. Specify the flow coefficient for a control valve in the quench section airflow (CVQ).

23. Calculate the pressure upstream of the control valve (PCVQ) to pass WAQ.

24. Compare PCVR and PCVQ. They must be equal. If not, select new values for CVR and/or CVQ.

25. Calculate the heater inlet air pressure (PH) assuming a total pressure loss of 1.2 based upon previous experience.

26. Specify the total combustor airflow venturi throat diameter (DVT).

27. Calculate the choked-flow, venturi upstream pressure (PATVUP*) required to pass WAT through DVT, and the overall venturi pressure ratio: TVPR = PATVUP* / PH. If TVPR < 1.2, specify a smaller value for DVT. The results from this twenty-seven step analysis was the specification of venturi diameters and control valve settings to establish the reference test condition, for the specified combustor geometry. The analysis was repeated with fixed venturi diameters to determine the control valve range required to establish other test conditions of interest such as parametric variations or other design points. During this process, the venturi diameters were redefined to maximize the operational range while preserving adequate sensitivity of flow control and measurement. These analyses formed the basis for specifying the control valves and venturiis installed in the RQL facility.

The analysis was used to both establish the flametube-scale RQL combustor dimensions and set target ranges for the rich combustor inlet airflow area and

the quench jet area that would produce acceptable pressure losses. In particular, considering the SSC condition and the UTRC flow resources available, it was decided that WAT = 3.0 lb/s and that the combustor diameter would be 5.0 in. A rich combustor residence time (TAUR) of 13 ms would be achieved for a 8-in. long rich combustor, with a lean combustor residence time (TAUL) of 4.3 ms for a 8-in. long lean combustor. Both of these values included the flow volumes associated with adapting conical transitions described below. These nominal values became targets for the combustor component designs.

Further, it was predicted that a rich combustor inlet airflow area of 1 $in.^2$ would produce a 3.2 pct loss, and a quench jet effective area of 2.7 $in.^2$ would produce a 4.4 pct pressure loss. While these two values were not matched (and did not have to be matched because the control valves set the airflow split), they were at practical levels. The quench jet pressure loss corresponded to the value J = 22, which set this level as a practical target for a cylindrical RQL combustor. The analysis also illustrated the importance of the quench-jet discharge coefficient; the percentage imprecision in its value results had twice the influence on J. It became apparent that quench mixing studies must correlate their results with J values based on effective area and not geometrical area.

The analysis was also useful to set alternative test conditions which preserved selected parameters of the RQL combustor. Table IV-2 illustrates the interactive nature of the combustor for two ways to achieve a parametric variation in ØR. The third column represents the SSC condition as defined above. As shown in the fourth column, as ØR was increased parametrically to 2.0 by raising fuel flowrate, the residence times changed mildly, but F/AOA, and hence TL, increased dramatically. Alternatively, the increased ØR can be attained at constant F/AOA by altering the airflow split, S, as shown in the last column. However, both the rich combustor residence time increased and, more importantly, the quench momentum ratio grew by 41 pct. The RQL system analysis provided a tool to assess the impact of test condition variation on RQL parameters, and a means to specify conditions which controlled these variations.

Table IV-2 Interactive Test Conditions for ØR

Parameter	Unit	SSC Condition	Fuel flow Parametric for ØR	Split Variation for ØR
P3	psia	150	150	150
T3	F	1200	1200	1200
ØR	---	1.8	2.0	2.0
F/AOA	---	0.030	0.033	0.030
S	---	0.243	0.243	0.219
TR	F	3400	3140	3140
TAUR	msec	13	14	15
J	---	22	24	31
TL	F	2870	3030	2870
TAUL	msec	4.3	4.1	4.4

RQL Flametube-Scale Combustor Specification

The flametube-scale, RQL combustor consisted of rich, quench and lean zones as shown in Fig. IV-2. The following sections describe the components of this combustor.

Combustor Sections

The rich combustion zone consisted of a cylindrical length section followed by a conical convergent section to the quench entrance; these two sections were individual modules of the RQL combustor. Three cylindrical spools were available which could be installed separately or in-combination to achieve alternative rich zone lengths. These spools were 4, 6 and 8 in. long; each had a 5-in. ID. Based on the above system analysis, these sections provided 5.6, 8.5, and 11.3 ms, respectively, of rich zone residence time to the cylinder end flange (i.e. not including the conical convergent section) at the SSC condition. Each section contained both a passage located 3 in. from one end to accept a hydrogen-oxygen torch ignitor, and three radial passages in one end flange to pass the rich sampling probes. The convergent section was 1.6-in. long, transitioning from the 5-in. ID combustor to the 3-in. ID quench section at an included angle of 64 degrees.

The lean zone consisted of a divergent section at the quench exit followed by a separate cylindrical section. The 3.2-in. long divergent section transitioned from the 3-in. ID quench to the 5-in ID combustor at an included angle of 34 degrees. Three cylindrical spools were available to achieve alternative lean zone lengths. These spools were 6, 9, and 11 in. long; each had a 5-in. ID. The exit sampling probes penetrated into the lean combustor cylindrical spools by

3 in.; the lean combustor exit was defined by these probe tips. Thus, the effective lengths of the lean spool sections were 3,6, and 8 in. When the volume of the divergent section was included, these lengths provided 2.2, 3.4, and 4.3 ms, respectively, of lean combustor residence time at the SSC condition.

Each cylindrical combustor section was fabricated as a double-wall spool with 8-in., 300 psi flanges. Each was specified to use commercially-available carbon-steel pipe or tube and achieve a 0.125-in. wide annular gap to pass an axially-flowing water coolant; spacer wires were used during fabrication to preserve gap uniformity. The active cooling was necessary to achieve a usable test section pressure rating of 200 psia. Typically, each spool was fed by four, 0.5-in. coolant delivery lines. Four lines were also used for the coolant exhaust; orifices were placed in each exit line to regulate the coolant flowrate and enhance uniform flow. Typically, a combustor section flowed water at a rate of 10 GPM. The 1.6-in. and 3.2-in. conical sections were machined from carbon-steel rings to achieve a 0.1-in. wide annulus that flowed coolant flows of 2 GPM and 4 GPM, respectively. The analysis used to prescribe the combustor coolant requirements is described below.

All rich and lean combustor sections contained a 1.25-in. thick castable ceramic liner to provide thermal insulation and achieve the diameters mentioned above. The insulating liners were cast from Plibrico Plicast 40, a commercially available ceramic consisting of mostly alumina. This material was selected because of its favorable thermal shock properties and its ability to withstand combustor temperatures up to 3400 F. The 1.25-in. castable ceramic thickness was chosen because of a "keystoning" effect due to the thickness. That is, while the liners developed cracks due to thermal stressing, the keystoning helped prevent pieces from becoming dislodged. A typical combustor spool is shown in Fig. IV-3. To help secure the castable ceramic in the conical sections, a wire reinforcement mesh of 0.125-in dia. weld rod was attached to the inner surface. When the ceramic was cast, the weld rods were embedded about a 1-in. below the ceramic surface. This procedure provided additional strength to the cast liner and prevented the liner from dislodging.

To aid in specifying the combustor component design, a simple thermal analysis was developed to predict combustor section heat transfer characteristics. The one-dimensional model, which was setup on a personal computer spreadsheet, approximated the effects of radiative and conductive heatloads, and the convective cooling through the combustor walls. The analysis was used to predict the maximum and mean combustor wall temperatures at an operating condition for a specified combustor design. The design specification included the wall material and thickness, coolant gap size, ceramic liner thickness, combustor diameter and length, and maximum permitted coolant wall temperature.

The analysis procedure began by specifying a test section inlet gas flowrate, temperature, and equivalence ratio. A calculated combusting gas temperature, combustor massflow, and an assumed emissivity were used to determine the heatload The hot surface temperature was obtained by using a Newton-Raphson iteration technique to balance this heatload with the heatsink for a specified coolant temperature adjacent to the combustor wall. Metal wall temperatures were derived through conduction calculations. The coolant flowrates were calculated to achieve sufficient heatsink for a nearly isothermal, design coolant temperature. Coolant temperature rise and pressure loss in the annular passages, pressure loss for specified coolant supply lines, and energy loss from the combustor gas to the coolant, were also predicted by this analysis. Separate representations were developed to accommodate axially or circumferentially flowing coolant. The spreadsheet permitted a comparison of the effectiveness of a design for several operating conditions.

Quench Section

Four candidate quench-jet configurations were evaluated for their ability to control NOx emissions by adequately quenching the rich combustor products. A slanted-slot configuration was the first quench mixer specified. Recognizing the critical importance of this component, three alternative quench configurations were defined and evaluated. These alternative designs were guided by a simplified analysis of jet penetration into a confined crossflow. This analysis helped define quench mixers based on layouts of eight, equal-diameter circular holes, twelve equal-diameter circular holes and multiple holes of three diameters ("multihole" configuration). The penetration analysis is described, followed by descriptions of each of the quench designs.

Penetration Analysis

An analysis of jet penetration into a crossflow was conducted to aid the definition of the quench section designs to evaluate in the RQL combustor. The purpose of the analysis model was to screen potential quench candidates by predicting the jet penetration for various orifice geometries consisting of single-diameter or multiple-diameter orifices, and pressure loss and momentum ratios they achieve.

In the RQL combustor, the higher flowrate quench-jets penetrate into a lower flowrate, confined crossflow. For high levels of jet penetration, the jets block the crossflow and locally causes it to accelerate. A personal computer spreadsheet model was developed to predict the quench-jet penetration into a confined crossflow with consideration of the blockage effect.

Studies of a fluid jet penetration when injected across an unconfined flow correlate as (Ref. IV-1):

$$\frac{y_0}{d} = K * J^{0.5} * \left(\frac{x}{d}\right)^{0.33}$$

where: y_0 = the jet penetration in the unconfined flow;
d = the jet orifice diameter;
J = the jet-to-crossflow momentum flux ratio in the unconfined flow;
x = the distance downstream of injection location.

The constant, K, depends on whether the inner or outer boundary, or jet centerline is being tracked; the above reference suggests K = 0.56 for the centerline penetration.

A jet injected into a confined crossflow, as found in the quench section, will locally accelerate the crossflow which, in turn, will reduce the penetration. Ultimately, the jet mixes with the crossflow and a general acceleration will occur due to mass addition. In and near the plane of injection, the jets are coherent and represent a blockage to the crossflow. The jets do spread and mix so that this effect changes as the flow develops.

As a simple model for rapidly penetrating jets it was assumed that the jet retains its exit diameter, d, for the penetration depth, y, evaluated one jet diameter downstream. Then N jets represent a blockage area (A_j) of:

$$A_j = N * d * y$$

and the remaining area for the cross-flow (A_{CF}) is

$$A_{CF} = A_{CF0} - A_j = A_{CF0} - N * d * y$$

where A_{CFo} is the cross-flow area with no jet blockage. The reduced crossflow area accelerates this flow which for a fixed jet momentum flux, decreases the momentum flux ratio to J_b which is given by:

$$J_b = J * \left(\frac{A_{CFo} - N * d * y}{A_{CFo}}\right)^2$$

The penetration with blockage, y, is:

$$\frac{y}{d} = K * J_b^{0.5} * \left(\frac{x}{d}\right)^{0.33}$$

The confined and unconfined flow penetrations can be combined to obtain:

$$\frac{y}{y_o} = \frac{1}{1 + \frac{N d y_o}{A_{CFo}}} = \frac{1}{1 + B_o}$$

where B_o is the potential jet blockage if the flow was not confined. The actual blockage is represented by

$$B = \frac{N d y}{A_{CFo}}$$

This representation of jet blockage, illustrated in Fig. IV-4, is more applicable for low x/d values. For such cases, the jet core from the wall to the extent of penetration is nearly in the same transverse plane, and the acceleration effect would be realized. For high x/d values, the jet trajectory is not contained in a single transverse plane; the jets penetrate such a plane as a collection of near-circular jets.

For N jets of various diameters, the above equation can be generalized to account for the penetration of each jet.

$$\frac{y_i}{y_o} = \frac{1}{1 + \frac{N_i d_i y_{io}}{A_{CFo}}}$$

The effect of jet blockage in a confined crossflow on the predicted jet penetration was dramatic. For example, at the flow conditions corresponding to SSC operation, eight, 0.719-in. dia quench jets produced a 4.8 pct pressure loss and a J value equal to 24. The predicted unconfined jet penetration was 2.0 in., whereas the predicted confined jet penetration was 0.76 in. That is, the former case was predicted to penetrate beyond the centerline of a 3-in. dia quench section while the latter would penetrate only to 50 pct of the radius. Substantially different quench mixer performance would be expected for designs achieving these two penetrations.

The penetration of the quench-jets for a specified quench hole layout was evaluated in selecting alternative quench configurations. Other considerations in the design were the quench-jet pressure loss (i.e. design momentum ratio) and the orifice spacing.

Eight Slanted-Slot Quench

A slanted-slot quench mixer was the first quench section specified. It was based on reported experience in applying the RQL combustor concept to control NOx emissions from industrial gas turbine combustors (Ref. IV-2). Further, based on cold-flow quench mixing studies, it was known that the slanted-slot layout produced a secondary swirling flow with the quench section that was believed to be beneficial to mixing (Ref. IV-3). In essence, the slanted slots acted as vanes to the inlet crossflow. Also, the slant angle and length of the slots tended to produce a full circumferential coverage of this crossflow which was also believed beneficial to enhanced mixing.

The slanted-slot quench specified for the HSCT application consisted of an array of eight equally-spaced slots located around the surface of a 3-in. ID cylinder (Fig. IV-5). The slots were slanted at a 45-deg angle to impart a counter-swirl to the incoming rich combustor flow. Each slot was 0.25-in. wide by 1.75-in. long to the full-radius end to provide 0.424-in^2 of geometrical area; the total for all eight slots was 3.392 in^2. The length and angle of the slots completely covered the circumference of the quench section. At the SSC condition and using an assumed slot discharge coefficient of 0.8, it was predicted that this slot geometry would produce a 4.4 pct pressure loss to the quench airflow, and achieve J = 22. That is, this quench-jet area was specified using the system analysis described above to achieve a practical level of pressure loss, and the associated mixing momentum ratio.

The quench section was fabricated as a separate, 3.375-in. long module in the combustor assembly. It contained one, 3-in. dia quench airflow inlet which fed the annular manifold around the quench-jet cylinder. The quench housing was constructed from 316 stainless-steel and had nominal side-wall thicknesses of 0.5 in. Since this quench section was not actively cooled, a 0.5-in. thick liner of Plicast 40 was cast on the combustion-gas side of the quench-jet cylinder. The quench section, like the conical sections, incorporated reinforcement bars constructed of 0.062-in. weld rod attached to the quench inner surface prior to casting the ceramic. These rods prevented the ceramic liner from rotating circumferentially or becoming dislodged. Wax plugs were used during liner casting to preserve the quench slot geometry and removed afterward by melting. The ID of the cast ceramic was 3 in. The depth of each slot was the sum of the 0.25-in thick metal cylinder and the 0.5 in thick ceramic, for a total of 0.75 in.

Eight Circular-Hole Quench

A second quench design introduced the quench airflow through eight, 0.719-in. dia, equally-spaced circular orifices (Fig. IV-6). The quench section length and inner diameter remained at 3.375-in and 3-in, respectively, and the axial plane of the hole centerlines was equidistant from the quench entrance and exit. The geometrical area of the eight quench orifices was 3.248 $in.^2$, which was within 4 pct of the slanted slot area. The eight-hole quench was predicted to produce a pressure loss of 4.8 pct and achieve J = 24 (for an assumed discharge coefficient of 0.8) at the SSC condition. Since these values were very close to those for the slanted-slot quench, the primary difference between the two designs was the degree of penetration and flow coverage achieved. That is, the circular jets were expected to penetrate deeper into the crossflow, but with a loss of flow circumferential coverage. As indicated in the Penetration Analysis discussion, the penetration of the eight, circular quench-jets into a confined crossflow was predicted to be 50 pct of the quench radius at the SSC condition. In contrast, the unconfined flow penetration was predicted to be 131 pct of the quench radius. Unlike the slanted-slot orifices, the circular-jet orifices were not overlapping; a 0.459-in. web existed between adjacent jets. The specification of this eight circular-hole quench satisfied the criterion identified by Holdeman for optimal mixing in a cylindrical configuration (Ref. IV-4). By considering the cylindrical geometry to be a limiting case for outer-wall injection for a curved rectangular duct, he formulated a desired relationship between the number of quench jets, N, and the momentum ratio, J, as:

$$N = \pi * \sqrt{2 * J} / C$$

where C = 2.5. For J = 24, the desired N = 8.7, close to the design.

The original eight-hole quench section design was similar to the slanted-slot quench. It had one air inlet, was fabricated from 316 SS, and was not cooled. It contained a ceramic liner that was cast and reinforced in a fashion similar to the slanted slot design. Again, the thickness of the quench-jet metal cylinder and the ceramic liner was 0.75 in.

The castable ceramic liner was successful at protecting the quench metal wall from the extreme temperature and heat transfer environment in the quench section. However, due to erosion caused by the harsh environment, the quench section ceramic liners survived only a few tests before needing to be recast. This feature was unacceptable for a test rig being used to develop RQL technology. This nuisance was remedied by fabricating water-cooled quench sections that did not require a ceramic liner for survival. Heat loss to the cooled surface was minimized with use of a 0.03-in. thick, flame-sprayed

coating of zirconia oxide; emission traverses obtained from the probe immediately downstream from the quench displayed no cool-wall influences.

The water-cooled versions of the quench section were fabricated by re-working a non-cooled device. The design included two, 0.10-in. high annular passages in a replacement, 0.75-in.-thick wall, quench-jet metal cylinder (Fig. IV-7). Each annulus was 1.10-in. wide and located to provide a 0.75-in. wide uncooled band at the center of the section for the quench-jet orifices. Water was supplied at a flowrate of 3 GPM to each cooling passage through flexible lines that passed across the quench manifold and out of the housing. The water-cooled quench sections proved to have the durability required to survive in this part of the combustor.

Initial test results with the uncooled, eight circular-hole quench indicated that a great degree of NOx control had been achieved. Therefore, the first water-cooled quench section contained a duplicate quench-jet design. It was identical to the first in hole diameter and pattern, and was predicted to achieve the same pressure loss and momentum ratio. The only difference between these two quench sections was that the second design included water-cooling.

Multihole Quench

The third quench-jet configuration was termed "multihole" because it injected the quench airflow through arrays of circular orifices using three hole diameters. The goal of the design was to promote a greater range of mixing length scales than would be experienced with a single hole diameter array. The multiple scales would develop from differences in both the hole diameters and the levels of penetration into the crossflow. It was also desired to achieve complete coverage of the quench cylinder circumference.

Iterations of multihole configurations using the Penetration Analysis led to the specification of a repeating array consisting of one 0.58-in. dia, two axially-aligned, 0.15-in. dia, one 0.29-in. dia, and two axially-aligned, 0.15-in. dia holes, in this sequence. The array was repeated eight times around the quench circumference (Fig. IV-8) resulting in a 48 hole pattern contained within a 0.71-in. wide band at the mid-plane of the quench section. The total array provided 3.207 $in.^2$ of geometrical area, 95 pct of the eight circular-hole quench, with a predicted pressure loss of 4.9 pct and an associated momentum ratio, J = 25 (for an assumed Cd=0.8). Since all orifices were plenum-fed, this value of J applied to all quench jets. However, because of differences in the hole diameter, the predicted penetrations, as a percentage of the quench radius, covered the range indicated in Table IV-3. The table also indicates the percentage of the quench flow, reflected as the percent of total quench-jet area, injected to each penetration.

Table IV-3 Multihole Orifice Penetration

Jet Diameter	Total Number	Jet Area	Penetration
in.	---	pct of total	pct of quench radius
0.58	8	66	38
0.29	8	16	24
0.15	32	18	15

Because the multihole layout contained a high density of orifices, casting a ceramic liner around them was not practical. Therefore, the 0.71-in. wide metal band containing the orifices extended radially inward to the 3-in. quench ID, with ceramic liner cast on either side of the band. The multihole quench was not water cooled.

Twelve Circular-Hole Quench

A fourth quench design introduced the quench airflow through twelve, 0.500-in. dia, equally-spaced circular orifices. The quench section length and inner diameter remained at 3.375-in and 3-in, respectively, and the axial plane of the hole centerlines was equidistant from the quench entrance and exit. The geometrical area of the twelve quench orifices was 2.356 $in.^2$, which was 72.5 pct of the eight circular-hole quench area; the web between orifices was 0.29 in.

The twelve-hole quench was predicted to produce a pressure loss of 8.7 pct and achieve J = 46 (for an assumed discharge coefficient of 0.8) at the SSC condition. The predicted penetration into the confined quench crossflow was to 48 pct of the quench radius, nearly identical to that predicted for the eight circular-hole quench. As for the eight-hole design, the twelve circular-hole quench followed the parameter identified by Holdeman for optimal mixing. That is, for J = 46, the desired N = 12.1.

The twelve-hole quench section design was similar to the water-cooled, eight circular-hole quench. It had one air inlet, was fabricated from 316 SS. Again, heat loss to the cooled surface was minimized with use of a 0.03-in. thick, flame-sprayed coating of zirconia oxide. The design included two, 0.10-in. high annular passages in a replacement, 0.75-in.-thick wall, quench-jet metal cylinder (see Fig. IV-6). Each annulus was 1.10-in. wide and located to provide a 0.75-in. wide uncooled band at the center of the section for the quench-jet orifices. Water was supplied at a flowrate of 3 GPM to each cooling passage through flexible lines that passed across the quench manifold and out of the housing.

Fuel Preparation

The rich combustor airflow was delivered to the fuel preparation spool, which housed the fuel injector, and where static pressures and stagnation temperatures to document the P3 and T3 conditions, respectively, were acquired. The fuel preparation section was internally insulated with a 0.5-in. thick Fiberfrax T-30R laminated tube to minimize heat loss. The fuel injector was secured to a water-cooled mounting flange that had a 1.93-in. ID and comprised the combustor bulkhead.

An individual Delavan Swirl-Air fuel nozzle was used for all combustion tests. This nozzle was mounted in the center of an annular, axial-flow swirler (Fig. IV-9). The swirler contained 18 curved vanes, with a final turning angle of 45 deg., in a 1.93-in. OD by 1.13-in. ID flow annulus. The tip of the nozzle was flush with the swirler exit plane, with the assembly being recessed into the rich combustor bulkhead. The effective airflow area of the nozzle-swirler assembly was 1.0 $in.^2$.

The Swirl-Air nozzle is an internal mix, air-assist nozzle. This design was selected because of demonstrated performance in previous studies applying the RQL concept to industrial gas turbine combustors (Ref. IV-5). The air-assist feature permitted control of the fuel atomization process independent of the test condition. The assist airflow was regulated, metered by a venturi, and included in WAR. The assist airflow was not heated, however, and the value of T3 denoting a test condition resulted from a mass-weighting of the air assist, rich combustor, and quench section airflow.

The specific model of the Delavan Swirl-Air nozzle was 32740-3. The nozzle had a nominal capacity of 2.5 GPM, far in excess of the fuel flowrate requirement of the flametube-scale RQL combustor, with a nominal spray cone angle of 100 deg. The nozzle capacity was selected to obtain internal air passages which did not excessively back-pressure the air-assist supply. Typically, the nozzle fuel-to-air flowrate ratio was unity.

The spray characteristics of the nozzle-swirler assembly were studied by performing ambient spray tests. First, the preferred recess length was determined. This length corresponded to achieving maximum interaction between the spray and the rich combustor airflow prior to entering the combustor, but avoiding spray impingement on the recess sidewalls. After observing the spray for three levels of recessed length, it was determined that the nozzle-swirler assembly should be recessed 0.5 in. from the combustor inlet. Once this length was established, the spray patternation and atomization qualities were studied using the UTRC Ambient Spray Facility. It was observed, however, that the atomization quality was very high, resulting in droplet sizes smaller than could be confidently measured by the setup of

the Malvern Particle Size Analyzer. The spray had a "fog" characteristic; droplet sizes were estimated to be less than 10 microns. The small droplets prohibited determining the spray pattern because of poor spray collection efficiencies of a fog.

RQL Facility

Layout

The flametube-scale RQL combustor facility included a high-temperature airflow distribution and control system, the modular RQL combustor, and an exhaust system (Fig. IV-10).

The total combustor airflow (WAT) was supplied to the test facility installed in Cell 1E of the Jet Burner Test Stand by continuous-flow compressors This flow was metered by a venturi and heated by a series of two electrical air heaters. The airflow exiting the second heater was divided into the rich combustor airflow (WAR) and quench airflow (WAQ). The rich combustor airflow traveled through a 2-in. control valve, a bellows expansion joint and then a metering venturi. The quench airflow was routed through a 3-in. control valve and a bellows before entering the quench manifold; the quench air flowrate was calculated as the difference between WAT and WAR.

A water-cooled instrumentation section containing six emissions sampling probes was located at the exit of the flametube-scale RQL combustor. A description of the emissions sampling system is described. Downstream of the instrumentation section, the combustor exhaust passed through a diffuser and transition sections upstream of the combustor back-pressure control valve. The transition section diverted the flow through two 90-deg turns prior to encountering high-pressure water sprays to cool the flow before entering the back-pressure valve. A window was located in the transition section along the combustor centerline to permit observation of the flame patterns. This section of the report describes the facility capabilities supporting the RQL combustor.

Airflow Delivery and Heating

Four centrifugal air compressors, capable of delivering airflow rates up to 20 lb/s at pressures of 400 psia, supplied the high pressure airflow required for the RQL combustor tests. At the SSC condition, the required total airflow rate was WAT = 3 lb/s; the maximum WAT was 4 lb/s at a parametric variation from SSC. These airflow rates were established by using a large capacity regulator to provide a fixed pressure to a total airflow metering venturi. Based on the System Analysis, the total airflow venturi was specified to have a 0.760-in. dia throat for the high-power test conditions. This venturi

operated choked at all test conditions. A secondary system, also supplying airflow at 400 psi, was divided into two separately regulated flows. One supply provided a metered air-assist flow to the Delavan fuel injector, and the second delivered unmetered cooling air to the viewing window.

Combustor inlet air temperatures (T3) up to 1300 F were achieved with multiple, non-vitiated heating systems. Two direct contact, electrical resistance heaters were plumbed in series to obtain a 1300 F inlet temperature at 200 psia. The first heater, rated at 600 VDC and 720 kW, raised the test model airflow temperature from ambient to approximately 850 F at the heater exit. The second unit, a 480 V, 3-phase, 650 kW system provided the additional energy required to boost the air temperature from 850 F to 1300 F. The design of the 650 kW boost heater was unique in that the heater housing was internally insulated with a 0.5-in. thick Fiberfrax laminated tube. This insulation method minimized heat loss while permitting the housing to maintain strength. This approach allowed the use of a standard 14-in., SC 40, 304 SS pipe for the pressure vessel. If external insulation was used, a 1.25-in. thick wall, 316 SS tube would have been required to satisfy the design pressure.

Part-power test conditions demanded combustor inlet temperatures up to only 850 F. This inlet temperature was achieved by using the 720 KW heater in series with an indirect, natural gas-fired system. The natural gas-fired system provided temperatures of 325 F to the inlet of the 720 KW heater. The 720 KW unit was then used to increase the air temperature to the 850 F combustor inlet condition.

Downstream of the air heaters, the total airflow was split into two separately regulated flows directed to either the rich combustor or the quench zone. Based on the results of the System Analysis, a 2-in., 1500-psi class globe control valve was installed to regulate the rich combustor airflow. This control valve had a maximum flow coefficient (CV) of 38 and allowed airflow rates up to 1.5 lb/s at 250 psid and 1400 F. Also based on the Analysis, the rich combustor airflow venturi was specified to have a 0.600-in. dia throat. At most test conditions, this venturi operated choked. The quench flow was determined from the difference of the metered total airflow and rich combustor airflow. Regulation of the quench flow was achieved by use of a 3-in., 1500 psi class globe control valve. It had a maximum CV of 99 and permitted airflow rates of up to 4 lb/s at 250 psid and 1400 F.

Due to the high inlet temperatures necessary to meet the HSCT requirements, special consideration was given to minimizing heat loss while maintaining the strength of the airflow piping. The piping was constructed of 316 SS and, where feasible, was internally insulated with 0.5-in. thick Fiberfrax T-30R insulation. Again, this internal insulation method permitted the use of standard schedule piping. Two stainless steel bellows rated at 250 psia and

1400 F were installed to accommodate thermal expansion of the rig. The bellows were also internally insulated to minimize heat loss.

Fuel flow

Jet-A fuel was supplied to the test cell from above ground storage tanks using a 1500 psi positive displacement pump capable of flowrates of 14000 lb/hr. The fuel was delivered to the test combustor by independently-controlled primary and secondary systems. The primary leg permitted flowrates of 150 to 400 lb/hr and the secondary leg delivered flowrates to 150 lb/hr. Fuel flows for each system were controlled with a pressure-reducing regulator in series with an appropriately-sized orifice, and metered with a turbine flowmeter.

Miscellaneous flows

Independently regulated hydrogen and oxygen flows for the torch ignitor were supplied from high pressure storage bottles. An automatic timing sequence controlled the torch firing by causing the reactants to flow to the torch body where firing was initiated with a spark plug. The timing sequence automatically terminated the torch firing after a specified time interval (nominally 1.5 sec). The stoichiometry of the torch reactants was hydrogen-rich, resulting in the injection of a hot hydrogen plasma into the combustor.

Most of the flametube-scale RQL combustor was cooled by low pressure water. The internal, cast ceramic liner reduced the heat loss from the combustor and maintained a hot combustor wall, but was not a sufficient insulator to restrict metal temperatures to acceptable limits. The required water flowrate was minimal; it was set to a conservative level of nominally 10 GPM for each combustor section. High pressure water was injected upstream of the back-pressure valve. This flow reduced the combustor exhaust gas temperature and suppressed noise. It was supplied by a high pressure, centrifugal water pump capable of flows up to 35 GPM at pressures of 200 psi.

High pressure gaseous nitrogen, used for fuel and sampling probe purge, was supplied from a 15000 SCF storage tank that was charged to 2400 psi by a liquid nitrogen vaporizer-compressor system. The nitrogen was regulated to provide adequate pressures and flows for purge.

Emissions Sampling and Analysis

The principle focus of the RQL combustion test program was to document the combustor emissions levels achieved at operating conditions for a HSCT aircraft engine. Emissions samples were acquired at three discrete axial locations in the flametube-scale combustor: the rich combustor exit, the quench exit and the lean combustor exit. Generally, these samples were

obtained at multiple radial and circumferential locations. A description of the sampling probe designs and analysis methods are described in the following sections.

Lean Combustor Sampling

The lean combustor sampling instrumentation consisted of an array of six emissions probes which defined the combustor exit plane. As indicated previously, the probe tips extended 3-in upstream into the combustor spool; the residence time for a lean combustor length was based on the position of the probe tips.

The six probes were distributed across the combustor exit plane. Samples could be obtained either from each probe individually or from all probes ganged together. Five of the probes were positioned at two different radii based on equal area segments and the sixth probe was placed on the centerline (Fig. IV-11). Three of the probes were located 120deg apart at a 1.4-in radius from the centerline and two were separated by 120 deg at a 2.0-in. radius.

The lean combustor probes were designed to provide an aerodynamic quenching of the sample at the probe tip (Fig. IV-12). This quenching process was accomplished by a rapid expansion to supersonic conditions in order to reduce the static pressure and static temperature and thereby freeze the composition. Energy was extracted from the sample by convective heat transfer to the probe coolant to reduce the sample total temperature. After achieving a sufficient reduction in this temperature, the sample flow was shocked to a subsonic condition at a stabilization step. If sufficient energy was removed from the sample, its static temperature after the shock would be too low to promote further chemical reactions. The aerodynamic-quenching probe concept is described in more detail in Ref. IV-6.

The probe design process was to first analyze the flow through the probe tip to predict pressure and temperature histories, establishing the tradeoffs between sample conditions and flowrate, expansion ratio, and length to shock step. An important consideration was the influence of friction during supersonic flow in the probe which reduced the sample Mach number and pressure. Next the influence of these histories on the conversion of NOx and CO was analyzed using chemical kinetic calculations.

Based upon several iterations of the aerodynamic quenching flow analysis, a probe tip design was specified to minimize NOx formation and CO oxidation. The design included a 0.030-in. dia sample inlet, a supersonic expansion area ratio of 4.27 and a supersonic quenching length of 1.97-in. The body of the probe consisted of three concentric, 304 SS tubes: an outer tube having 0.50-in. OD x 0.028-in. wall; a mid-tube having 0.34-in. OD x 0.015-in. wall; and an inner tube having 0.12-in. OD x 0.013 wall. Water cooling, necessary for

probe survival in the combusting flow and for heat extraction from the sample, was supplied to each probe at a nominal flowrate of 2.5 GPM.

Predictions of the flow conditions in the probe tip are shown in Fig. IV-13 for the SSC condition. As indicated, the Mach number increased to 2.5 after the tip expansion but decayed to 1.3 during the heat extraction primarily because of friction; the total pressure was similarly reduced from 150 psia to 30 psia. The static temperature was held below 1500 F while the total temperature was reduced by approximately 850 F in the 1.97-in long water cooled passage.

Chemical kinetic calculations were performed to predict any changes in CO or NOx concentrations during the aerodynamic quench. The initial conditions for the chemical composition assumed equilibrium concentrations at the probe entrance except for the two species of interest. NO and NO_2 were set to be 100 ppm and 0 ppm, respectively, and CO set to correspond to a 0.2 pct level of combustion inefficiency (nominally 300 ppm). At the SSC condition, the CO predictions indicated a minimal oxidation loss of about 5 pct of the initial level (Fig. IV-13). The calculations predicted virtually no formation of NOx within the probe tip or transfer line, although a 10 pct conversion from NO to NO_2 was possible in the transfer line (Fig. IV-14).

Rich Combustor Sampling

The rich combustor sampling instrumentation consisted of two emissions probes located at the exit of rich zone cylindrical section. The two probes were separated by 120deg with one positioned on the combustor centerline and the other at a 1.25-in. radius. These probes were inserted into the combustor by use of access ports through the flange of a rich combustor spool section.

The rich probes were not designed as aerodynamic quenching probes because of the concern that rich combustor soot would plug the small sampling orifice. Additionally, the combustor layout and access would not accommodate the probe tip length required for that design. As presented in the results, there was no evidence that specie conversion was experienced in rich combustor samples.

The rich sampling probe was constructed using 0.50-in. OD x 0.035-in. wall, 304 SS tube for the straight body (Fig. IV-15). The body was compressed over a 3.5-in. length to achieve a 0.35-in. frontal width for the portion of the probe inserted into the combustor. The sample line was a 0.125-in. OD x 0.028-in. wall, 304 SS tube welded to the body to form the inlet orifice located on the side of the probe near the end. Water coolant was supplied to the probe at a flowrate of 2 GPM. Due to the soot generated in the rich zone, a 25 micron filter was installed in the probe sample line to prevent clogging of the transfer system or emissions analyzers.

Samples extracted from the rich combustor contained CO concentrations that were beyond the highest scale of the available gas analyzer. An alternate means of determining the CO level was used which compared direct and nitrogen-diluted emissions samples. That is, two samples for the test condition were analyzed, with one of them diluted by nitrogen to reduce the CO concentration to be within the analyzer range. The CO2 concentrations were recorded for both samples and used to monitor the dilution ratio. In particular, designating the diluted sample concentrations as CO_d and $CO2_d$, then:

$$CO = CO_d * \frac{CO_2}{CO_{2_d}}$$

Quench-Mixer Sampling

Emissions samples were acquired near the quench-mixer exit to determine the fuel-air ratio profile for use as an indicator of the mixing effectiveness of the quench-jets during combustion. The concentration of NOx was also measured.

The quench-mixer sampling probe spanned the flow diameter in a plane within the conical transition to the lean combustor. This location was the closest accessible plane to the quench-mixer exit; it was 2.3 in. downstream of the plane of quench-jet centerlines. The probe was designed to traverse 3.25 in. across the test section allowing samples to be acquired over the full extent of the 3.0-in. dia quench section exit.

The quench-mixer traversing probe design was identical to the rich combustor probe except that it spanned fully across the flow diameter. This configuration minimized both the flow bias that a single-ended probe might impose and the pressure loads that are common to traversing probes which are partially submerged into a high pressure flowfield. The housing contained two diametrically-opposed fittings with o-rings to both accommodate movement of the probe and achieve a pressure seal Water was supplied at a rate of 5 GPM to provide adequate probe cooling.

Since the quench mixing effectiveness was unknown at the outset of the test program, it was anticipated that the quench sampling probe might ingest a highly fuel-rich sample. Precise determination of fuel-air ratio for rich samples would require the measurement of hydrogen concentration, but such analysis capability was not available on-line. An alternative procedure was developed in which the sample was diluted with air and completely oxidized on a catalyst. However, initial quench-mixer samples indicated that all samples were fuel-lean; a significant oxygen concentration was always present. Hence, only standard analysis techniques were required for quench-mixer samples.

Emission Analysis Procedures and Performance Parameters

The UTRC emissions sampling and analysis system is maintained and operated in accordance with ARP 1256A specifications. The emissions cart employed is capable of continuous monitoring of emissions of carbon monoxide, oxygen, carbon dioxide, unburned hydrocarbons and oxides of nitrogen (Fig. IV-16). CO_2 levels are determined from a Beckman Model 864 instrument and CO levels are obtained with a ASC Model 3300 instrument. Both of these devices are non-dispersive infrared analyzers. A Thermo Electron Model 10 chemiluminescence analyzer is used to measure NOx composition. A Rosemount Model 755 paramagnetic device is used for oxygen analysis and a Beckman Model 402 flame ionization detector is used to monitor unburned hydrocarbons.

Emissions samples were routed from the probes through electrically heated lines to a valving system where the samples could either be combined or extracted individually, and then delivered to the gas analyzers. The samples were then transferred from the valving system to the emissions cart through an externally insulated 304 SS line that was maintained at 350 F. The transfer line had a 0.18-in. ID and was approximately 75 ft long. At the cart the sample was divided for distribution to the five analyzers. The NOx and UHC samples were plumbed directly to the corresponding analyzers and measured as wet samples. The CO_2, CO and O_2 samples passed through a capillary dryer which is used to remove the moisture before those samples are analyzed. The composition of NOx, UHC, CO, CO_2 and O_2 were determined from the appropriate analyzer reading and a corresponding calibration curve.

The results from analyses of the emission sample were used to calculate the primary performance parameters for a combustion test. These parameters included the fuel-air ratio, the emissions index, flame temperature, and combustion efficiency. Since each of these was based on the sample analysis, the parameter reflected either a local value when individual probe samples were analyzed, or a global value when all probes were ganged together.

Fuel-Air Ratio

The fuel-air ratio calculated from the emissions analysis followed the technique outlined by Spindt (Ref. IV-7). This procedure has been used by UTRC for analysis of emission-based fuel-air ratio because it has a greater precision for samples which approach stoichiometric. The fuel-air ratio was calculated as:

$$f/a = \left\{ F_b \left(11.492\, F_C \cdot \frac{1 + R/2 + Q}{1 + R} + \frac{120\,(1 - F_C)}{3.5 + R} \right) \right\}$$

where:

$$F_b = \frac{PPM_{CO} + PPM_{CO_2}}{PPM_{CO} + PPM_{CO_2} + PPM_{UHC}}$$

$$F_C = \frac{12.01}{12.01 + 1.008\left(\frac{H}{C}\right)}$$

$$R = \frac{PPM_{CO}}{PPM_{CO_2}}$$

$$Q = \frac{PPM_{O_2}}{PPM_{CO_2}}$$

PPM_i = parts per million molar concentration of specie i

C, H = number of carbon and hydrogen atoms contained in the fuel, respectively.

The Spindt technique combined CO, CO_2, O_2 and UHC emissions to determine the fuel-air ratio, but as for any similar procedure, the result was largely influenced by the CO_2 and O_2 content.

Emissions Index

An emissions index of specie i (EI_i) was calculated for NOx, CO, and UHC according to:

$$EI_i = \frac{PPM_i}{1000} \cdot \frac{(1 + f/a)}{f/a} \cdot \frac{MW_i}{MW_{comb}}$$

where: PPM_i = parts per million molar concentration of specie i;
MW_i = molecular weight of specie i;
f/a = fuel-air ratio based on the sample analysis;
MW_{comb} = molecular weight of the combustor composition.

Combustion Efficiency

The combustion efficiency (η_{comb}, pct) was calculated from the sample analysis, where inefficiencies were represented by concentrations of the incompletely oxidized species, UHC and CO, greater than equilibrium:

$$\eta_{comb} = 100 - 0.1\left(0.235\,EI_{CO} + EI_{UHC}\right)$$

The efficiency calculation assumed that the unburned hydrocarbons have the same heat of combustion as the Jet-A fuel, 18500 BTU/lb.

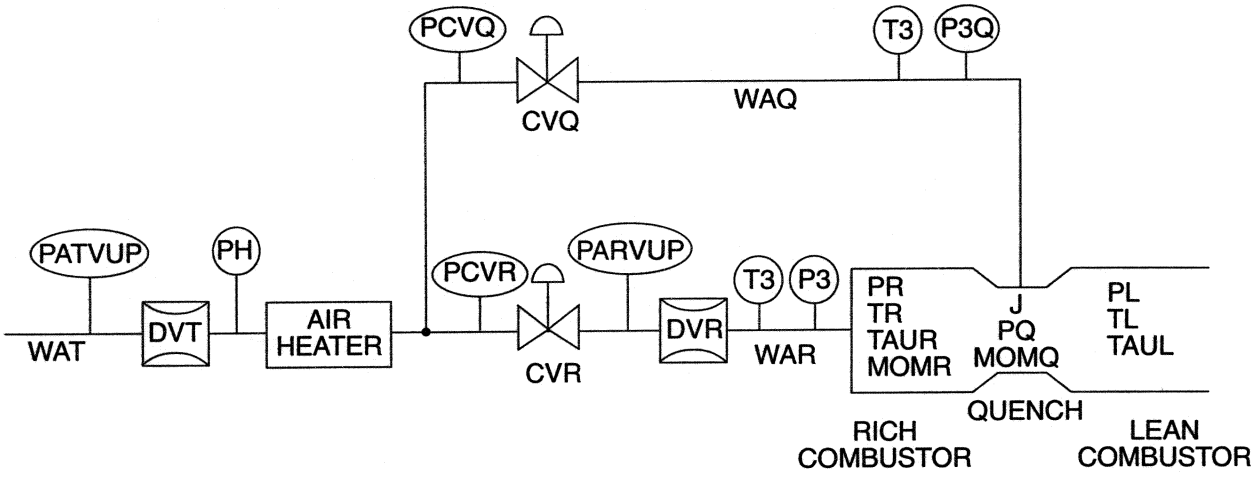

Figure IV-1 RQL Airflow Control System

NOTES: 1. DESIGN: P3 = 200 psia, T3 = 1400 F
2. COMBUSTOR SECTIONS ARE WATER COOLED WITH INTERNAL, CAST CERAMIC

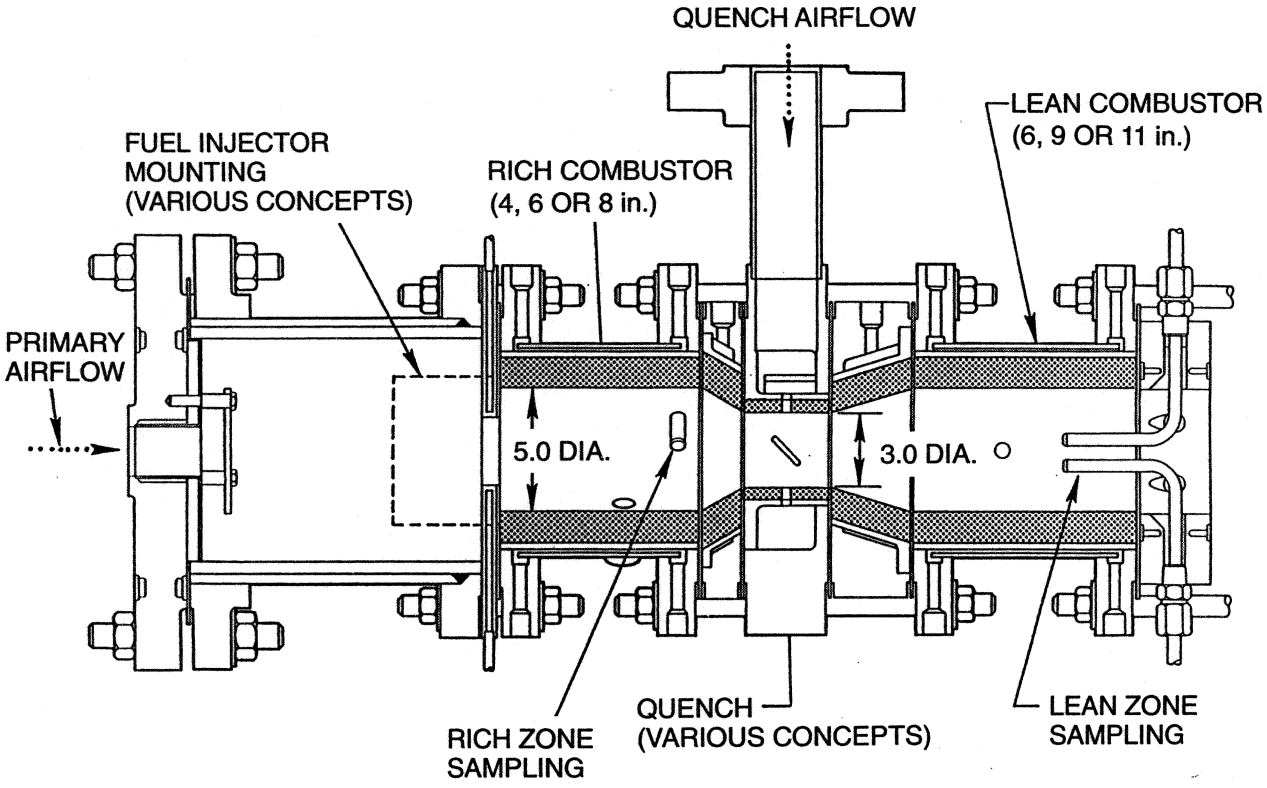

Figure IV-2 Modular RQL Combustor

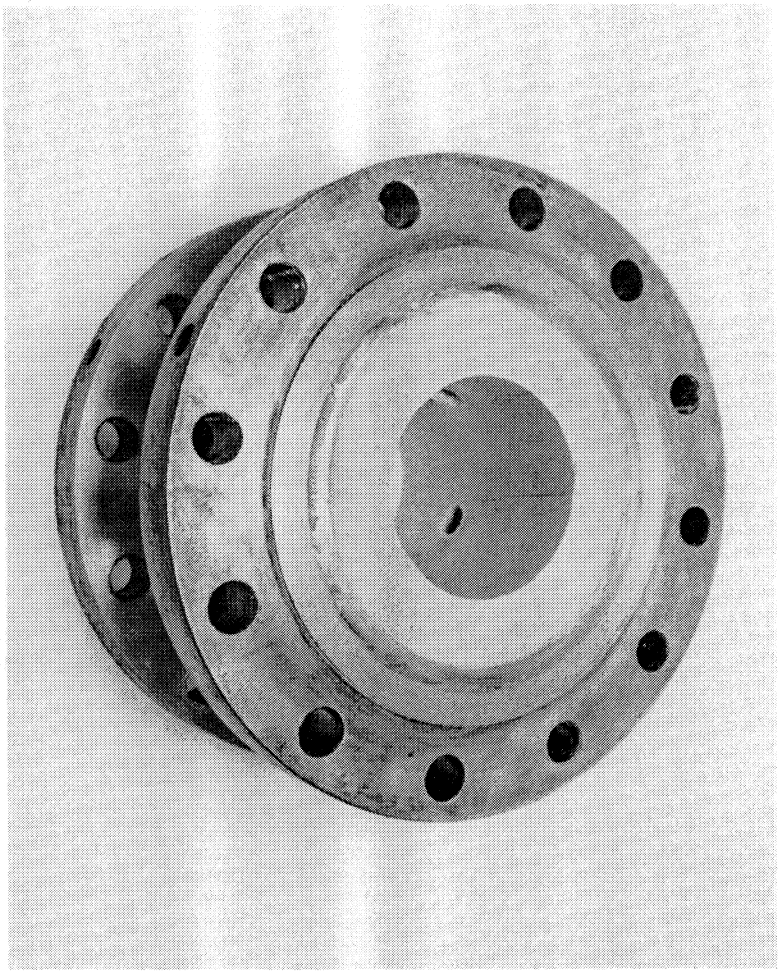

FEATURES:
- WATER-COOLED PRESSURE CONTAINMENT
- 5 IN. ID
- PENETRATIONS FOR
  - — IGNITOR
  - — DIAGNOSTICS
- REUSABLE

Figure IV-3 Ceramic Lined Cylindrical Test Section

UNCONFINED

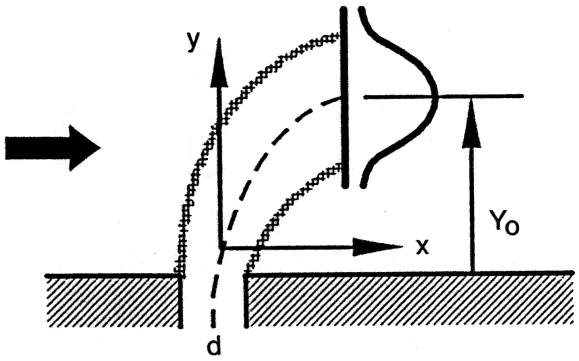

$$\frac{Y_o}{d} = K J^{1/2} \left(\frac{X}{d}\right)^{1/3}$$

CONFINED

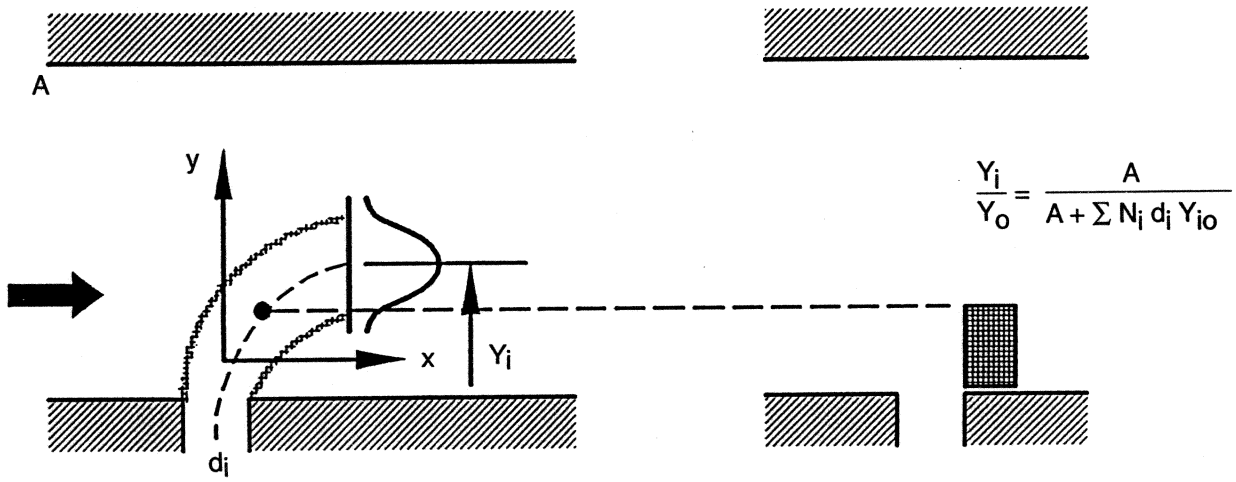

$$\frac{Y_i}{Y_o} = \frac{A}{A + \Sigma N_i d_i Y_{io}}$$

Figure IV-4 Quench Jets in Confined Flow

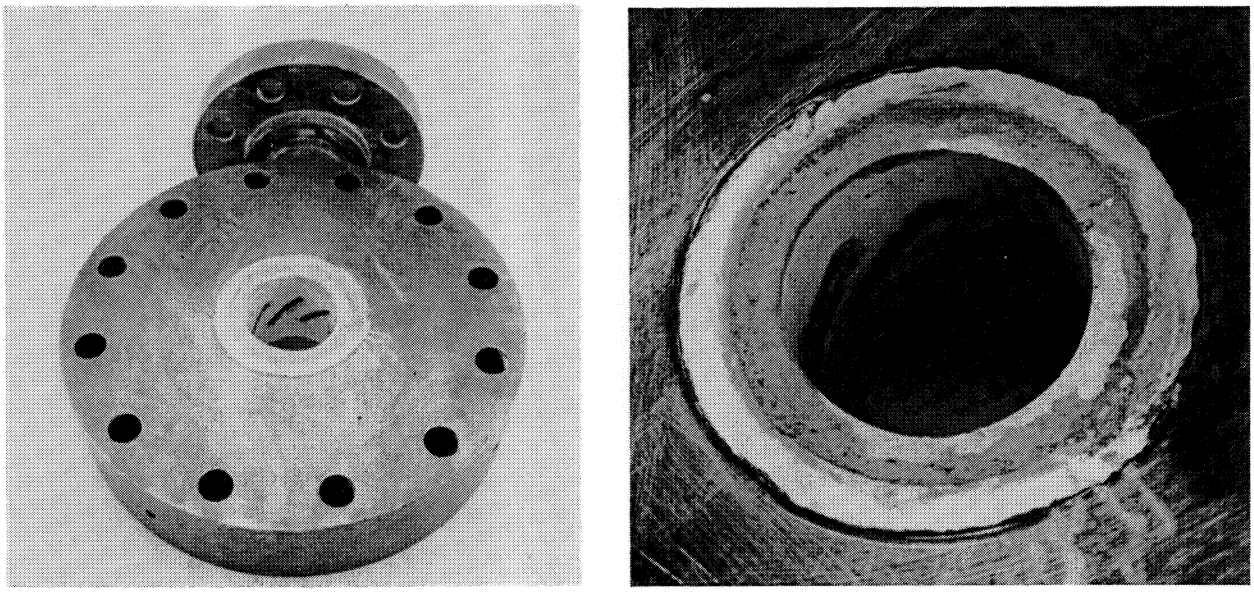

Figure IV-5 Ceramic-Lined Slanted-Slot Quench Section

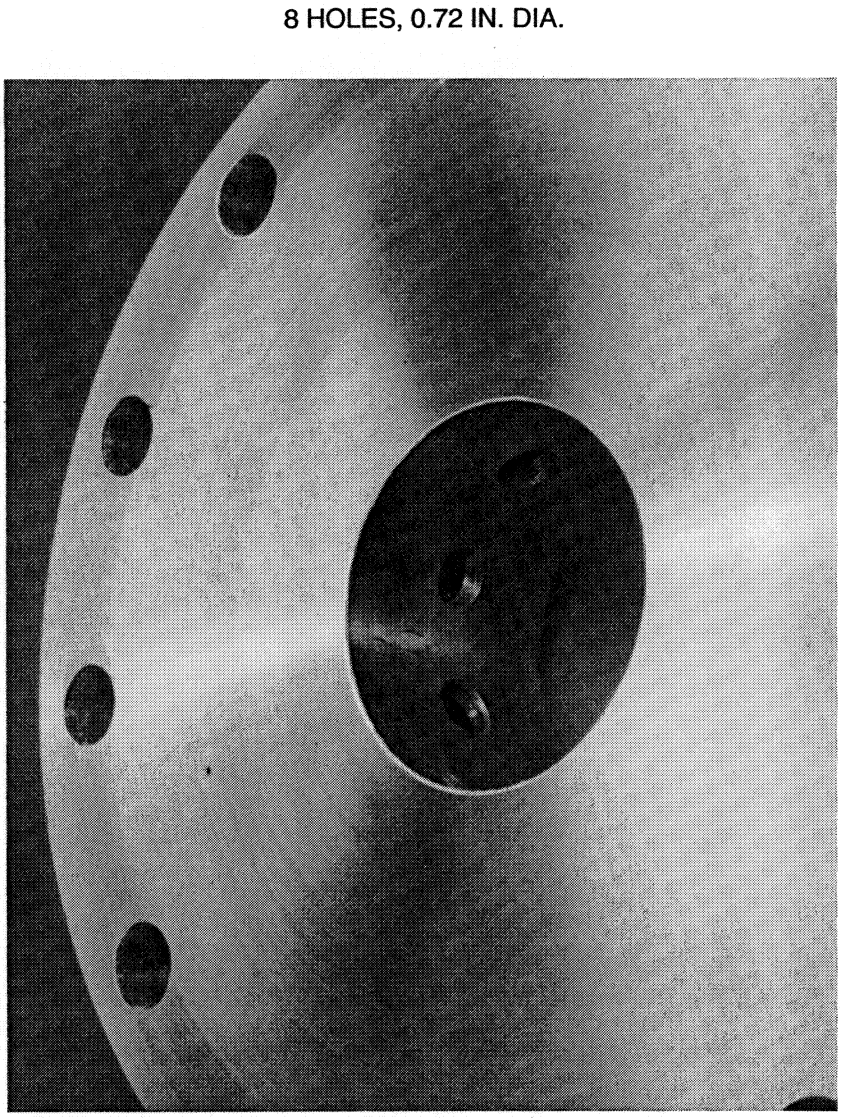

Figure IV-6 Eight Circular Hole Quench

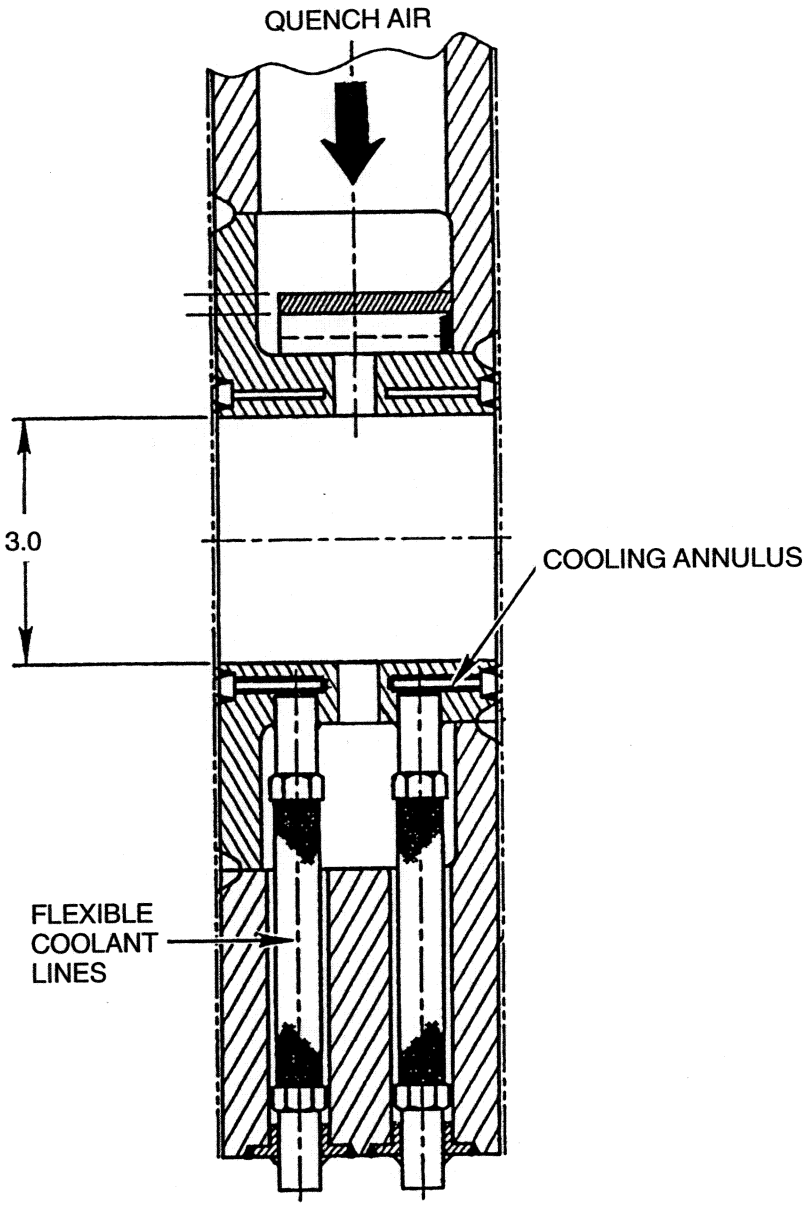

Figure IV-7 Water Cooling for Quench

8 HOLES @ 0.58 IN. DIA., 8 HOLES @ 0.29 IN. DIA., 32 HOLES @ 0.15 IN. DIA.

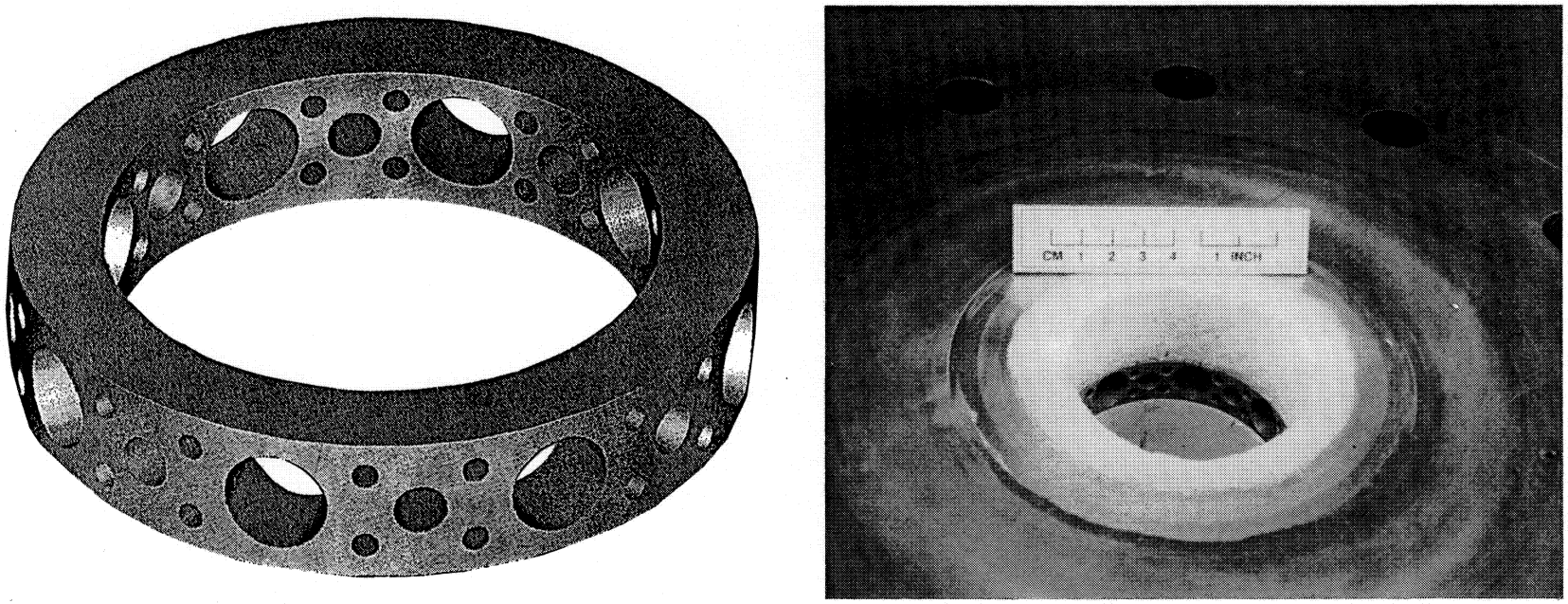

Figure IV-8 Multihole Quench

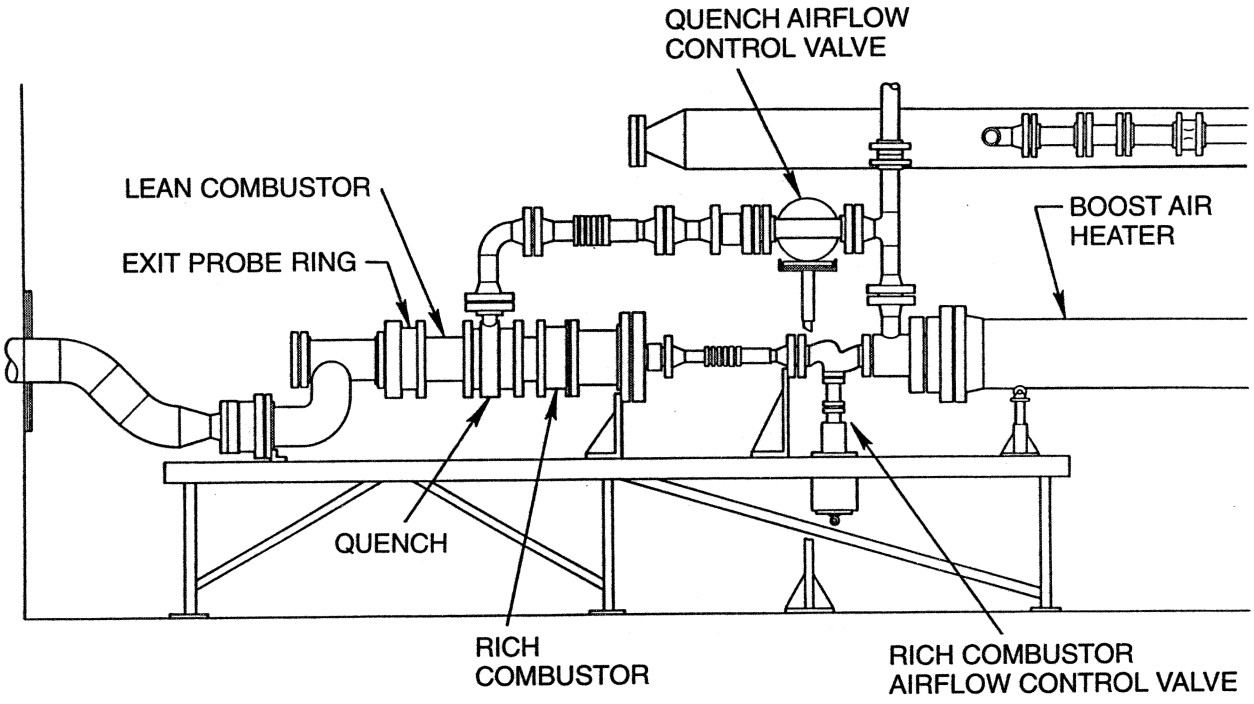

Figure IV-10 Modular RQL Combustor Installation

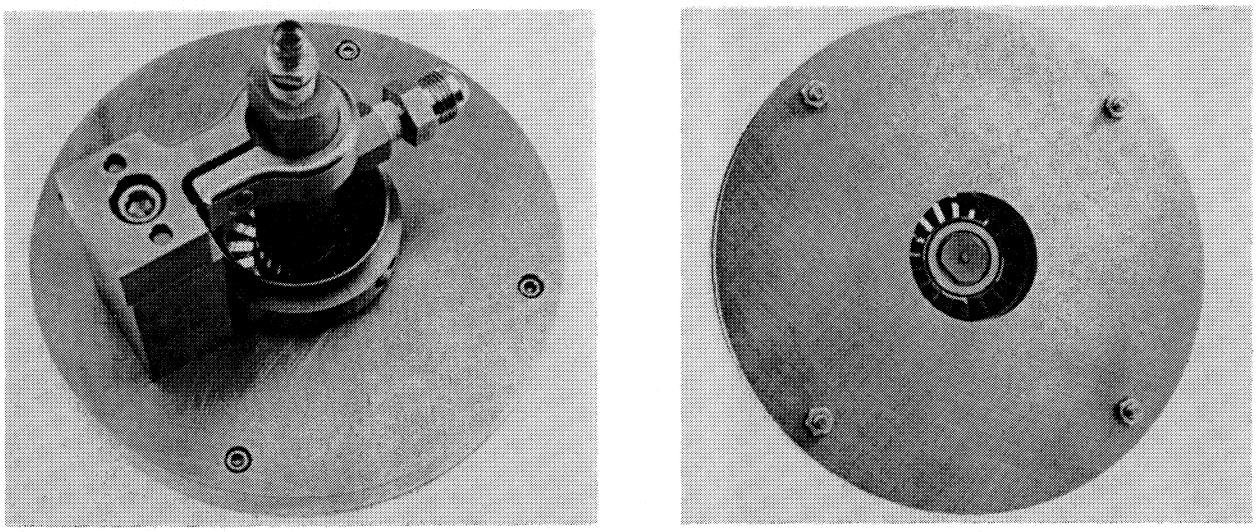

Figure IV-9 Delavan Swirl-Air Fuel Preparation

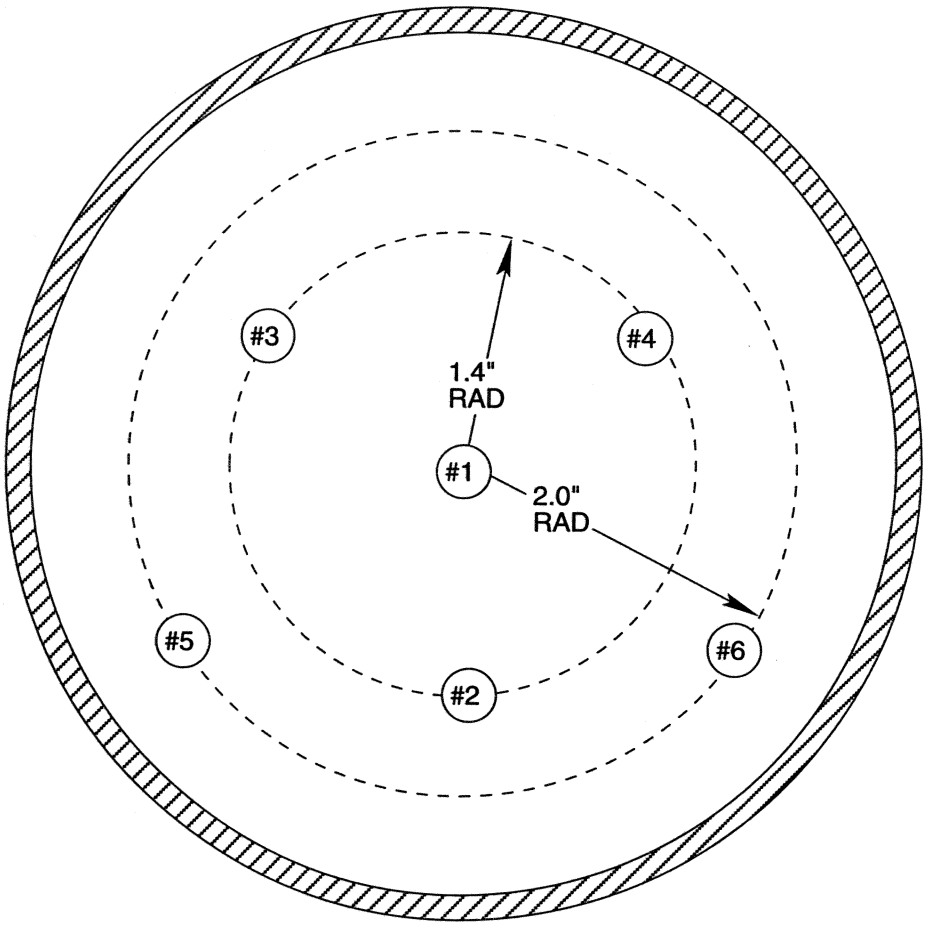

Figure IV-11 Lean Zone Probe Layout

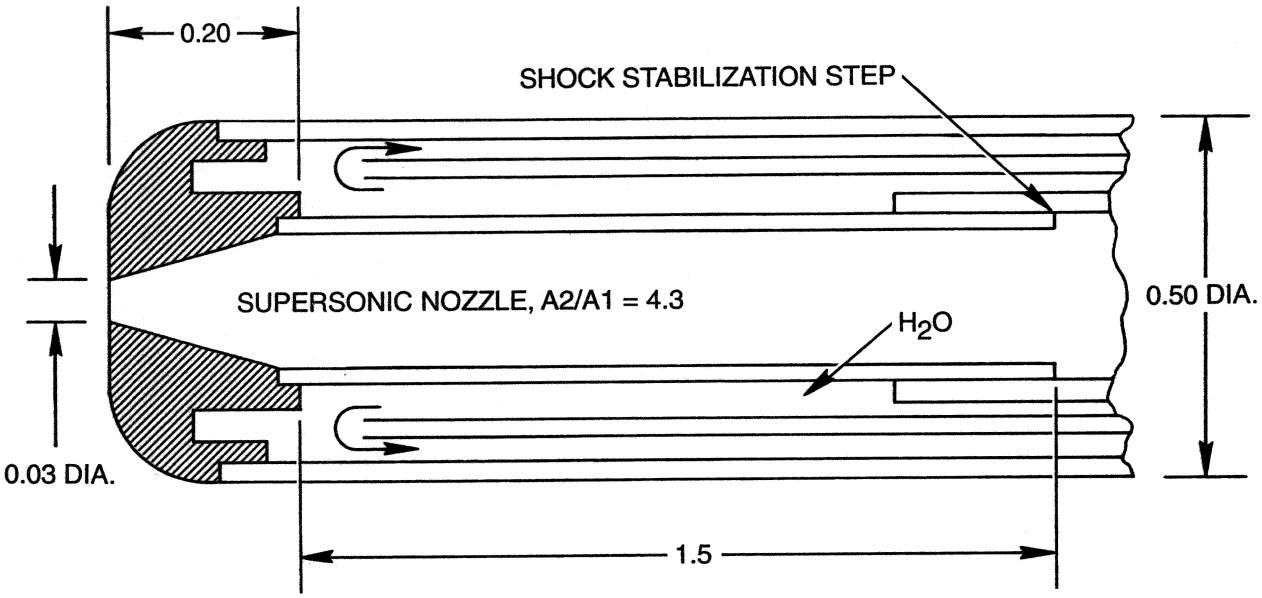

NOTE: ALL DIMENSIONS IN INCHES.

Figure IV-12 Aerodynamic-Quench Emission Probe Tip

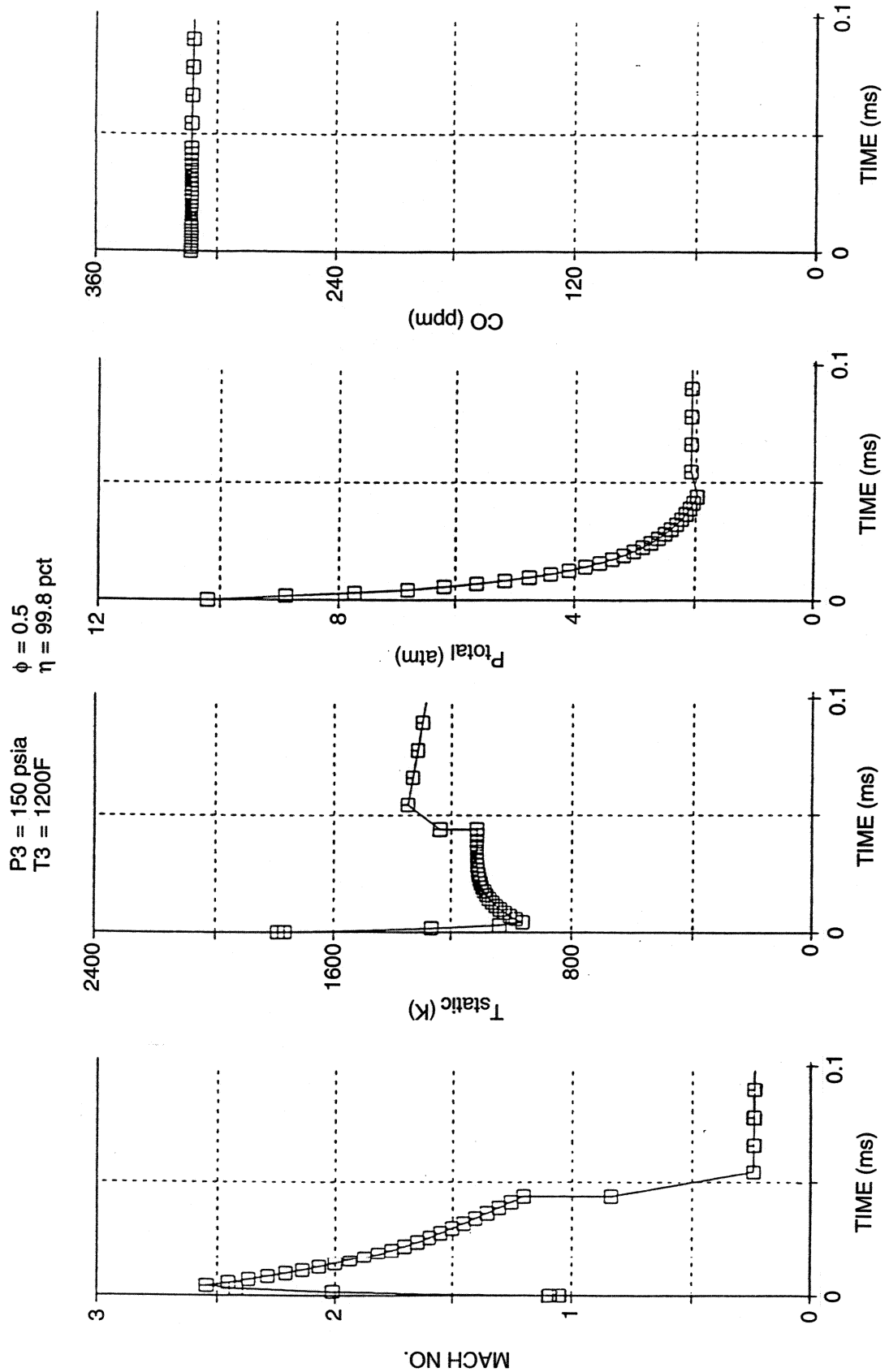

Figure IV-13 Aerodynamic Quenching of CO

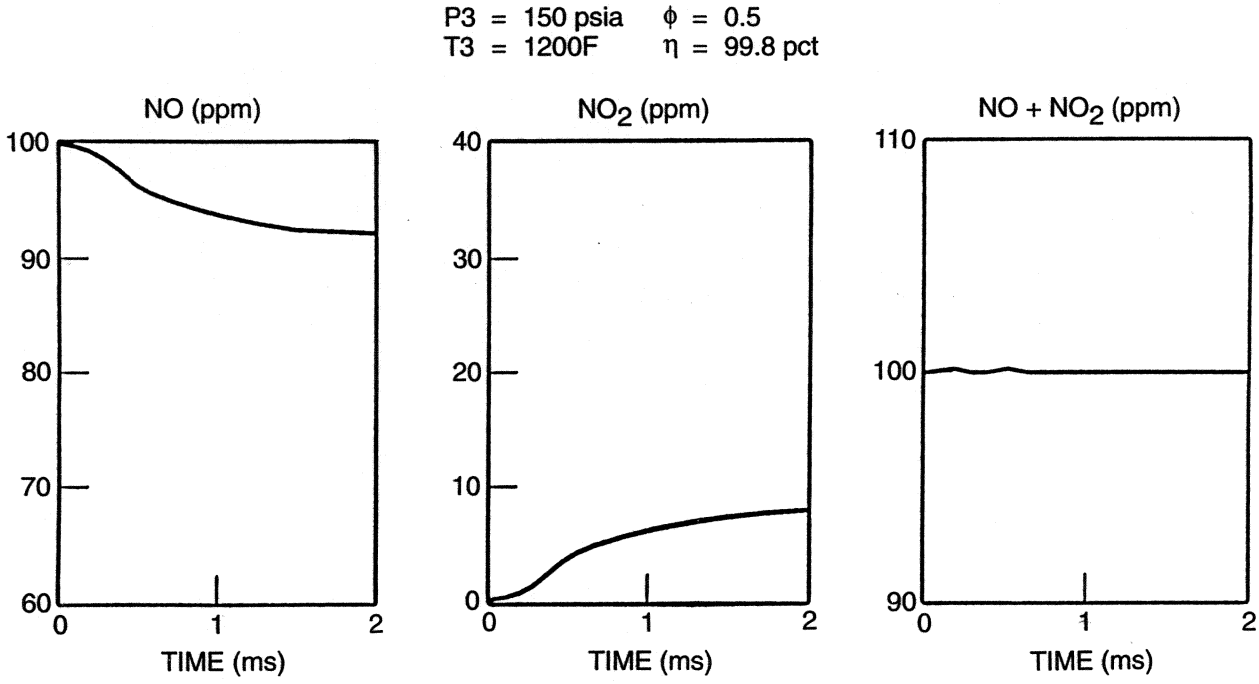

Figure IV-14 Aerodynamic Quenching of NO_x

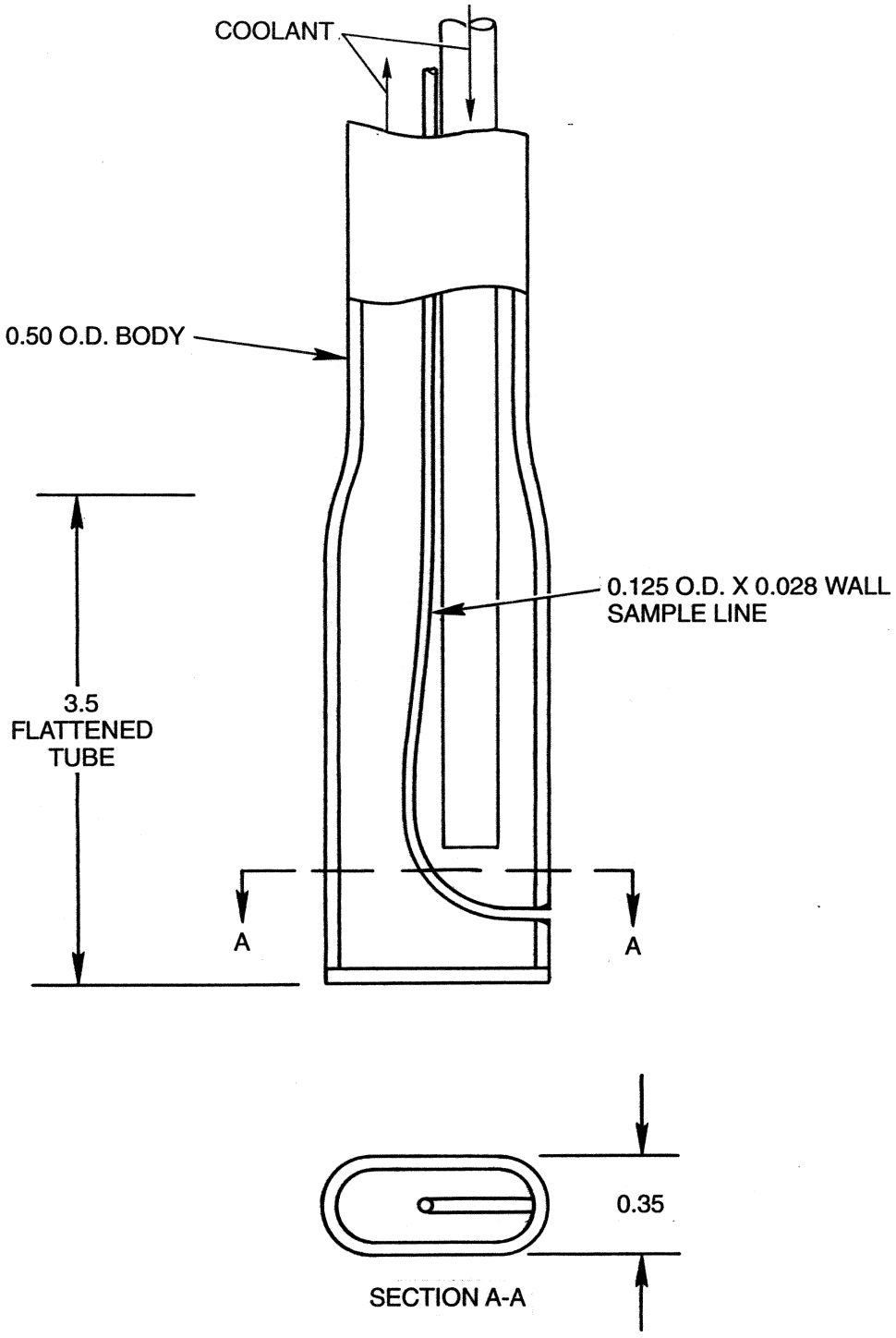

NOTE: ALL DIMENSIONS IN INCHES.

Figure IV-15 Rich Combustor Probe

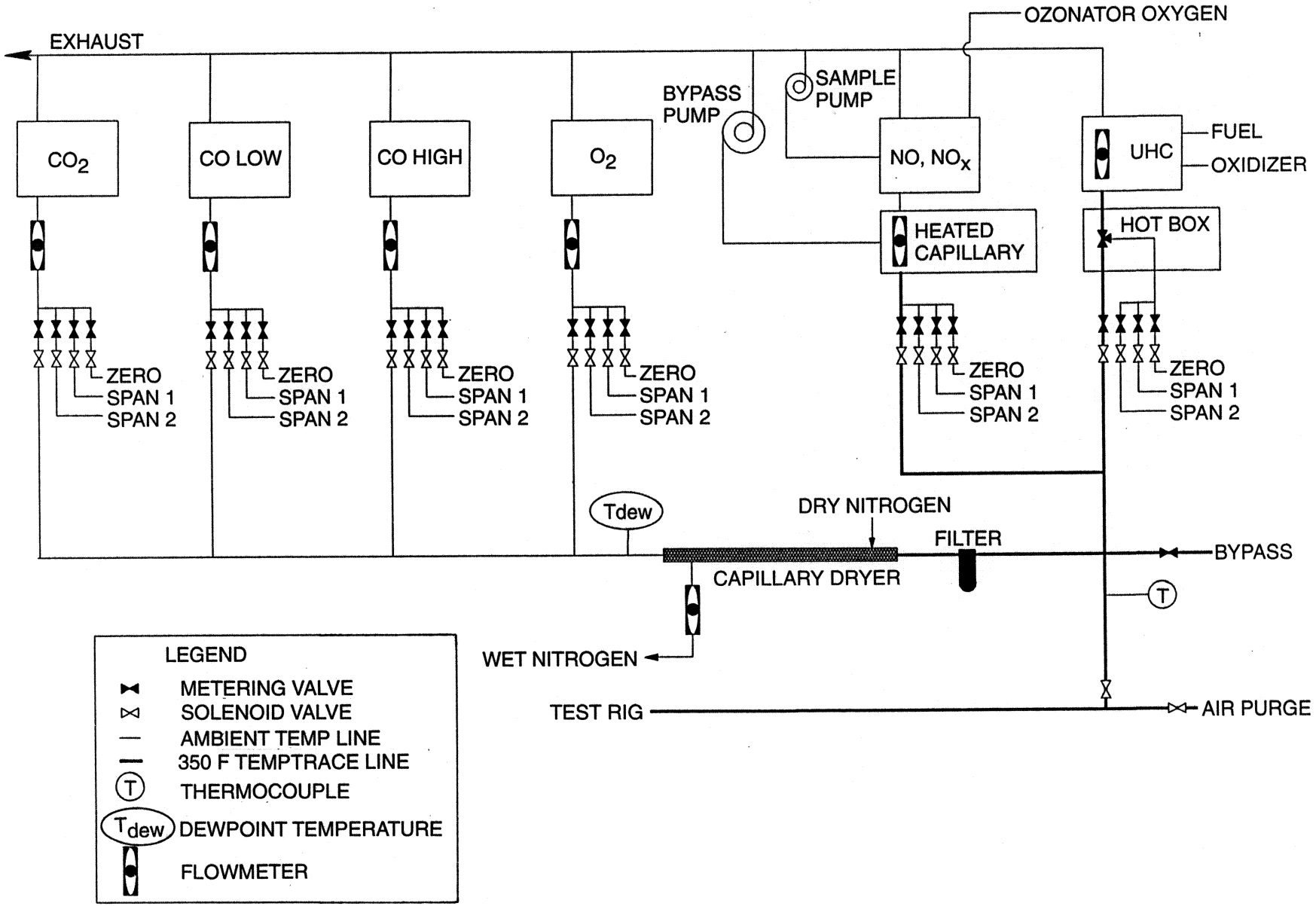

Figure IV-16 Emissions Analysis System Schematic

SECTION V SUPPORTING STUDIES

The definition of the flametube-scale RQL combustor was supported by waterflow visualization and CFD studies of the flowfield inside the combustor. The former focused at displaying the key features of the flowfield, particularly in the rich combustor, and the extent these features were altered by changes in the fuel nozzle design. The visualization also served as a reference for CFD predictions of the flowfield. Once these predictions reasonably matched the visualizations, the quality of the flow entering the quench section was assessed by limited CFD analyses. This section of the report describes each of these two supporting activities, and the manner that they affected the RQL combustor design.

Waterflow Visualization

Waterflow visualization studies were performed to provide an opportunity to directly observe the flowfield produced in a flametube-scale, cylindrical RQL combustor, and the manner that the flowfield was altered by changes in the fuel nozzle design. This study was performed using a Plexiglas model of the RQL combustor. Flow patterns in water flowing through the model were traced by either illuminating minute air bubbles in the flow or injecting dye.

Visualization Setup and Flow Conditions

The waterflow visualization study used a Plexiglas model of the cylindrical RQL combustor (Fig. V-1). The model was modular to permit the exchange of the fuel preparation device, the length of the rich combustor spool section, and the configuration of the quench mixer.

Three fuel preparation devices were evaluated. Two of them were a high airflow capacity airblast nozzle with an outer flow turning angle of either 40 deg or 65 deg; the inner flow was co-swirled with a turning angle of 50 deg. These devices represented current fuel atomization technology in a device with an effective airflow area of approximately 1 $in.^2$. As described in Section IV, this capacity was the level required to pass the rich combustor airflow at the SSC condition in the flametube-scale RQL combustor tests. As such, these nozzles represented the basis for the design of an airblast nozzle to be evaluated a subsequent study with the RQL combustor. The third fuel preparation configuration consisted of a Delavan Swirl-Air air-assist nozzle mounted in the center of an axial-flow swirler. This configuration was identical to the one described in Section IV for the flametube-scale RQL combustor. The swirler consisted of 18 curved vanes with a final turning angle of 45 deg. This swirler had an effective flow area of 0.9 $in.^2$, also suitable

for the flametube scale RQL combustor. No flow was delivered through the air-assist nozzle during the visualization tests.

The rich combustor was represented in the visualization model by 5-in dia cylindrical Plexiglas spool sections. As for the flametube-scale combustor, spool section lengths of 4, 6 or 8 in. could be used in the model.

The quench mixer design had a 3-in dia and permitted the exchange of the inner cylinder to alter the configuration of the quench jets. Since the primary purpose of the visualization study was to assess the flowfield in the rich combustor, and not to evaluate the mixing efficiency of alternative mixer designs, only two quench-jet cylinders were fabricated and their evaluation was in terms of their influence on the rich combustor flow. The two mixers replicated the eight, slanted-slot and the eight, circular-hole quench configurations.

The cylindrical model was contained in an outer rectangular box which was also filled with water to eliminate the effect of surface curvature when viewing the flowfield. The exit of the visualization waterflow consisted of a weir setup which permitted undistorted visual access upstream along the model axis. The flow was visualized by illuminating either minute air bubbles formed by cavitation in the water supply or dye injected at discrete locations using small diameter tubing. Axial or transverse planes of the model were usually illuminated by a light sheet formed by an Argon-ion laser. The images were recorded by either a video camera for playback or a still camera for greater resolution.

The water flowrate to the model was set to always achieve a fully turbulent flow. True Reynolds number matching to the flametube-scale RQL combustor at SSC conditions would require a flowrate of approximately 650 GPM. However, the facility flowrate limit was 150 GPM, and operation at this level produced pump-induced flow oscillations. Most of the visualization study was performed using bubble tracers produced at a flowrate of 100 GPM. This flowrate translated to a Reynolds number, based on the combustor diameter, of 60,000, which was considered sufficiently great to replicate the key features of the flowfield. Limited testing was performed using dye tracers at approximately half this flowrate to improve the resolution of the dye streaks. There were no noticeable differences in the flowfield structure for these two flowrates.

The total water flowrate was split between the rich combustor and the quench mixer as would be experienced during combustor operation. The reference flow split was intended to represent the SSC combustion test condition. However, since the visualization tests were isothermal, the flow split was adjusted from the SSC combustion test value to achieve the same quench jet to crossflow momentum flux ratio (J). As described in Section III:

$$J = C1 \times T3Q/TR \times (WAQ/WAR)^2 = C1 \times T3Q/TR \times (1/S - 1)^2$$

Then to achieve the same J for an isothermal flow with flow split S_{ISO}:

$$T3Q/TR \times (1/S - 1)^2 = (1/S_{ISO} - 1)^2$$

which for the SSC conditions yielded:

$$S_{ISO} = 0.33$$

The flow split was varied from this value in the visualization tests to determine its influence on the general flowfield.

Flow Visualization Results

The focus of this study was to document the key flowfield features existing in the rich combustor, and the response of them to alterations of the fuel nozzle and rich combustor length. During the study, general observations were also made for the flowfields in the quench mixer and lean combustor.

Rich Combustor Flowfield

The flowfield structure in the rich combustor was most strongly influenced by the following factors:

- Swirl strength of inlet flow
- Rich combustor length
- Fuel preparation type
- Flow split and quench-jet design

The swirl strength of the inlet flow through the fuel nozzle had the strongest effect on the flowfield. Figure V-2 is a schematic diagram of the major flow characteristics associated with the airblast fuel injector having a 65 degree outer swirler. The high swirl generated by the injector caused a vortex core to develop in the center of the spool which extended throughout the entire length. Dye injection at various locations indicated that the flow would be entrained into the vortex core only if it came close to the boundary which was located at a radius of approximately 0.5 in. Inside the vortex core, high axial velocities directed toward the quench mixer were observed.

The main flow from the nozzle exit spread radially outward at an angle of 38 deg and attached to the liner approximately 2.5 in. downstream. It then continued downstream and passed through the quench-mixing section. A

small downstream recirculation zone was present at the beginning of the converging section to the quench mixer.

Recirculation zones formed both inside and outside of the main flow near the front end of the fuel-rich combustor. A dome recirculation zone formed between the nozzle bulkhead and the main flow while a central recirculation zone formed between the main flow and the vortex core. Dye injection revealed short residence times within the vortex core and long residence times in both the dome recirculation zone and the central recirculation zone.

Figure V-3 depicts the flowfield generated by the airblast nozzle having a 40-deg outer swirler. The reduced swirl strength eliminated the presence of a vortex core. The main flow exited the fuel injector at 25 deg and there was no obvious attachment to the liner. The dome recirculation zone split into two counter rotating regions, one located very close to the injector face with the other located between the wall and the main flow. It appeared that the lack of attachment allowed more water to flow back upstream along the wall toward the dome recirculation zone. The reduced inlet flow swirl strength also decreased the size of the central recirculation zone.

The flow contraction at the entrance of the quench mixer caused the small development of a vortex core in the downstream end of the fuel-rich section for the 40-deg nozzle. However, the strength of the core was small compared to that for the 65-deg device and it did not extend the length of the fuel-rich section. A downstream recirculation zone was again present at the end of the fuel-rich section.

Changes in the rich section length only had small effects on the overall flowfield. Figure V-4 is a schematic diagram generated from tests using a 4-in. long rich section fed by an airblast nozzle having a 65-deg outer swirler. The flow structure of the dome recirculation zone, central recirculation zone, and the vortex core remained unchanged with the shortened spool, being similar in size to the 8-in. section. Again, the main flow attached to the liner approximately 2.5 in. downstream. However, because of the reduced overall length, the central recirculation zone became much closer to the downstream recirculation zone and the two zones appeared to interact. These interactions appeared as brief bursts of unsteadiness superimposed on the time-average flowfield.

Visualizations from tests conducted using the air-assist/45-deg axial flow swirler configuration closely resembled the 65-deg swirl airblast fuel nozzle (Fig. V-5). A dome recirculation zone, downstream recirculation zone, and vortex core developed in the rich section similar to those with the high swirl airblast nozzle. The vortex core extended into the recessed cavity in the front end. Flow exiting the cavity remained in the axial direction for about 0.5 in. before rapidly expanding in the radial direction at approximately 45 deg. The

main flow attached to the liner at approximately 2.5 in. from the bulkhead. Observations did not indicate the strong presence of a central recirculation zone.

Most of the visualization were conducted at the S=0.33 condition (33 percent of the flow through the fuel injector and 67 percent added in the quench-mixing section). Sensitivity studies were performed by varying the flow split over a wide entire range. Results indicated that main flow patterns in the rich section were not significantly affected when more than 20 percent of the flow was introduced through the fuel preparation device. For lower splits, a reverse flow from the quench into the rich combustor was observed and the vortex core in the downstream portion of the rich section was shifted from the centerline toward the liner. Diverting more flow from the fuel nozzle to the quench mixing section increased the residence time in the rich section, particularly in the recirculation regions.

The rich combustor flowfield features were independent of the two quench jet configurations evaluated, for equivalent values of S.

Quench Mixer Flowfield

Effective emission control from the RQL combustor relies upon achieving rapid mixing in the quench section. If mixing is to occur uniformly in this section, the vortex core that was generated in the rich section must be eliminated. Figure V-6 is a photograph showing the compression of the vortex core as it entered the convergence upstream of the quench. The vortex core remained compressed until it reached the quench slots shown in the figure. Mixing occurred and the vortex core was completely dispersed as it flowed through the diverging transition at the quench exit. Observations indicated that the diverging section played a key role in the vortex core breakup.

As expected, the flowfield characteristics in the quench-mixing section were strongly dependent upon the quench jet to crossflow momentum ratios which was changed by altering S.

Lean Combustor Flowfield

Visual observations in the lean section did not reveal any significant flow patterns except for the decay of the central recirculation zone in the first third of the section. The flow appeared well-mixed and was primarily in the axial direction. The swirl generated by the fuel nozzle interacted with the quench jets and was largely canceled. It was observed that the circular-hole quench allowed more swirl to persist than for the slanted-slot quench.

CFD Predictions

As a compliment to the water flow visualization, predictions of the flowfield established in the rich combustor of the RQL combustor were computed. The purpose of these calculations was to obtain a preliminary assessment of the flow quality entering the quench zone. In particular, it was desired to anticipate the degree of velocity and temperature uniformity at the quench inlet since all scalar mixing evaluations of alternative quench configurations have been performed with uniform profiles only. Originally, it was hoped that predictions of NOx formation in the rich and quench sections could also be accomplished. This goal was not pursued, however, when it became apparent that a practical kinetics model for the various NOx formation pathways could not be efficiently included in the CFD equation set.

The CFD predictions of the rich combustor flowfield were accomplished using FLUENT, a commercially-available solver for the Reynolds-averaged form of the Navier-Stokes equations in general curvilinear coordinates. The entire RQL water flow model was represented in the computational grid so that the downstream boundary condition could be imposed at the exit of the lean combustor. However, since the purpose of the predictions was to assess the rich combustor flowfield, the solutions were obtained assuming the flow to be axisymmetric. The flow visualization tests showed this to be a valid assumption in the rich combustor but not true once the flow entered the quench section.

The flowfield predictions were performed in two steps. First, the isothermal flow produced in the flow visualization tests was predicted to confirm that the key flow features were replicated. Initial attempts to achieve this goal were not successful. In particular, the vortex core established with the 65-deg-swirl fuel nozzle was not predicted until the turbulence representation was changed from a k-e model to an algebraic-stress model. With the former model, an eddy viscosity was computed to represent an ensemble viscous influence on all velocity components. While this model is widely used for turbulent flows, it is known to exaggerate the dissipative stresses for the tangential velocity of swirling flows. The algebraic-stress model calculated the viscous stress components individually. As a consequence, the flowfields predicted with the k-e model displayed a vortex breakdown on the flow centerline because of the high dissipation. In contrast, the flowfields predicted with the algebraic-stress model retained a vortex core along the centerline because the dissipation was less. The second step of the flowfield prediction was to activate a simple one-step combustion model to generate temperature maps within and exiting from the rich combustor. In preparation for these calculations, the thermodynamic representation of the energy release had to be modified to model the decreasing temperature-rise for increasingly rich, fuel-rich mixtures.

Figures V-7 and V-8 represent the quality of isothermal flowfield prediction achieved by the FLUENT code using the algebraic-stress turbulence model for the flametube-scale RQL combustor. Both of these flowfield predictions were achieved for a 8-in. long rich combustor and a waterflow split S = 0.33. The figures display the computed streamlines for the use of the high-swirl, 65-deg airblast fuel nozzle (Fig. V-7) and the low-swirl, 40-deg airblast fuel nozzle. The dimensions of the RQL combustor were normalized by the combustor radius (R_{max}); the radial and axial scales of the figures are not equivalent.

The predicted flowfield for the high-swirl fuel nozzle (Fig. V-7) displayed the features observed in the corresponding waterflow visualization (Fig. V-2). The center vortex core was reflected by nearly parallel streamlines throughout the rich combustor. The corner recirculation zone was predicted to have an axial extent of approximately X/Rmax = 1, equal to the 2.5-in. dimension observed in the visualization. A second, predicted recirculation zone outside of the vortex core also matched the observations. The separated zone at the beginning of the combustor exit contraction was predicted to be smaller than observed; while not displayed in the figure, it is embedded in the curvature in the outermost streamline by these CFD analyses

The predicted flowfield for the low-swirl fuel nozzle (Fig. V-8) also displayed the features observed in the flow visualization, particularly the presence of a vortex breakdown on the flow centerline. The corner recirculation extended further downstream, also as observed.

The CFD prediction of the key rich-combustor flow features observed in the waterflow visualization justified extending the analyses to combusting flow. Figures V-9 and V-10 depict predictions of the rich combustor flowfield and temperature distribution, respectively, for a simulation of the SSC condition. These predictions were obtained for an 8-in. long rich combustor, using a 40-deg airblast fuel nozzle. The flow structures for combusting and non-combusting flow were similar, with strong corner and centerline vortical structures being predicted. The temperature map indicated that the combustion process was completed by the entrance to the quench section and a relatively uniform temperature profile was present; the map suggested that these features would also be experienced for a shorter, 4-in. long rich combustor.

Supporting Studies Summary

Waterflow visualization and CFD studies were performed to support the definition of components of the flametube-scale RQL combustor, and to anticipate the combusting flow features that would be achieved. The waterflow visualization study illustrated the key flow structures in the rich combustor, and their response to changes in the swirl strength of the fuel

nozzle. Both low and high swirl strength nozzles produced steady vortical regions suitable to stabilize the combusting flow. These regions were present for either a shorter (4-in.) or longer (8-in.) combustor length. They were present for a wide variation in the flow split, S, and independent of the specific configuration of the quench jets. CFD predictions replicated the observed rich combustor flow features with the use of an algebraic-stress turbulence model. Combusting flow predictions indicated that a stabilizing flowfield and a near-uniform temperature profile would enter the quench section for 4-in. to 8-in. long combustors.

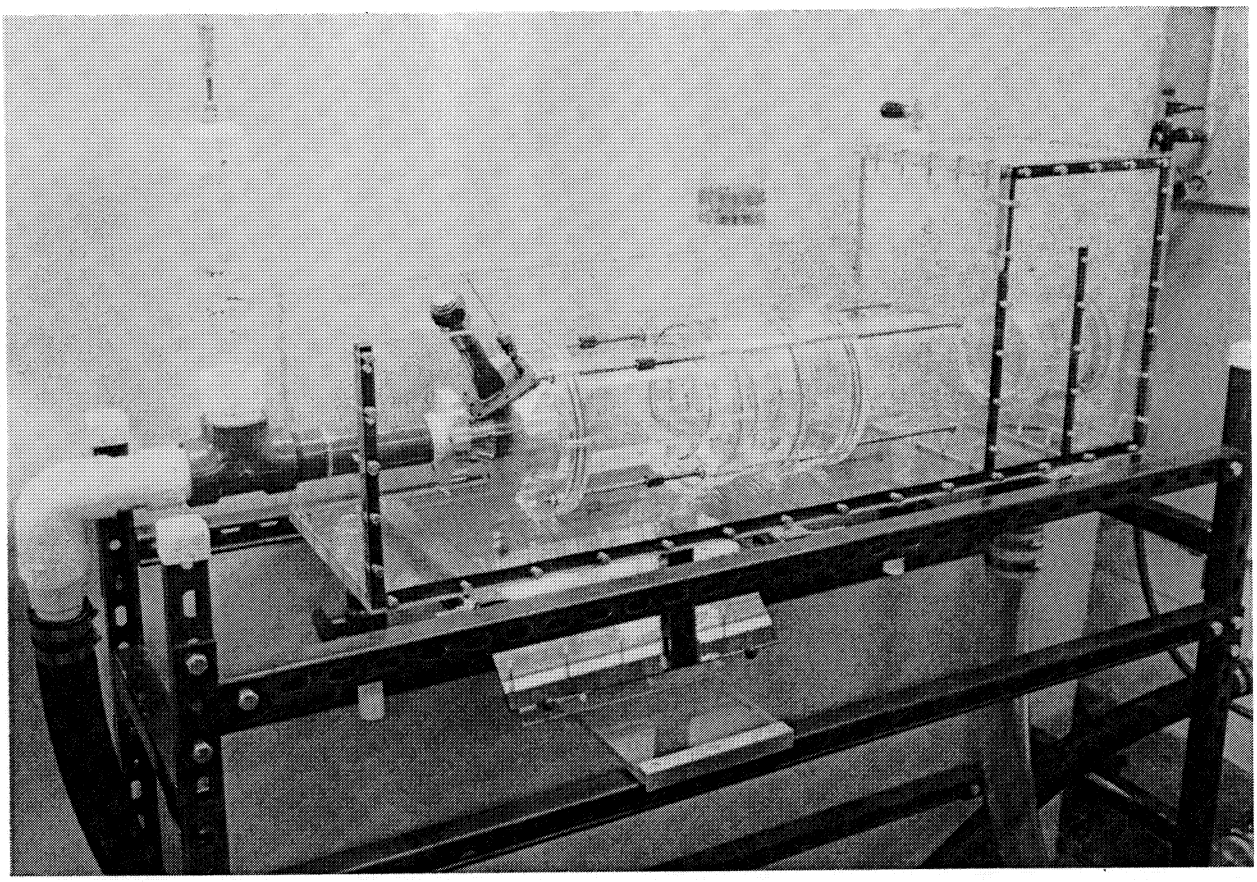

Figure V-1 RQL Combustor Flow Visualization

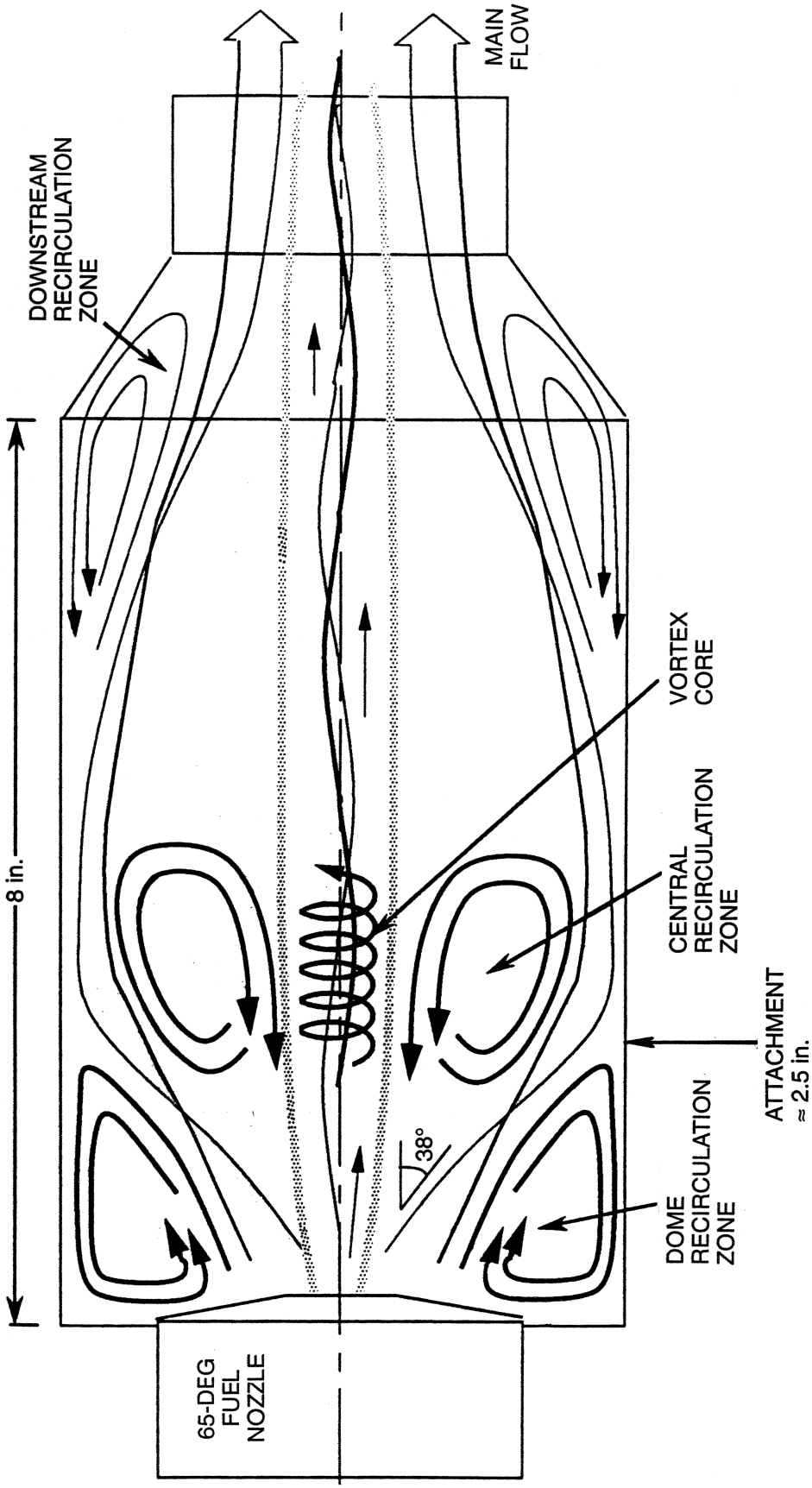

Figure V-2 Flow Structure in 8-in. Long Rich Combustor Using High-Swirl Airblast Nozzle

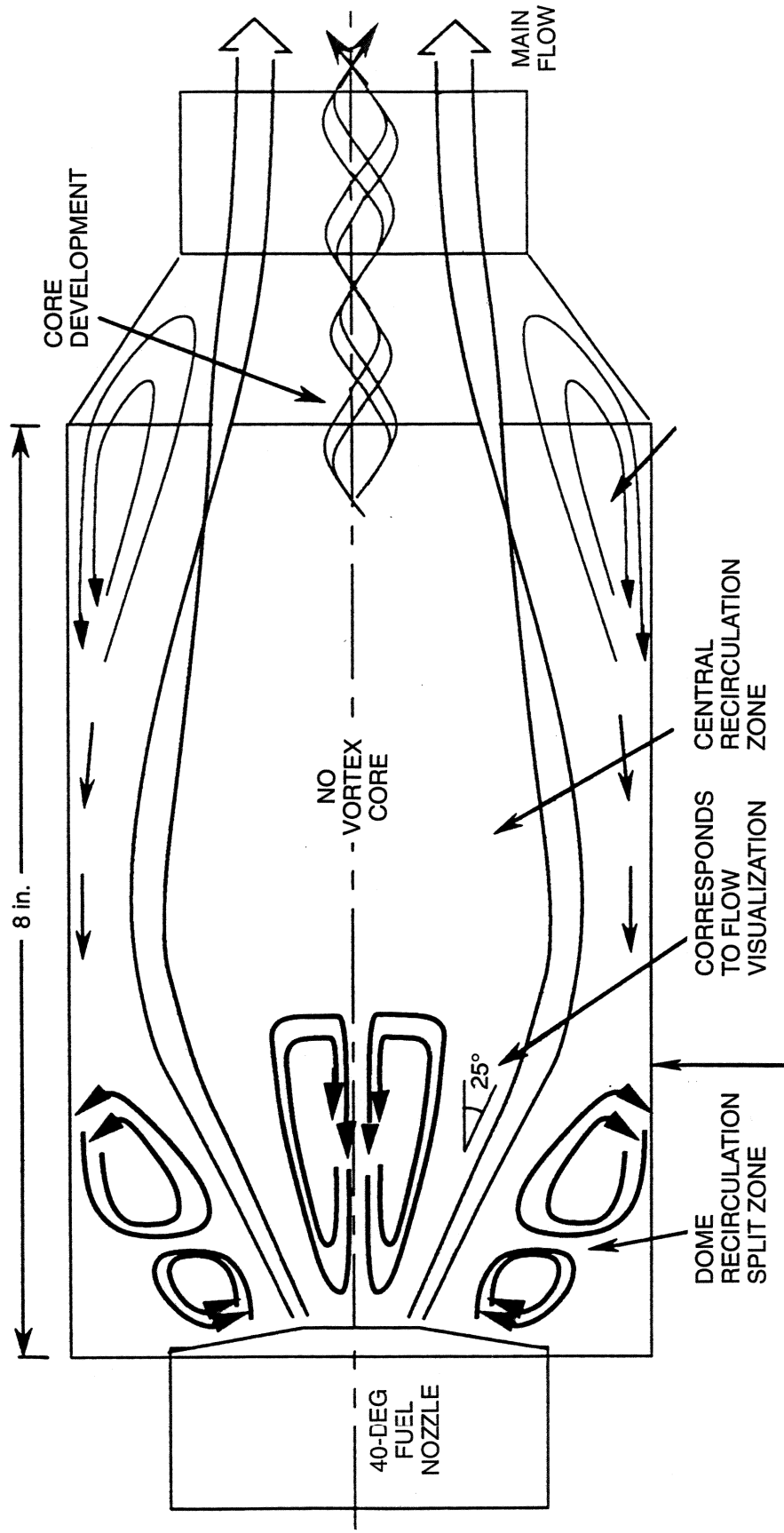

Figure V-3 Flow Structure in 8-in. Long Rich Combustor Using Low-Swirl Airblast Nozzle

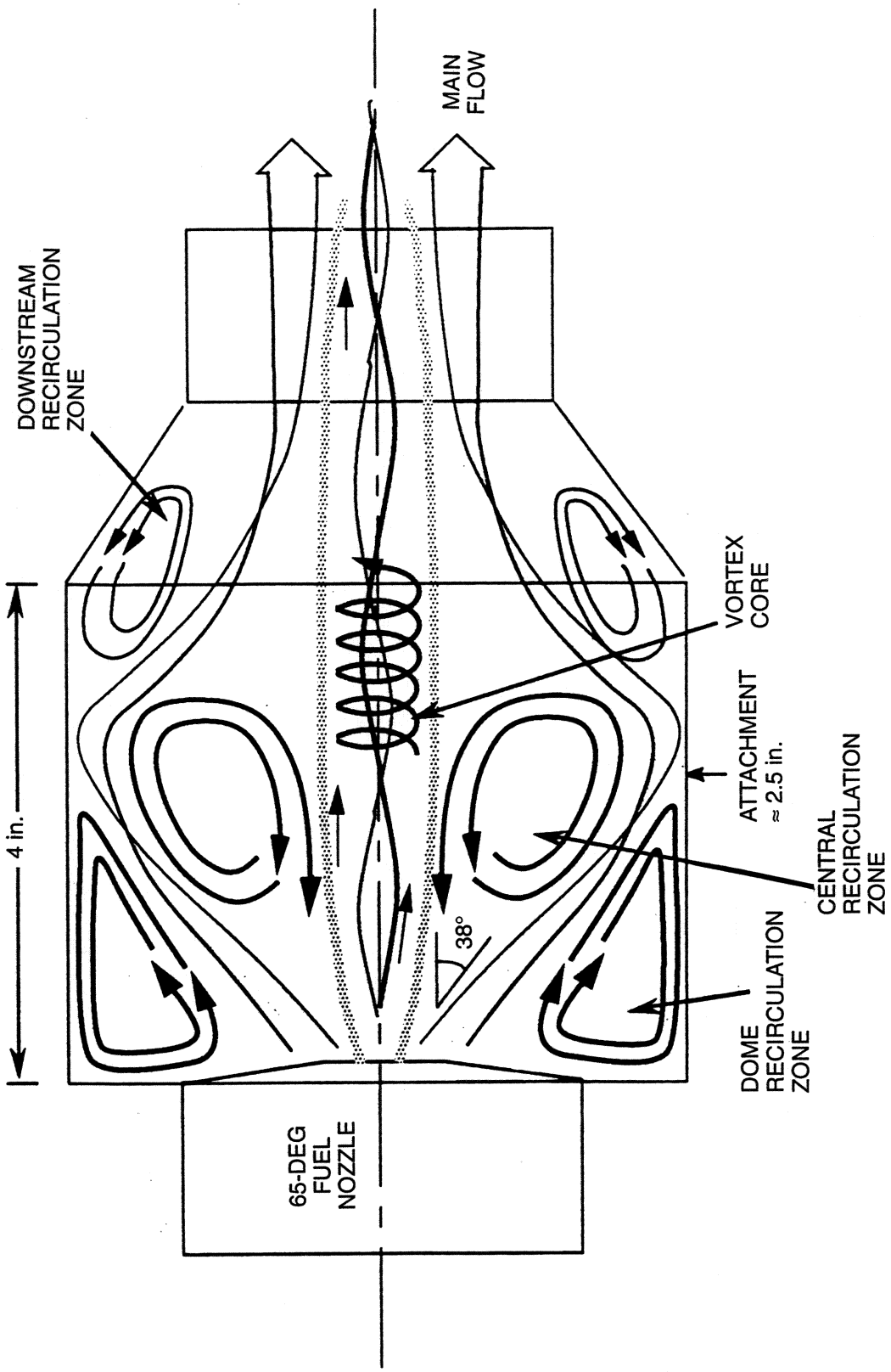

Figure V-4 Flow Structure in 4-in. Long Rich Combustor Using High-Swirl Airblast Nozzle

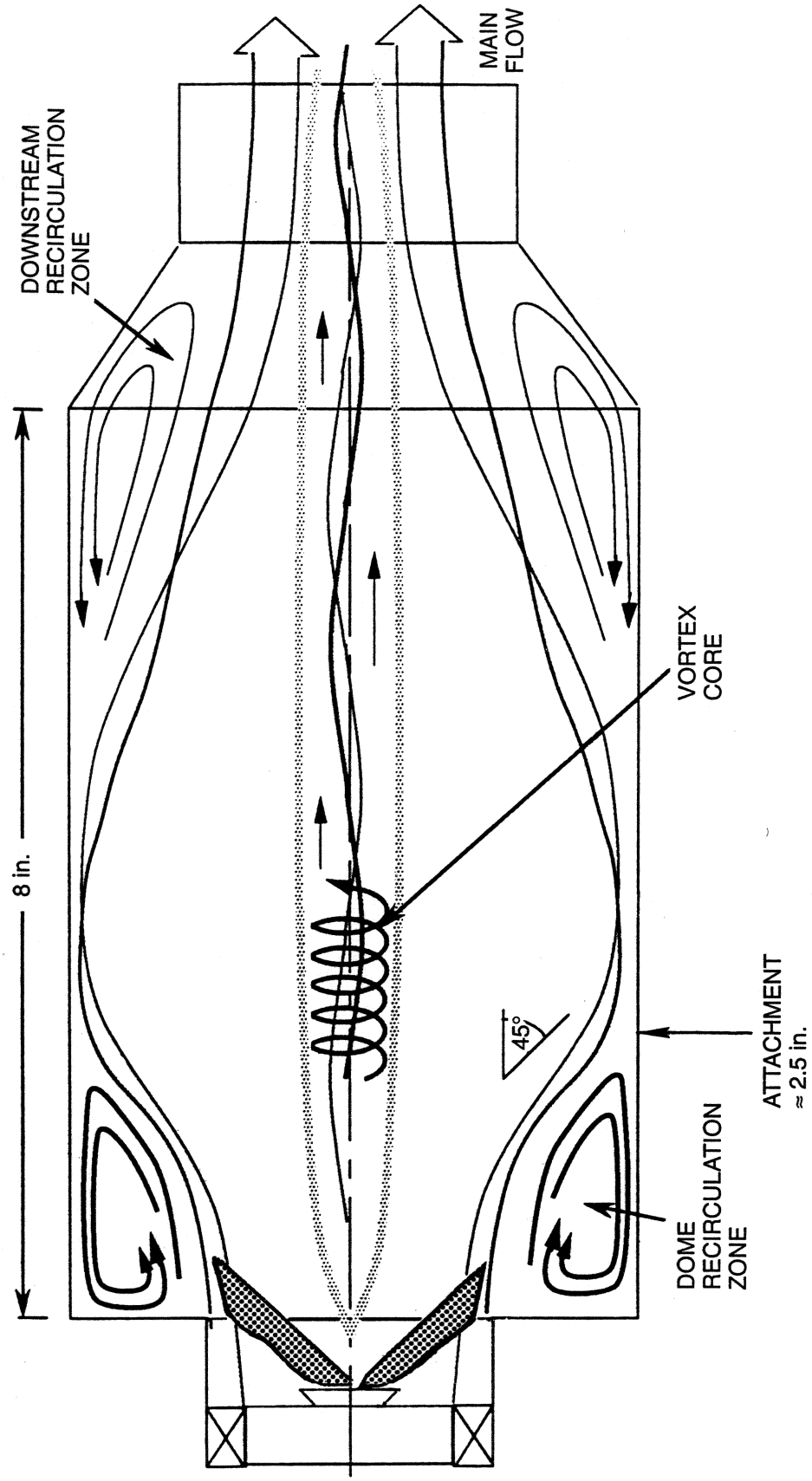

Figure V-5 Flow Structure in 8-in. Long Rich Combustor Using Delavan/45-Deg Swirler

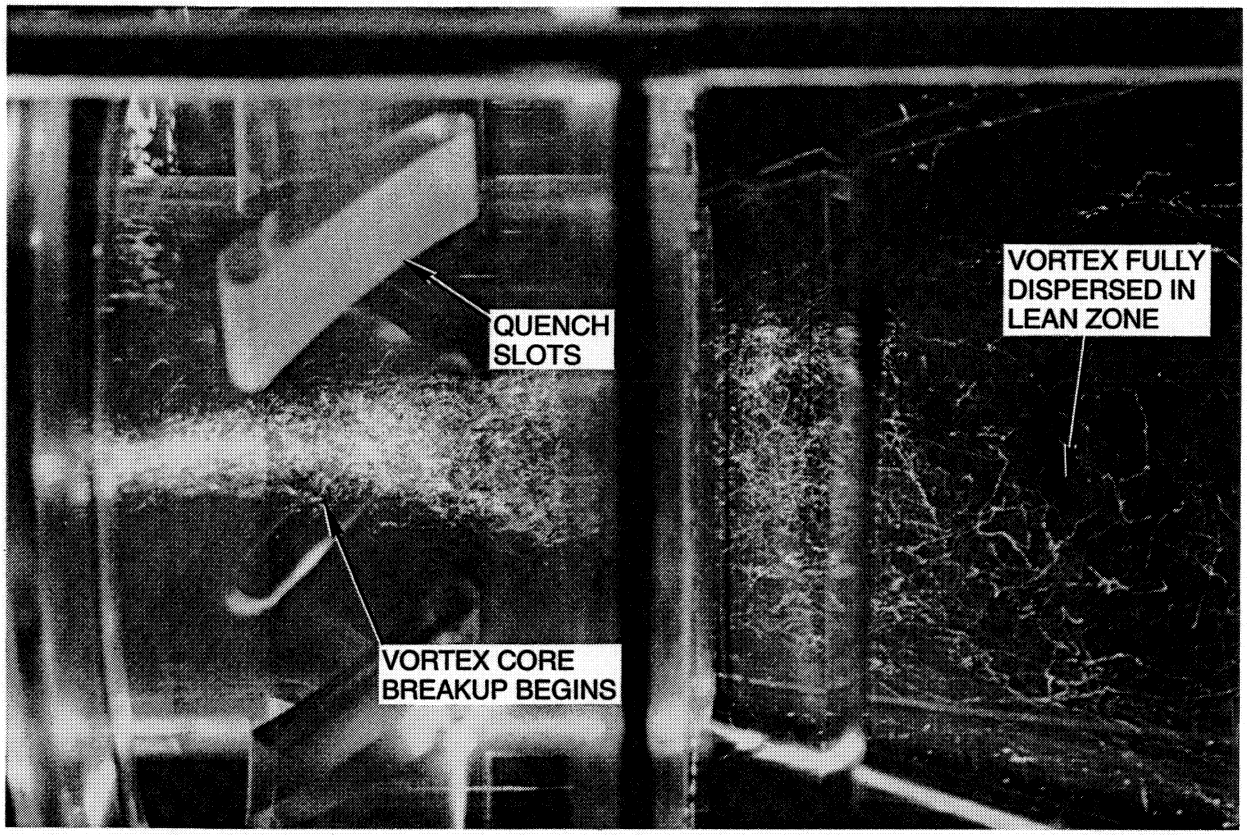

Figure V-6 Breakup of Vortex Core by Quench Flow Through Slots

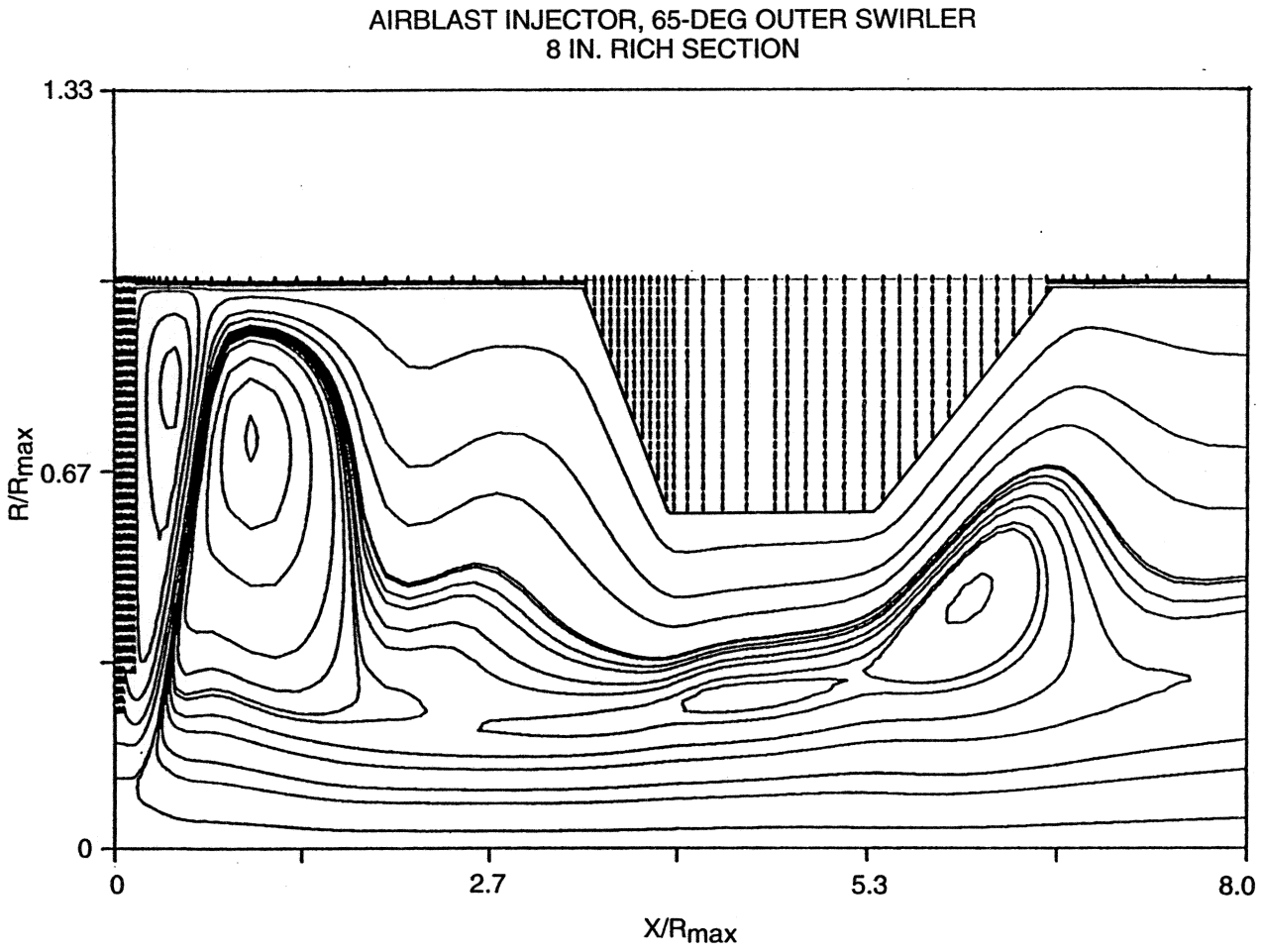

Figure V-7 Predicted High-Swirl Stream Function Contours

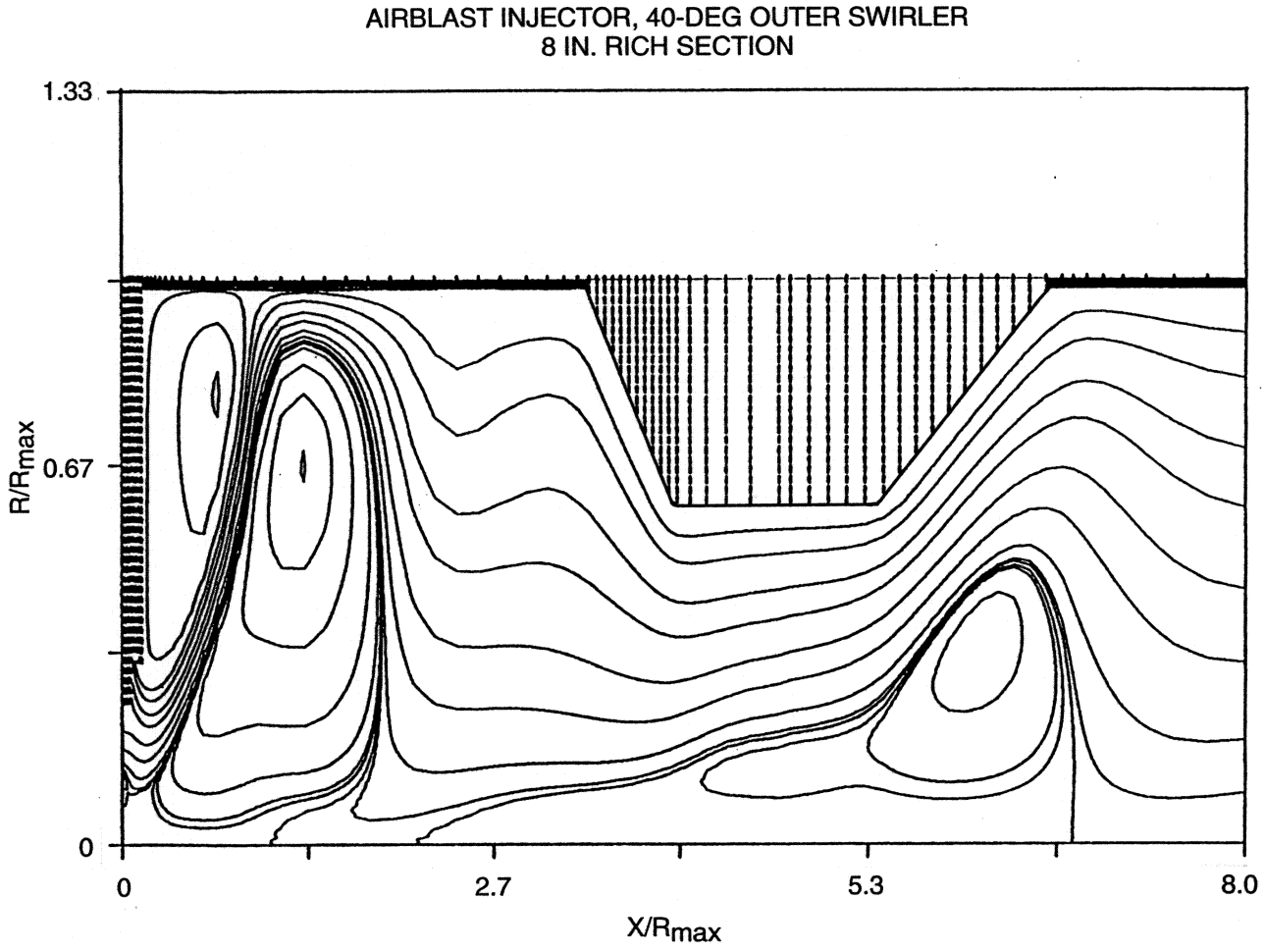

Figure V-8 Predicted Low-Swirl Stream Function Contours

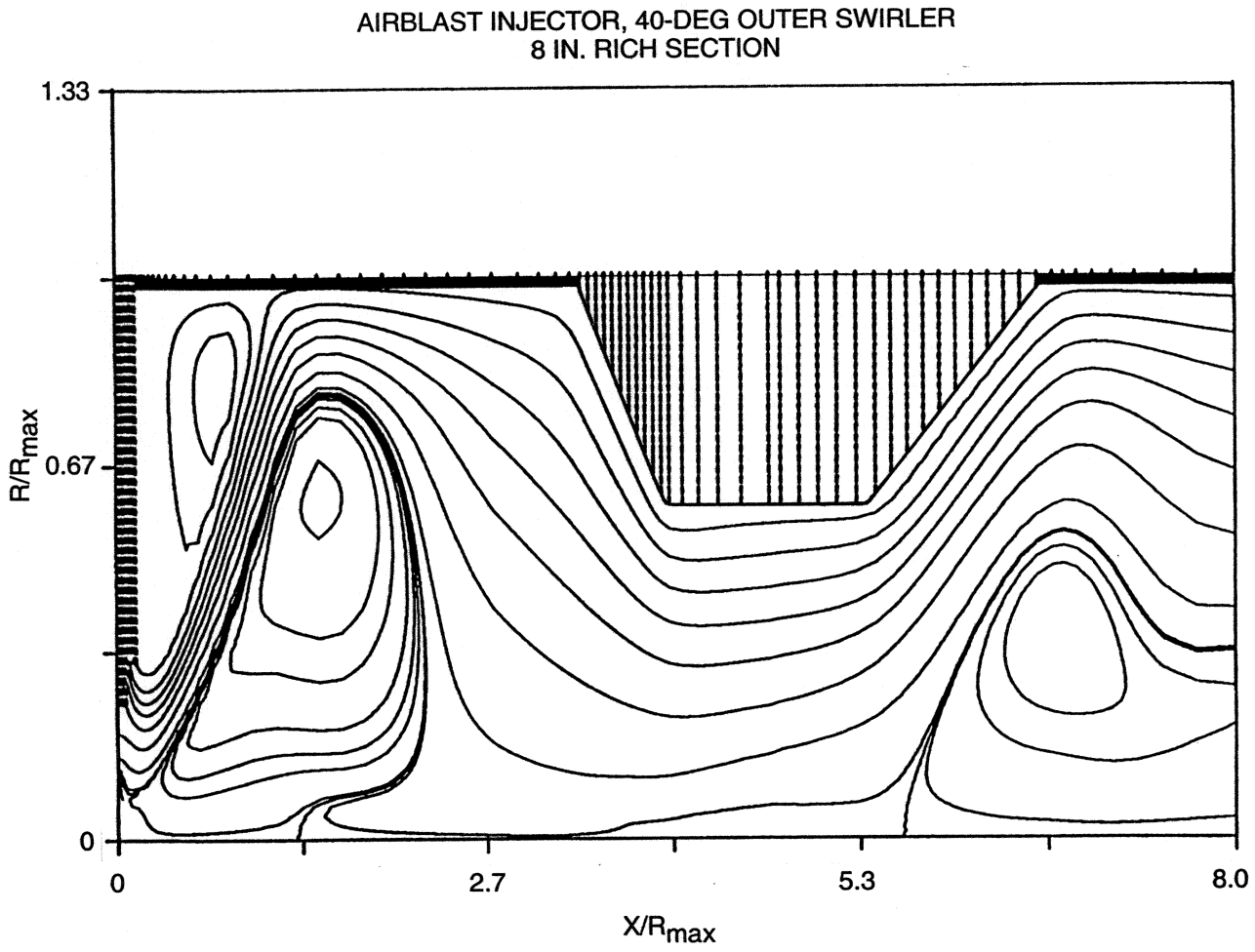

Figure V-9 Predicted Reacting-Flow Stream Function Contours

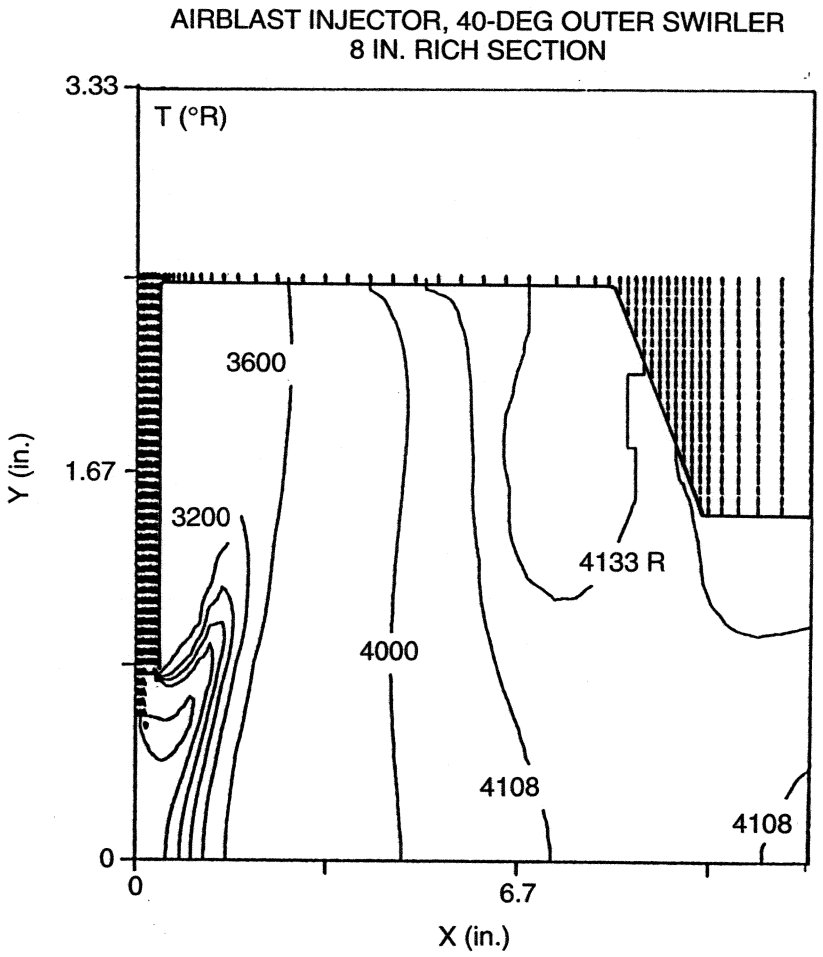

Figure V-10 Predicted Reacting-Flow Isotherms in Rich Combustor

SECTION VI RQL COMBUSTION TEST RESULTS

Combustion tests were performed using the flametube-scale RQL combustor described in Section IV to assess its performance and emissions control characteristics. Tests were performed at HSCT engine cycle operating conditions and at parametric variations from them. The test variables also included geometrical variations to achieve different residence times in the rich and lean combustors, and variations in the quench-jet configuration. The primary data were analyses of emissions samples extracted from the exit of the lean combustor; limited analyses of samples from the exit of the rich combustor or the quench section were also performed. This section of the report presents and interprets the data acquired in these tests.

Combustion Test Conditions

HSCT Engine Cycle Conditions

Combustion tests were performed at conditions representing one HSCT engine cycle. The chosen cycle corresponded to a Turbine Bypass Engine configuration since it imposed the most severe range of combustor operating conditions; they are listed in Table VI-1. However, to satisfy maximum values for either test facility total airflow heating or flametube-scale combustor pressure, some of them were pressure-scaled from these actual cycle conditions; actual test conditions are given on each data plot. The first five conditions correspond to those used to calculate the EPAP for supersonic aircraft as defined in Section II. The value for ØR is not specified in this table because its value depends on the part-power control strategy established for the RQL combustor. As stated previously, ØR = 1.8 was the design condition for SSC. Data were acquired at various ØR at other cycle conditions to establish the preferred control strategy.

Table VI-1 HSCT Combustor Cycle Conditions

Condition	P3	T3	F/AOA	UREF
	psia	F	---	ft/s
Idle	67	425	0.0090	70
15 pct	103	524	0.0090	76
34 pct	165	653	0.0112	78
65 pct	239	790	0.0175	78
Sea-Level Takeoff (SLTO)	264	819	0.0373	67
Subsonic Climb (SuCl)	104	667	0.0402	59
Supersonic Cruise (SSC)	150	1200	0.0300	90
Subsonic Cruise (SuC)	92	635	0.0139	75
Supersonic Climb (SSCl)	207	1250	0.0318	88

Many of the combustion tests focused at RLQ combustor performance and emissions control at the SSC condition. In addition to the true SSC condition defined above, tests were also performed at a scaled-SSC (S-SSC) condition based on T3 = 850 F. This condition was used for initial combustion tests and other intermittent test periods when the boost air heater required to achieve T3 = 1200 F was not operational. The S-SSC condition was defined in the manner described below for parametric variations of T3. Generally, the flametube-scale RQL combustor contained 8-in. long cylindrical rich and lean combustors; studies of the influence of residence time in each combustor led to length reductions in both.

Parametric Test Conditions

Four types of parametric variations from a cycle condition were studied:

- Air-assist level (WAA)
- Inlet air pressure (P3)
- Inlet air temperature (T3)
- Rich combustor equivalence ratio (ØR)

As discussed in Section IV, the RQL combustor can be very interactive, with variations in one parameter causing a significant change in other important features of the combustor. Such an interaction was not expected for the parametric variations in WAA or P3, but was recognized for variations in either T3 or ØR.

Air-Assist Parametric

Parametric variations in the air-assist flowrate to the fuel nozzle were performed to alter the atomization quality of the fuel. The assist air flowrate was nearly equal to the fuel flowrate in all cases, being approximately 3 pct of the total airflow or 12 pct of the rich combustor airflow. The variation from these values had less than a 5 pct effect on the combustor residence times and J.

Inlet Air Pressure Parametric

Parametric variations on the combustor inlet pressure were performed to assess the pressure-scaling influences on the performance and emissions control of the RQL combustor. For these tests, the combustor air flowrate was scaled to P3 to preserve UREF. Table VI-2 presents a P3 variation from the SSC and S-SSC conditions. In all cases, the rich and lean combustor residence times and J matched the SSC condition.

Table VI-2 P3 Variation from SSC and S-SSC

Parameter	Unit	SSC	P3-1	P3-2	S-SSC	P3-4	P3-5
P3	psia	150	100	75	119	150	90
T3	F	1200	1200	1200	850	850	850
ØR	---	1.8	1.8	1.8	1.8	1.8	1.8
F/AOA	---	0.030	0.030	0.030	0.028	0.028	0.028
UREF	ft/s	90	90	90	90	90	90
S	---	0.243	0.243	0.243	0.227	0.227	0.227
TR	F	3400	3400	3400	3180	3180	3180
TAUR	msec	13	13	13	11	11	11
J	---	22	22	22	22	22	22
TL	F	2870	2870	2870	2470	2470	2470
TAUL	msec	4.3	4.3	4.3	3.9	3.9	3.9

Inlet Air Temperature Parametric

Parametric variations on the combustor inlet temperature were performed to assess its influence on the performance and emissions control of the RQL combustor. These variations were expected to alter both the effectiveness of the quenching process and the ability of the lean combustor to consume CO while controlling NOx production. However, analyses of parametric variations in T3 resulted in consequent variations in both the rich and lean combustor residence times, and in the quench jet momentum flux ratio. The possible means to control these variations are illustrated in Table VI-3. The third column represents the SSC condition, with the subsequent columns displaying the effects of a T3 reduction alone, a combined T3 and F/AOA reduction, and a combined T3, F/AOA, and P3 reduction, respectively.

For a fixed airflow split, a reduction in T3 lowered the combustor temperatures. In the rich combustor, the momentum of the flow entering the quench increased. As a consequence, J reduced; in the table it reduced by 18 pct. As the lean combustor temperature reduced, it extended the lean residence time; in the table it increased by 12 pct. Both of these influences reflected the lower reference velocity for a T3 reduction alone.

A combined reduction in T3 and F/AOA altered the combustor temperature and the airflow split for a fixed ØR as shown in the table. However, while the value for J at the SSC condition was matched, the rich and lean residence times were extended by 15 pct and 16 pct, respectively. Again, this reflected the reduction in UREF.

Table VI-3 Alternative T3 Variation Strategies

Parameter	Unit	SSC	Reduced T3 Alone	Reduced T3 and F/AOA	Reduced T3, P3, F/AOA,
P3	psia	150	150	150	119
T3	F	1200	850	850	850
ØR	---	1.8	1.8	1.8	1.8
F/AOA	---	0.030	0.030	0.028	0.028
UREF	ft/s	90	71	71	90
S	---	0.243	0.243	0.227	0.227
TR	F	3400	3180	3180	3180
TAUR	msec	13	14	15	11
J	---	22	18	22	22
TL	F	2870	2580	2470	2470
TAUL	msec	4.3	4.8	5.0	3.9

The addition of a P3 reduction to the T3 and F/AOA combination achieved a better match of J, TAUR, and TAUL to the SSC condition; UREF was matched. Using this strategy, a series of test conditions were defined to achieve a range of T3 variations from the SSC condition as shown in Table VI-4. The S-SSC condition was defined by this strategy for a T3 = 850 F.

Table VI-4 T3 Variation from SSC

Parameter	Unit	SSC	T3-1	T3-2 S-SSC	T3-3	T3-4
P3	psia	150	109	119	132	141
T3	F	1200	750	850	1000	1100
ØR	---	1.8	1.8	1.8	1.8	1.8
F/AOA	---	0.030	0.028	0.028	0.029	0.029
UREF	ft/s	90	90	90	90	90
S	---	0.243	0.223	0.227	0.235	0.235
TR	F	3400	3120	3180	3280	3340
TAUR	msec	13	11	11	12	13
J	---	22	22	22	22	23
TL	F	2870	2360	2470	2650	2730
TAUL	msec	4.3	3.8	3.9	4.1	4.2

Rich Combustor
Equivalence Ratio Parametric

Previous studies of RQL combustors concluded that the value of ØR was important to optimizing the NOx control capability of the concept. Generally,

the ØR =1.8 design value for the SSC condition is higher than the value suggested by the prior studies because of the need to reduce the rich combustor liner temperature. It was desirable to assess the influence of ØR for the HSCT engine application and determine whether its design point compromised NOx emissions control.

Further, data were desired to define a control strategy for part-power operation of a RQL combustor. Since the HSCT engine cycle defined the overall operating conditions, a control strategy would specify desired values of ØR at all conditions to preserve combustor stability, maximize combustion efficiency, and minimize NOX and smoke emissions. For example, if the combustor geometry was fixed, ØR would scale directly with F/AOA and the engine cycle would dictate the value of ØR at each condition. Alternatively, if the airflow split was variable, the combination of the airflow schedule and the cycle condition would establish ØR. Data were desired for a range of ØR at part-power operating conditions to provide a basis of specifying the control strategy.

Variations in ØR were achieved in either of two ways:

- Vary the combustor fuel flowrate for fixed air flowrate and split,
- Vary the airflow split for fixed fuel and air flowrates

Each of these techniques caused an alteration to other processes important to the performance and emissions control of a RQL combustor.

The technique of altering ØR by varying the fuel flowrate for fixed air flowrate and split minimized changes to the rich combustor residence time and J but promoted changes in the lean combustor temperature. For instances where the lean combustor was not a strong contributor to NOx production because its temperature was low, the combustor NOx emissions were related directly to ØR, and this variation was referred to as a ØR-Signature. The trade-offs encountered in a ØR-Signature are illustrated in Table VI-5 for the SSC and S-SSC conditions where it is evident that the dominant variation accompanying the ØR change is the lean combustor temperature.

Table VI-5 ØR-Signature at SSC and S-SSC

Parameter	Unit	SSC	ØR-1	ØR-2	S-SSC	ØR-3	ØR-4
P3	psia	150	150	150	119	119	119
T3	F	1200	1200	1200	850	850	850
ØR	---	1.8	1.6	2.0	1.8	1.6	2.0
F/AOA	---	0.030	0.027	0.033	0.028	0.025	0.031
UREF	ft/s	90	90	90	90	90	90
S	---	0.243	0.243	0.243	0.227	0.227	0.227
TR	F	3400	3670	3140	3180	3450	2920
TAUR	msec	13	12	13	11	11	12
J	---	22	21	23	22	21	23
TL	F	2870	2700	3030	2470	2310	2630
TAUL	msec	4.3	4.6	4.1	3.9	4.1	3.7

Variations in ØR by altering the airflow split while keeping the total air and fuel flowrates constant changed the rich combustor residence time and J. This was the issue discussed in Section IV and illustrated in Table IV-2. In that case, reducing S from its value at SSC to achieve ØR = 2.0 increased TAUR by 12 pct and J by 41 pct. Often the interpretation of combustor emissions data resulting from an airflow split change is difficult because of the magnitude of the ØR and J interactions. However, alterations to ØR by changing S can be the proper way to acquire data to develop a part-power control strategy since the engine cycle sets the overall flowrates. This technique was termed a ØR-Split Variation.

Table VI-6 provides an example of Idle conditions which achieved a rich or a lean equivalence ratio in the first combustion stage. A lean value could be achieved for a fixed geometry combustor at low power. However, to avoid any operating condition with ØR < 1.0, an airflow control strategy could be defined to always keep ØR greater than unity at idle; it would therefore be fuel-rich for all operating conditions.

For the Idle condition, specifying ØR = 1.4,which was the minimum value to prevent excessive rich combustor temperature, resulted in a very low S and large J. It could be expected that the rich combustor products would be quenched with an abundance of CO causing the overall combustion efficiency to be low. The specification of ØR = 0.6 could likely operate at high efficiency however the NOx emissions might be higher than a conventional combustor because of the longer residence time in the rich combustor.

Table VI-6 ØR-Split Variation at Idle

Parameter	Unit	Idle-R	Idle-L
P3	psia	67	67
T3	F	425	425
ØR	---	1.4	0.6
F/AOA	---	0.009	0.009
UREF	ft/s	70	70
S	---	0.094	0.219
TR	F	3450	2840
TAUR	msec	24	12
J	---	120	21
TL	F	1050	1050
TAUL	msec	6.9	6.7

General RQL Combustor Operating Characteristics

The flametube-scale RQL combustor was operated at the HSCT engine cycle conditions from Idle to SuCl (i.e. maximum power), and at parametric variations from several of these conditions. The following comments summarize the combustor behavior with regard to combustion efficiency, combustor pressure distribution, stability, smoke emissions, and rich combustor composition.

Combustion Efficiency

The combustion efficiency of the overall flametube-scale RQL combustor was determined from analyses of gas samples obtained at the exit of the lean combustor. The efficiency was calculated according to the procedures described in Section IV.

Most of the combustion tests were performed at the SSC condition. For them, the combustion efficiency was always greater than 99.8 pct. Typically, the EICO was less than 5 and the unburned hydrocarbons were negligible.

The combustion efficiency at other operating conditions depended on the mode of the rich combustor. That is, the level of efficiency depended on whether the combination of F/AOA and S resulted in ØR > 1 or ØR < 1. Tests performed at the lower power conditions of Idle and 34-pct Power with a lean first stage of combustion (i.e. ØR < 1) yielded combustion efficiencies greater than 99.9 pct. Tests performed at higher power conditions always had ØR > 1. For them, and for low power conditions with ØR > 1, the combustion efficiency dropped slightly; the lowest was for a rich-Idle at 97.1 pct. Generally, these data suggested that sufficiently efficient operation throughout the HSCT engine cycle could be obtained. A more complete description of these data is

contained in a subsequent portion of this report section entitled "NOx/CO Emissions at Part-Power Conditions."

Combustor Pressure Levels at SSC

Static pressures were measured in the rich combustor, the entrance and exit of the quench crossflow and in the lean combustor. Static pressures of the airflow entering the rich combustor and the quench sections were also measured. Two pressure taps were positioned at each axial station and recorded independently. During the data processing these separate measurements were averaged to provide a single value for each location.

The air pressure drop percentage across the fuel nozzle/swirler assembly (DP/P-NS) was determined by normalizing the difference between the rich combustor inlet pressure (P3R) and the rich combustor pressure (PR) by P3R:

$$DP/P\text{-}NS = DPR/P3R * 100 = (P3R - PR)/P3R * 100$$

The actual pressure loss for this device was 3.4 pct which is within seven percent of the predicted loss of 3.2 pct. This difference may be attributable to a slight deviation in the discharge coefficient under combusting and non-combusting conditions.

The air pressure drop percentage across the quench orifices (DP/P-Q) was determined by normalizing the difference between the quench inlet pressure (P3Q) and the quench crossflow entrance pressure (PQIN, which was nearly equal to PR) by P3Q:

$$DP/P\text{-}Q = DPQ/P3Q * 100 = (P3Q - PQIN)/P3Q * 100$$

A discharge coefficient of 0.8 was assumed when specifying the quench orifice design for each of the four configurations. However, the actual pressure losses measured at SSC conditions indicate this figure to be off by as much as 25 pct. The predicted pressure losses for the multihole and eight circular hole quench designs were 4.8 pct. The predicted pressure losses for the slanted slot and twelve circular hole quench configurations were 4.4 pct and 8.9 pct, respectively. Actual pressure losses and discharge coefficients for the quench sections are shown in Table VI-7. Typical pressures for both the rich and lean combustors are also displayed in the table for each quench configuration.

Table VI-7 Combustor Pressure Distribution at SSC

Pressure Parameter		Quench Configuration			
		Slanted Slots	Eight Circular Hole	Twelve Circular Hole	Multihole
P3R	psia	150	150	150	150
DP/P-NS	pct	3.4	3.4	3.4	3.4
P3Q	psia	157	154	159	153
DP/P-Q	pct	7.9	6.7	8.7	5.9
Cd	---	0.59	0.68	0.81	0.73
PR	psia	145	145	145	145
PQIN	psia	144	144	145	144
PQEX	psia	140	137	136	137
PL	psia	142	140	139	140

Combustor Stability

The stability of the flametube-scale RQL combustor was assessed by both the visual operation of it at the several operating conditions and the conditions at which a blow-out of the combustor was experienced.

Visually, the combustor operated stably at all HSCT engine cycle and parametric conditions. The combustion process was viewed by use of a video camera sighting upstream through a viewport in the exhaust T-section transition. Typically, the image consisted of two concentric circles. The outer circle was the moderately illuminated lean combustor, and the inner circle was the brightly illuminated quench section. The latter resulted from the strong visible radiation originating in the rich combustor from soot. This concentric-circle image was sharp and constant; there was no indication of unstable combustion in either combustor zone. This observation was consistent with the RQL design concept that the rich combustor would always ensure stable operation.

Combustor blow-outs were observed for two conditions: a lean blow-out (LBO) at Idle and a rich blow-out (RBO) at SuCl. The Idle blow-out was obtained by gradually reducing the fuel flowrate while maintaining the Idle test condition values for T3 and WAT; P3 diminished slightly as the energy release was reduced. A LBO occurred at:

$$\text{ØR}_{\text{Idle LBO}} = 0.4$$

This LBO value was close to the level generally observed for well-mixed systems and suggested that mixing processes within the fuel preparation and rich combustor sections was thorough. In turn, this result indicated that a

moderately lean Idle operating condition (e.g. ØR = 0.6) could provide sufficient stability margin for HSCT engine operation.

The RBO was observed during ØR-Split tests at the SuCl condition. For this condition, F/AOA = 0.040. If the airflow split was held at the SSC design value of S = 0.243, then ØR = 2.4. While this split maintained J = 26 in the quench, the high value for ØR resulted in a measured smoke emission at a Smoke Number (SN) = 15. Reducing the value for ØR by reducing S suppressed the SN. However, as discussed above for ØR-Split variations, the value for J reduced to 10 which resulted in high exhaust CO and poorer combustion efficiency. During these ØR-Split variations, a ØR = 2.5 condition was established and the combustor extinguished. This result was also consistent with values for well mixed systems for which the lean and rich combustion limits, occur for similar levels of flame temperature. and hence was consistent with the LBO level.

Smoke Emissions

The smoke emissions from the flametube-scale RQL combustor were evaluated from a single-point sample extracted on the exhaust flow centerline just downstream from the lean combustor probe array. The sample was collected and converted to a SAE Smoke Number in accordance with ARP 1179.

No significant exhaust smoke emission was detected for any operating condition except for SuCl. Typical values were SN < 2 for all other operating conditions including SSC. As noted in the "Combustor Stability" section above, the values recorded at SuCl reached SN = 15 for an extreme in a ØR-Split variation. The SN data for this condition are presented in a subsequent report section entitled "NOx/CO Emissions at Part-Power Conditions."

Soot was present in the RQL combustor. Post-test inspections showed that significant particulate carbon was formed in the rich combustor; the liner color was dark gray. However, no significant carbon or liner discoloration was found in either the quench or lean combustor sections, indicating that the rate of carbon consumption in these sections was very high.

Rich Combustor Composition

The role of the rich combustor was to process a fraction of the total airflow and all of the fuelflow in a manner to assure stable combustion and deliver a near-equilibrium composition gas flow to the quench section. Since the fuel originated as a liquid, it was possible that regions of diffusion flame combustion would be present, with the associated high rate of NOx production. The rich combustor had to cope with such instances and allow them to revert to the low equilibrium NOx concentrations corresponding to fuel-rich combustion. In a sense, the rich combustor reformed the injected

liquid fuel to a high heating value gaseous fuel for consumption in the lean combustor.

Gas samples from the exit of the rich combustor were analyzed to determine whether a complete fuel reformation was achieved. The samples were extracted using two sampling probes of the design described in Section IV. The probes were located in the plane of the rich combustor cylindrical spool, with one probe on the flow centerline (CL) and one at a radius of 1.25 in., or at the mid-radius (MR) of the combustor.

Samples from either probe were analyzed individually after transfer to the emission cart. An in-line filter was used to collect the soot in the sample and prevent contamination of the gas analyzers. Generally, both a non-diluted sample and a N2-diluted sample were analyzed for each probe and test condition. This dual analysis was required to reduce the CO concentration in the sample to be within the analyzer calibration as described in Section IV. Typically, dilution ratios of approximately four were required, with the precise value being determined by comparing the CO2 concentrations of the two samples.

The concentration of O2 and UHC were zero and the EINOx < 1 for all samples extracted from the rich combustor. These results were consistent with equilibrium predictions of complete consumption of O2 and UHC, and minimal production of NO ($NO_{equilib}$ < 30 ppm for ØR > 1.6). Equilibrium calculations also predicted that other nitrogen compounds would be minimal in the operating ØR range. This result established that any NOx concentration measured at the combustor exit was formed in the quench section or lean combustor. Note, however, that studies performed with fuels containing fuel-bound nitrogen have indicated that NOx from this nitrogen source can lead to significant concentrations in both combustors. (Ref. VI-1).

CO data from analyzed samples are plotted in Fig. VI-1. These data were obtained for the flametube-scale RQL combustor during a ØR-Split parametric variation from the SSC condition. The quench jet configuration was the slanted-slot, and the rich combustor cylindrical spool section was 8 in. long. The data represented the CO concentration dependence on ØR for samples extracted from either the centerline (CL) or mid-radius (MR) position. Also plotted are calculated equilibrium concentrations for the global value of ØR. As shown in the figure, the measured CO concentrations for the two sampling locations were equal to within 7 pct. indicating that a uniform composition was present. Further the concentrations were within approximately 10 pct of the predicted equilibrium level. Small variations in the local fuel-air ratio could easily account for both of these differences suggesting that essentially complete fuel reformation had occurred by this axial station. Similar results were obtained for the measured concentrations of CO2; other major gas species, such as H2O and H2, should also be at near equilibrium levels. The uniformity and composition of the flow approaching

the quench section was in agreement with the CFD prediction of the flow as presented in Fig. V-10.

In order to assess the effect of a shortened rich combustor residence time on the specie composition, samples were analyzed from flametube-scale RQL combustor tests using a 4-in. long rich combustor spool section. The quench jet configuration was the slanted-slot. At the nominal SSC condition, the shortened rich combustor length reduced TAUR from 13 msec to 7 msec.

As for tests with the 8-in. long rich combustor, no significant concentrations of O2, UHC, or NOx were present for the 4-in. long rich combustor. Superimposed on the Fig. VI-1 data for the longer combustor are the measured CO concentrations from the two probe locations in the shorter combustor (closed triangle symbols). As shown, the data for the shorter combustor were consistent with the magnitude and uniformity observed for the longer combustor; near-equilibrium compositions were again achieved.

Together, combusting and non-combusting studies indicated that a reduced residence time combustor could be used as the first zone of a RQL combustor. The rich combustor sampling data indicated that a shortened device would not compromise the NOx control potential of the RQL concept. Further, the waterflow visualization studies indicated that comparable flowfield features, particularly those believed to be important for combustor stability, would be established in the shortened combustor. The ability to shorten the rich combustor was significant because of the associated reduction of liner area which demands cooling without the use of air films.

NOx/CO Emissions at Supersonic Cruise Conditions

A primary objective of the combustion test program was to determine both the NOx and CO emission levels that could be achieved by a flametube-scale RQL combustor operating at the SSC condition, and the sensitivity of them to operational and design features of the combustor. The test program which acquired the data for these issues began with a combustor configured with the slanted-slot quench. Initial tests were performed at the scaled-SSC (S-SSC) condition defined for operation at T3 = 850 F and proceeded through parametric variations in P3 and T3 to achieve the true SSC condition. The influences of the level of fuel nozzle air-assist airflow, equivalence ratio, and rich and lean combustor residence times were assessed at this condition. Subsequently, alternative quench designs were evaluated. This section of the report presents the results from studies at the SSC condition, and parametric variations from it. The results are organized according to the quench configuration.

SSC Emissions Using the Slanted-Slot Quench

Combustion tests performed with the flametube-scale RQL combustor configured with the slanted-slot quench began with operation at the S-SSC condition. Initially, the combustor contained 8-in. long cylindrical sections in both the rich and lean combustor to provide 11 ms and 3.9 ms hot residence time for the rich and lean combustors, respectively, at the S-SSC condition; at SSC, these values were 13 ms and 4.3 ms. As described below, the influence of reduced rich or lean combustor length was studied. At both the S-SSC and SSC conditions, J = 22.

Efficiency and Composition Uniformity at Scaled-SSC

The RQL combustor operated stably at the S-SSC condition, with high combustion efficiency and uniform composition profiles at the combustor exit. Figure VI-2 depicts the variation in the fuel-air ratio, EICO, and EINOx determined from analyses of samples extracted from either individual combustor exit probes, or from all the probes ganged together. The layout of the sample probes and the analysis procedures are described in Section IV of this report. As indicated, the emission-based fuel-air ratio was both nearly uniform and near the metered value of F/AOA = 0.028 for S-SSC. The values for EICO ranged from 1 to 3, which corresponded to a combustion efficiency of 99.9 pct or greater. The NOx emissions for this condition and RQL configuration were also uniform near a value of EINOx = 5. The composition uniformity indicated by each of these parameters indicated that the slanted-slot quench promoted thorough mixing in this lean combustor.

P3 Sensitivity

A combustion test sequence was performed following the parametric P3 variation from the S-SSC condition. Nominally, the sequence consisted of the S-SSC, P3-4, and P3-5 conditions described in Table VI-2. The value of T3 was held constant, with data acquired for ØR values of 1.8 and 2.0 as achieved from a ØR Signature. The principle effect of the ØR Signature (i.e. variation of fuel flowrate for constant airflow rate and split) was a variation in the lean combustor temperature, TL. However, as indicated in Table VI-5, the expected TL variation was approximately 2300 F to 2600 F. Since these levels were below the threshold for high thermal NOx formation rates (nominally 2900 F), it could be expected that all the data should primarily reflect the pressure influence on NOx emissions for this combustor. However, the quench process controls the NOx emissions and the temperature history through the quench will not be the same for both values of ØR.

The EINOx data acquired for the P3 variation from the S-SSC condition are shown in Fig. VI-3. These data were analyzed to determine the NOx sensitivity to P3 following a power law of the form:

$$EINOx = a * P3^{n}$$

where a = constant. Regression analyses to fit this form were performed for both values of ØR, resulting in:

n = 0.64	with R^2 = 0.99	for ØR = 1.8
n = 0.86	with R^2 = 0.72	for ØR = 2.0

where R^2, the square of the regression coefficient, reflects the fraction of data variation represented by the correlation.

The fit for the higher value of ØR was poor, possibly because either the correct relationship was not of the power-law form, or the data were sparse. The fit for ØR = 1.8 was excellent and was applied for subsequent data analyses.

The CO emissions decreased slightly with increased P3 during this variation, with EICO = 3.5 at P3 = 90 psia and EICO = 2.7 at P3 = 150 psia (Fig. VI-3). This trend was representative of a combustor operating with constant stoichiometry and flows, but with CO oxidation responsive to its concentration, and hence responsive to the combustor pressure. The combustion efficiency always remained above 99.9 pct.

T3 Sensitivity

Combustor test sequences were performed following parametric T3 variations at ØR = 1.8 as described in Table VI-4. This variation ranged from T3 = 750 F to 1200 F. As described previously, in order to maintain near constant values for J, TAUR, and TAUL, a P3 variation was included with the T3 variation which resulted in the highest T3 condition matching SSC.

The EINOx data representing this T3 parametric are shown in Fig. VI-4. As indicated, the NOx emissions increased with T3 from a value of EINOx = 4 at T3 = 750 F to EINOx = 10.9 at T3 = 1195 F. The value achieved at the SSC condition was higher than the program goal, reflecting that improvements in the NOx control in either the quench or lean combustor were required. These data were analyzed to determine the NOx sensitivity to T3 when included in an exponential format; since P3 was also varied, a P3 power-law term as determined above at ØR = 1.8 was also included. That is, the form of the dependence was represented:

$$EINOx = b * P3^{0.64} * \exp(c * T3)$$

where b. c = constants and the units of T3 = R. Regression analyses to fit this form yielded values:

b = 0.022, c = 0.00183

for a fit with R^2 = 0.98 or a standard error for predicted EINOx of 0.4. This data fit indicated that for departures from the SSC condition:

+/- 10 psia in P3	corresponds to	+/- 0.5 EINOx
+/- 50 F in T3	corresponds to	+/- 1.0 EINOx.

It should be noted that only slight changes in the overall fuel-air ratio, F/AOA, (or ØL) accompanied the T3 variation. Therefore, for each T3 value there was a corresponding value for the lean combustor temperature, TL. Hence, a correlation of EINOx with TL would also fit these data. This issue was revisited later in this section during data analyses for dependencies on the combustor stoichiometries.

Figure VI-4 depicts the measured CO emissions variation for this T3 parametric. The values of EICO were low for all T3 levels, decreasing from EICO = 5 at T3 = 750 F to EICO = 1 at T3 = 1195 F. At the highest level of T3, approximately half of the CO was due to equilibrium composition; equilibrium CO was negligible for lower T3. However, the low CO levels measured corresponded to a combustion efficiency of 99.9 pct or greater for all T3.

Efficiency and Composition Uniformity at SSC

The RQL combustor operated stably at the SSC condition, with high combustion efficiency and uniform composition profiles at the combustor exit. Figure VI-5 depicts the variation in the fuel-air ratio, EICO, and EINOx determined from analyses of samples extracted from either individual combustor exit probes, or from all the probes ganged together, for two ØR values as achieved in a ØR Signature. As for operation at the S-SSC condition, the emission-based fuel-air ratio was both nearly uniform and near the metered values of F/AOA. The values for EICO ranged from less than 1 to 2 for ØP = 1.8, which corresponded to a local combustion efficiency always greater than 99.9 pct. The EICO variation for ØR = 2.0 was greater, with values ranging from 1 to nearly 8. Other data suggested that the highest value, which corresponded to Probe 4, was artificially high, reducing the maximum EICO to 4. For any of these values, the local combustion efficiency was 99.8 pct or greater. The NOx emissions for SSC with this RQL configuration were less uniform than measured at the S-SSC condition. For operation at ØR = 1.8, the local variation was EINOx = 8 to 11.5; the ganged sample indicated EINOx = 9.5. For operation at ØR = 2.0, and ignoring the value for Probe 4, the range was 11 to 15.5; the ganged sample indicated EINOx = 12. Despite these mild spatial variations in combustor exit NOx emissions, the fuel-air uniformity and effective CO burnup indicated that the slanted-slot quench promoted thorough mixing in this lean combustor.

Lean Combustor Residence Time Influences at SSC

The emission levels measured at the SSC operating condition indicated that a reduced lean-combustor residence time could be used to reduce NOx without compromising combustor efficiency. Data were acquired with a flametube-scale RQL combustor obtained by substituting a 3-in. long lean combustor for the 8-in. long rich combustor of the original configuration. This change

reduced the lean-combustor residence time at the SSC condition from 4.3 ms to 2.2 ms.

The variation in EINOx measured with the shortened lean combustor for a T3 parametric (as described above) is shown in Fig. VI-6. The behavior of the NOx emissions was similar to that obtained for the 8-in. long, lean combustor but with reduced EINOx levels. For T3 = 1205 F, EINOx = 8.5 as compared to the 11.9 value obtained at 1195 F with the longer lean combustor. The three data were analyzed by regression analysis for compliance with the form determined previously, namely:

$$EINOx = d * P3^{0.64} * \exp(e * T3)$$

where d and e were constants and the units of T3 = R. Analyses to fit this form yielded values:

$$d = 0.021, \quad e = 0.00169$$

for a fit with $R^2 = 0.98$ or a standard error for predicted EINOx of 0.3. This data fit indicated that for departures from the SSC condition:

+/- 10 psia in P3	corresponds to	+/- 0.4 EINOx
+/- 50 F in T3	corresponds to	+/- 0.7 EINOx.

If the same dependencies on P3 and T3 prevailed for the shortened combustor as for the longer one, then the lead constant in the above regression analysis should have reduced in proportion to the reduction in measured EINOx. However, the constant was nearly invariant, indicating that the one or both of these dependencies had changed, or that the few data did not allow an accurate determination. Data for a P3 parametric with the shortened lean combustor did not exist to help resolve these issues.

It was noted that the reduction in lean-combustor residence time did not produce a proportionate reduction in EINOx. That is, at the SSC condition, TAUL reduced to 51 pct but EINOx reduced only to 71 pct of the longer combustor values. This non-linear character could be due to production in either the quench because of flow-chemistry interactions or in multi-dimensional flow features of the lean combustor. If the former was true, then the emissions could be represented as:

$$EINOx = EINOx_q + f * TAUL$$

where $EINOx_q$ was the quench contribution to the total NOx and f was a constant. Using the data obtained for the two values of TAUL at the SSC condition:

$$EINOx_q = 4.9, \quad f = 1.6 \text{ EINOx/ms} \quad \text{at SSC.}$$

This model indicated that the quench was a major contributor to the exit NOx emissions. The simple extrapolation was that the slanted-slot quench configuration would produce EINOx = 4.9 for zero lean combustor residence time, and did provide 58 pct of it for the shortened lean combustor.

The CO emissions for the shortened lean-combustor decreased with increasing T3 as for the longer lean combustor, but were measured to be approximately three times higher (Fig. VI-6). That is, at T3 = 850 F, EICO = 10

for the shorter combustor but EICO = 3 for the longer one. At T3 = 1200 F, EICO = 3 and 1 for the shorter and longer combustors, respectively. The corresponding combustion efficiency was 99.7 pct at T3 = 850 F and increased to greater than 99.9 pct at T3 = 1200 F.

As for the NOx emissions at SSC, the response of the EICO could only be linearly related to TAUL:

$$EICO = EICO_0 + g * TAUL$$

where $EICO_0$ represented the contribution emerging from the quench and non-one-dimensional flow regions, and g was a constant. Using the data obtained for the two values of TAUL at the SSC condition:

$$EICO_0 = 5.1, \quad g = -0.95 \text{ EICO/ms} \quad \text{at SSC.}$$

This model indicated that a slanted-slot quench configuration would produce EICO = 5.1 for zero lean combustor residence time, and hence achieve a combustion efficiency > 99.8 pct. This performance could be altered by the degree of non-ideal flow actually produced in the transition to the lean combustor.

Rich Combustor Residence Time Influences at SSC

The flametube-scale RQL combustor was configured with a 4-in. long rich combustor substituted for the 8-in. long device in the original combustor.; the lean combustor length was 3 in. At the SSC condition, these combustor lengths provided 7 ms and 2.2 ms of hot residence time in the rich and lean combustors, respectively. As described in an earlier portion of this report section, analyses of rich combustor samples for these two combustor lengths indicated no significant difference in the flow composition entering the quench. Figure VI-7 superimposes the EINOx measured with the shortened rich combustor on the data trend with the longer rich combustor. The shorter rich-combustor data match the longer combustor data. This match also supported the conclusion from the waterflow visualization studies that the flowfield entering the quench was similar for both combustor lengths.

Fuel Nozzle Air-Assist Influence at SSC

All combustion test data presented in this report were acquired using the Delavan Swirl Air, air-assist fuel nozzle mounted in an axial-flow air swirler. The details of this fuel preparation setup are described in Section IV. Typically, the air-assist flowrate was set to achieve a nozzle fuel-air ratio (F/ANOZ) of unity. Limited tests were performed to determine whether variations to the assist airflow, and hence to the fuel atomization quality, would affect the measured combustor emissions.

Data depicting the response of the measured EINOx to changes in the fuel nozzle fuel-air ratio, achieved by variations in the air-assist flowrate, are

contained in Fig. VI-8. Only a mild reduction in F/ANOZ could be achieved before the airflow capacity of the nozzle became limiting. The maximum value of F/ANOZ, or minimal assist airflow, was set by the ability to accurately meter the flow. With these limits, the turndown range of F/ANOZ studied was approximately 1.4/1. As shown in the figure, over this range, the value of EINOx changed minimally, with a slight tendency to increase with larger values of F/ANOZ. This trend could be expected as higher values corresponded to a lower air-assist and a slightly degraded atomization quality. The insensitivity of the emissions to this turndown indicated that the performance of fuel nozzle, either alone or in conjunction with the axial-flow air swirler, was constant and likely preserved a high atomization quality. This conclusion was consistent with the ambient spray qualities reported in Section IV.

Rich and Lean Combustor
Equivalence Ratio Influence at SSC

The SSC design point set the value of ØR = 1.8 to restrict the rich combustor maximum temperature to 3400 F while avoiding higher ØR values which would promote soot formation. Hence, the parametric variation range on ØR was minimal, typically being from 1.8 to 2.0 for the SSC condition. In the course of investigating ØR influences, ØL effects were discerned.

Data were acquired for ØR Signature variations for a limited ØR range for flametube-scale RQL combustor configurations using lean combustor lengths producing either 4.3 ms or 2.2 ms of hot residence time. The EINOx response for these configurations is shown in Fig. VI-9. In both cases, an increase in ØR elevated the measured EINOx. The effect was greatest for the highest level of T3 and negligible for T3 = 850 F. A reduction in TAUL diminished both the absolute and the percent increase in EINOx.

In principle, the ØR Signature test maintained the combustor flow character constant while increasing both ØR and ØL. Among the primary considerations was whether either the rich combustor composition or the quench effectiveness changed with ØR, or whether the lean combustor NOx production increased with the higher TL because of higher ØL. This was a broader consideration for the effect of increasing the fuel flowrate for constant air flowrate and split than typically given to previous RQL data analyses such as for ØR Signature tests with industrial gas turbine combustors. In those cases, the level of TL would be sufficiently low so that increases in it would not greatly accelerate NOx formation. As described in Section IV, a NOx bucket was found near ØR = 1.5 because of a trade-off of reduced NO and increased XN formations in the rich combustor.

In contrast, the role of an elevated TL was the major consequence of a ØR Signature test for the HSCT application. The results from the rich combustor composition study indicated that near-equilibrium products entered the quench; no significant NOx was present. As shown in Table VI-5 for the SSC

condition, the variation of J for ØR values from 1.8 to 2.0 was minimal, but that the corresponding rise in TL was from 2870 F to 3030 F. Other thermochemical calculations indicate that for T3 = 1080 F, the corresponding increase in TL was from 2760 F to 2930 F. Therefore, for both of the high T3 cases shown in Fig. VI-9, TL rose above the threshold for high NOx production rates. In contrast, the values of TL for T3 = 850 F were below the threshold. The EINOx responses to the ØR Signature were consistent with these TL distinctions.

The NOx response for the data of Fig. VI-9 from the longer lean combustor can be related to the change in the lean combustor equivalence ratio (ØL) by adding it to the exponential T3 relationship. That is, using previously determined forms:

$$EINOx = h * P3^{0.64} * \exp(i * T3 + j * ØL)$$

where h, i, and j were constants and the units of T3 = R. Analyses to fit this form yielded values:

$$h = 0.0086, \quad i = 0.00152 \quad j = 3.30$$

for a fit with $R^2 = 0.97$ or a standard error for predicted EINOx of 0.6.

An alternative analysis for the longer lean-combustor data considered whether the T3 and ØL dependence could be replaced with a TL dependence alone of the form:

$$EINOx = k * P3^{0.64} * \exp(m * TL)$$

where k and m were constants and the units of TL = R. Only the four higher temperature data (ØR = 1.8, 2.0 at T3 = 1080 F, 1195 F) were used in this analysis to avoid bias from the constant ØR, lower T3 range. While regression analyses to this data range yielded a good fit, when the determined TL dependence was applied to the full T3 range, the fit was poor. That is, for the limited, higher T3 range:

$$m = 0.00042, \text{ with } R^2 = 0.98.$$

However, when this value for "m" was used to fit the entire T3 range, the best fit achieved only $R^2 = 0.71$.

These analyses indicated that a data representation relying upon TL alone did not preserve the previously determined T3 relationship for constant ØL. The form which combined T3 and ØL dependencies retained the T3 relationship and added a ØL influence. Such a combination was a hybrid between pure diffusion combustion and premixed combustion. In the former case, the heat release would occur at stoichiometric conditions (i.e. ØL =1) and the flame temperature influence on the emissions would be represented by T3 alone. For premixed combustion, the flame temperature (a special combination of T3 and Ø) of the mixture would dominate, not a mixed combination of these parameters. The hybrid nature of the RQL could have derived from the mixing dominated processes in the quench followed by the mixture burnout in the lean combustor.

The EINOx data on Fig. VI-9 for the shortened lean combustor were also analyzed in the same manner as described above using the combined dependence on P3, T3 and ØL of the form:

$$EINOx = r * P3^{0.64} * \exp(s * T3 + t * ØL)$$

where r, s, and t were constants and the units of T3 = R. Analyses to fit this form yielded values:

$$r = 0.014, \quad s = 0.00156 \quad t = 1.40$$

for a fit with $R^2 = 0.98$ or a standard error for predicted EINOx of 0.3. The dependence on T3 was similar, but the dependence on ØL reduced to 42 pct, from the values for the longer lean combustor. As speculated above, if the ØL term reflected the NOx production during CO burnout in the lean combustor, then the reduced ØL dependence was consistent with earlier observations for lean-combustor residence time.

Emissions data were also acquired from combustion test with the flametube-scale RQL combustor following a ØR-Split variation. As discussed earlier, ØR-Split parametrics retained constant total air and fuel flowrates but altered the split of airflow between the rich and quench sections. As a consequence, the values of ØR and J changed for a constant F/AOA.

The measured EINOx was relatively insensitive to changes in the rich zone equivalence ratio as achieved in the ØR-split parametric (Fig. VI-10). This insensitivity indicated that competing processes were occurring in the quench. That is, while an increased quench vigor would be expected for the higher J values at higher ØR, the NOx was not lower. Among the possible explanations for not achieving lower NOx could be that the quench jets over-penetrated at the high J and no benefit resulted. Alternatively, while the quench was more vigorous, the range of stoichiometries to be spanned in reaching F/AOA was greater. While the fuel-air ratio range important for NOx production was likely restricted to values near stoichiometric, the probability of encountering it for a longer time was increased for the wider transition.

The more vigorous quench as achieved at higher values of ØR tended to produce higher CO (Fig. VI-10), although the level of increase was sufficiently small to have a minor effect on combustion efficiency. Based on the near-equilibrium behavior in the rich combustor, as ØR increased, the concentration of CO produced in the rich combustor increased. The corresponding increase in the lean combustor suggested that a portion of this higher CO did not mix and oxidize in the quench airflow despite a higher J. If the quench jets over-penetrated in this case, CO contained in flow near the circumference of the quench duct might persist. Analyses of samples from a traverse across the quench flow could clarify this issue.

SSC Emissions Using a Circular-Hole Quench

Combustion tests were performed with the flametube-scale RQL combustor configured with either an eight or twelve circular-hole quench to assess the influence of these alternative designs. Minimal test condition parametric testing for them was performed. Except as noted, the combustor contained a 4-in. long rich combustor and a 3-in. long lean combustor to provide 7 ms and 2.2 ms hot residence time for the rich and lean combustors, respectively, at the SSC condition. As described in Section IV, at the SSC condition, the eight-hole quench was designed to achieve J = 24, and the twelve-hole quench was designed to achieve J = 46.

Primarily, data were acquired at the exit of the flametube-scale RQL combustor to compare the emissions control achieved with these quench designs to that achieved with the slanted-slot quench. Samples from either the individual or ganged probes were analyzed. Limited data were also acquired from samples extracted during a traverse across a flow diameter in a plane 2.3 in. downstream of the quench-jet centerline. This plane was approximately in the middle of the conical transition to the lean combustor where the flow had expanded from the 3.0-in ID quench to a 3.25 in. diameter These two types of data are presented and discussed in the following sections.

Combustor Exit Emissions

Emission data were acquired from tests with the two constructions of the eight circular-hole quench described in Section IV: (1) 0.5-in. thick ceramic quench-cylinder cast inside a 0.25-in. thick, uncooled metal quench-cylinder, and (2) 0.75-in. thick, water-cooled metal quench cylinder. Both constructions achieved a 3.0-in. ID. The difference in the quench-cylinder constructions reflected an attempt to achieve a more durable component for the flame-tube scale RQL combustor testing. Both were designed to achieve J=24.

The initial data were obtained at the SSC condition using the uncooled, eight-hole quench (Fig. VI-11). The rich combustor contained an 8-in. long cylindrical spool section which yielded a greater residence time than stated above. Based on test results with use of the slanted-slot quench, it was believed that the longer rich-combustor residence time would not affect the emissions from the overall combustor. As indicated in the figure, a relatively uniform level of NOx was measured. Samples from individual probes ranged from EINOx = 4.5 to 5.7 with an arithmetic average of 4.9; the ganged sample value was EINOx = 6.0. It was unknown why the gang sample differed from the individual probes. Total pressure measurements obtained at each sampling location were nearly identical, suggesting that the gas flow radial-profile was also nearly uniform. The sample pressure within the transfer line was sufficiently low for either individual or ganged sampling to achieve aerodynamic quenching of NOx at the probe tip. Possibly the

difference between the individual and ganged sample analyses should be taken as a global indicator of uncertainty.

As noted on the figure, these data were acquired for a value of ØL which was slightly less than the SSC setpoint; the data corresponded to ØL = 0.41 instead of 0.44. The effect of this difference was assessed by applying the data correlation determined above for the flametube-scale RQL combustor configured with the slanted-slot quench and operating at conditions up to SSC. That correlation was:

$$EINOx = 0.014 * P3^{0.64} * \exp(0.00156 * T3 + 1.40 * ØL)$$

with the units of T3 = R. Applying this description to the two values of ØL predicted only a 4 pct reduction in NOx at the leaner condition, within the measurement uncertainty. The prediction of only a slight reduction was believed to result from the dominant role of the quench process on NOx formation, and the lesser role of the lean combustor.

The corresponding CO data displayed a trend of growing concentration with radius, increasing from EICO = 3 to 16. The ganged sample value was EICO = 10 which corresponded to a combustion efficiency of 99.8 pct. The CO concentration profile suggested that the quench jets penetrated deep into the quench-section crossflow to promote oxidation in the central region with slightly retarded oxidation in the outer regions. It should be recognized, however, that a substantial oxidation did occur over all regions of the flow as the measured CO was less than 1 pct of the equilibrium EICO at the ØR condition.

Together, the NOx and CO data indicated that the eight circular-hole quench offered the emissions control required to achieve the HSCT NOx goal at the SSC condition while retaining high degrees of combustor operability and efficiency. The reduced levels of NOx were obtained by use of rapidly penetrating quench jets which suggested that quench designs should focus on terminating the undesired kinetics quickly rather than promoting the global mixing to achieve mixture uniformity throughout the flowfield. That is, small-scale non-uniformities will be acceptable if regions of high potential NOx production are minimized. The NOx data indicated that the eight circular-hole quench was a good mixer; the CO profile was not a significant residual of the quench inlet composition.

A second set of emissions data were acquired with the water-cooled construction of the eight, circular-hole quench. The data (Fig. VI-12) did not match some trends obtained with the uncooled quench. The NOx emissions were uniform, but at a greater level; the ganged sample registered EINOx = 7.9, nearly two units greater than observed with the uncooled quench. Also, the CO level was lower, and displayed no significant radial profile; the ganged sample indicated EICO = 1.2 which corresponded to a combustion efficiency greater than 99.9 pct.

The emission data for the two constructions of the eight, circular-hole quench were analyzed in an attempt to discern the cause of the differences. There was no evidence that the water cooling affected the emissions. If present, the cooling would have increased the CO emissions because of heat extraction and reaction quenching on the walls, but the opposite response was observed. Also, heat removal would reduce local NOx formation rates, but again the opposite response was observed.

One difference in the combustor configurations used for the eight, circular-hole quench evaluations was the length of the rich combustor. As indicated above, the data for the uncooled quench were obtained with an 8-in. long rich combustor; the data for the cooled quench were obtained with a 4-in. long rich combustor. The role of the rich combustor length could be to affect the flow structure and composition entering the quench. The flow structure issue was studied as part of the rich-combustor waterflow visualization which had a primary objective of discerning the response of the global flowfield to changes in the fuel nozzle swirl strength and combustor length. In these studies, it appeared that the quench inlet flowfield was qualitatively invariant. Rich combustor sampling also indicated that the quench entrance flow composition was nearly identical for these two combustor lengths. Indeed, rich combustor length was not a significant influence on the emissions control achieved by the slanted-slot quench. However, data were not acquired to confirm that the eight-hole quench was also insensitive to this change. Since the quench section has been shown to be the critical, emission-control component of the RQL, studies of inlet flow influences on both the crossflow and the quench jets should be performed.

Data were also obtained at the SSC condition using a cooled, twelve-hole quench. The rich combustor contained a 4-in. long cylindrical spool section as used with the cooled, eight-hole quench. As described in Section IV, the twelve-hole quench was designed to achieve a quench-jet penetration into the crossflow similar to that for the eight-hole design by using a greater quench-jet pressure loss (and hence J) to compensate for the smaller jet diameter; at design, J=46. Figure VI-13 compares the NOx and CO data obtained with the two circular-hole quench designs. Both designs achieved nearly identical levels and profiles of these species, with ganged samples yielding: EINOx = 8 and EICO = 2.0. These data indicated the importance of the quench-jet penetration to achieve emissions control for a RQL combustor.

Quench Exit Emissions

Emission data were acquired from samples extracted during a traverse across a flow diameter in a plane 2.3 in. downstream from the quench-jet centerline. In this plane, the flow had expanded from the 3.0-in ID quench to a 3.25 in. diameter. The traversing probe was in-line with two opposed quench jets. Samples, extracted following the procedures described in Section IV, were obtained in tests at SSC using cooled constructions of either the eight or twelve circular-hole quench, and 4-in. and 3-in. long rich and lean

combustors, respectively. In all cases, the sample compositions were lean as denoted by containing approximately 8 to 13 pct oxygen. That is, no sample reflected the pure penetration of rich combustor gases. The oxygen levels were consistent with the value of F/AOA and with the locally-determined emissions-based fuel-air ratio.

Data from a flow traverse during tests using the cooled, eight circular-hole quench are presented in Fig. VI-14, with the flow centerline at the 1.6 in. location. A complete traverse was acquired for F/AOA = 0.030; a traverse at F/AOA = 0.025 was limited because of test rig problems. For both of these data sets, the airflow split was set to maintain ØR = 1.8 while altering the quench-jet penetration. This variation was the inverse of the ØR-Split variation which held F/AOA constant. However, in both types of split variation, reductions in S increased J. Table VI-8 illustrates the changes for the two conditions of the eight circular-hole quench traverse tests, particularly the 62 pct increase in J at the lower FA/OA.

Table VI-8 J Variation for Traverse with Eight Circular-Hole Quench

Parameter	Unit	SSC	S-1
P3	psia	150	150
T3	F	1200	1200
ØR	---	1.8	1.8
F/AOA	---	0.030	0.025
UREF	ft/s	90	90
S	---	0.243	0.203
TR	F	3400	3400
TAUR	msec	7	9
J	---	24	39
TL	F	2870	2620
TAUL	msec	2.2	2.4

Increased quench-jet penetration suppressed the emissions-based fuel-air ratio and EICO near the flow centerline. At the nominal SSC condition, the fuel-air profile was center-peaked, whereas the increased J appeared to depress it below the nominal setting. The CO remained center-peaked but was reduced. Recognizing that the equilibrium level entering the quench was approximately EICO = 1700, over 80 pct of it was consumed by the quench exit.

The NOx profile was mildly depressed on the flow centerline for either condition, with levels ranging between EINOx = 4 to 6. This level was approximately 60 pct of the value measured at the combustor exit, indicating that NOx formation in the quench process was the dominant contributor to the combustor emission, with the balance formed downstream of this traverse plane (i.e. in the lean combustor).

At the nominal SSC condition (lower J), the higher CO and lower NOx centerline values might reflect some persistence of the rich combustor composition (i.e. high CO, zero NOx) with under penetrating quench-jets. However, the measured centerline fuel-air ratio was lean and the NOx was lowest. That is, the centerline mixture had transitioned from fuel-rich to fuel-lean with sufficient vigor to avoid high NOx production. The label "under-penetrating quench-jets" conveyed an image of modest mixing near the centerline, and hence likely higher NOx formation. Therefore, the simplistic "under-penetrating" flow model did not explain both the CO and NOx response to J.

Figure VI-15 presents similar data for tests conducted with the cooled, twelve circular-hole quench. This nominal design was predicted to achieve J= 46 at SSC, and a quench-jet penetration equivalent to the eight-hole design. For operation maintaining ØR = 1.8, attaining F/AOA = 0.025 or 0.033 produced J = 74 or 35, respectively. Again, the emissions-based fuel-air ratio and the EICO were center-peaked, and the EINOx center-depressed, for the nominal SSC condition. However, the ranges of variation were less than for the eight-hole quench; the flow composition was more uniform. A higher level of NOx was determined, with close to 75 pct of the NOx measured at the combustor exit present in the quench exit samples. Since the combustor exit emissions for each quench design were nearly identical (Fig. VI-13), the attainment of the greater uniformity by the twelve-hole design was not beneficial; a greater percentage of the final value was achieved with this design at the quench exit. Again, the flow details within the quench dictated its effectiveness.

The fuel-air and CO profiles changed in predicted fashions, with increased centerline values for reduced J, and decreased values for increased J. As for the eight-hole quench, this was the expected response for a flow model based on jet penetration. However, as also for the eight-hole quench, the NOx centerline value was depressed at the SSC condition and increased with greater jet penetration. Again, the simple quench-jet penetration flow model did not explain both the CO and NOx behavior.

Limited quench-exit traverse data were acquired. They did confirm the important role of the quench process in controlling NOx formation in a RQL combustor. However, the data did not fit a simple model of the muti-dimensional flow within the quench; contradictory CO and NOx trends were observed. These observations affirmed that the quench contained a complex flow which requires more detailed studies to describe its behavior.

SSC Emissions Using the Multihole Quench

Combustion tests were performed with the flametube-scaled RQL combustor configured with the multihole quench to assess its influence on emissions

control. The combustor contained a 4-in. long rich combustor and a 3-in. long lean combustor to provide 7 ms and 2.2 ms hot residence time for the rich and lean combustors, respectively, at the SSC condition.

As described in Section IV, this quench configuration was termed "multihole" because it injected the quench airflow through arrays of circular orifices using three hole diameters. The goal of the design was to promote a greater range of mixing length scales than would be experienced with a single hole diameter array. The multiple scales would develop from differences in both the hole diameters and the levels of penetration into the crossflow. It was also desired to achieve complete coverage of the quench cylinder circumference. As tested, the multi-hole quench contained eight repeated arrays consisting of one 0.58-in. dia, two axially-aligned, 0.15-in. dia, one 0.29-in. dia, and two axially-aligned, 0.15-in. dia holes, in this sequence (Fig. IV-8). The total array provided 3.207 $in.^2$ of geometrical area, 95 pct of the eight circular-hole quench, with a predicted pressure loss of 4.9 pct and an associated momentum ratio, J = 25.

Figure VI-16 presents the NOx and CO profiles obtained during a combustion test at SSC. The NOx values were uniform at a level of EINOx = 8.5, which was modestly higher than observed with either circular-hole quench designs. The CO was center-peaked with EICO = 10.5 on the centerline and decreasing to EICO = 1 at a radius 80 pct to the combustor wall. The ganged sample registered EICO = 3 which corresponded to a combustion efficiency greater than 99.9 pct.

The use of multiple-diameter quench-jets was intended to promote quench zone mixing by introducing the multiple length scales associated with the diameters and penetrations. As presented in Table IV-3, the smallest and largest holes were predicted to penetrate 15 pct and 38 pct, respectively, of the quench radius. In contrast, both circular-hole designs were predicted to penetrate 50 pct of the quench radius. The CO data for the multihole configuration suggested that the quench air efficiently oxidized the rich zone species in the outer regions of the flow, but was less effective near the centerline. This was consistent with the predicted quench-jet penetrations. Similar behavior was also observed for tests performed at Scaled-SSC.

While the level of measured NOx indicated a slightly less effective quench process for the multihole design, the NOx profile did not reflect the reduced quench-jet penetration; the profile was relatively uniform. This result indicated that the multihole design was a good mixer, but not an improved NOx quencher. The existence of a CO profile did not contradict this assessment as its presence reflected less than 1 pct of the CO entering the quench.

Figure VI-17 presents NOx data obtained for P3, T3, and F/AOA parametric variations from SSC for the flametube-scale RQL combustor configured with

the multihole quench. These data were analyzed to determine whether they fit the correlation previously developed from data with the slanted-slot quench. The F/AOA variation was achieved in a ØR-Signature variation, but it was assumed that ØR was not a significant factor in the exit NOx emissions. The limited NOx variation with P3 was fit to a power-law:

$$EINOx = a * P3^{n}$$

with n = 0.64. This value was equivalent to that determined for the slanted slot quench. The NOx response to the T3 and F/AOA parametrics was determined by fitting the data to the exponential dependencies:

$$EINOx = u * P3^{0.64} * \exp(v * T3 + w * ØL)$$

where u, v, and w were constants and the units of T3 = R. Analyses to fit this form yielded values:

$$v = 0.0010, \quad w = 2.3$$

for a fit with $R^2 = 0.94$ or a standard error for predicted EINOx of 0.3. Corresponding constants for the slanted-slot quench data were:

$$s = 0.0016, \quad t = 1.4.$$

Both of the constants for the multihole quench configuration were substantially different from the values determined for the slanted-slot quench. The multihole displayed a reduced dependence on T3 and a greater dependence on ØL. However, the ranges of T3 and ØL variation used for the multihole correlation was very limited and should not be used to extrapolate the NOx response far from SSC. Additional data would be required to extend the correlation if this quench concept was to be evaluated at other conditions.

NOx/CO Emissions at Part-Power Conditions

Candidate RQL Control Strategy

Operation of the RQL combustor at part-power conditions, which for the purposes of this study relates to operation at any non-SSC condition, requires a control strategy that minimizes emissions and maximizes performance over a range of power settings. A major hurdle in the development of a possible control strategy is managing the rich combustor equivalence ratio to avoid near-stoichiometric conditions and excessive temperatures. Operation under these conditions would produce unacceptably-high levels of nitric oxides and impose extreme challenges in the development of a suitable rich liner material.

A candidate control strategy was identified that required minimal variation of the distribution of combustor airflow by means of variable geometry. At low power conditions, such as Idle, CO and UHC formed in a rich combustor would be frozen by the quench mixer and, because of the low lean combustor operating temperature, contribute to high levels of inefficiency. At these power conditions, it would be desirable to operate the combustor in a lean-lean mode At high power conditions, the NOx emission control capability of the RQL combustor strategy would be desired. While a fixed geometry

combustor could achieve the airflow distribution to globally satisfy these desires, it would result in a considerable portion of the operation cycle with near-stoichiometric values for ØR. Some degree of airflow redistribution was required to minimize such operation.

The candidate operating schedule, shown in Fig. VI-18, was based on a fixed airflow distribution at low power passing through ØR = 0.8 at Idle, and a variable airflow distribution to maintain the SSC design value of ØR = 1.8 at high power conditions. On the graphical relationship between ØR and F/AOA shown in the figure, the low power operation translates to a straight line passing through the origin, while the high power operation is represented by the horizontal line denoting ØR = constant. As a consequence of satisfying the Idle and SSC values for ØR, the two line segments intersect at F/AOA = 0.020.

The definition of the HSCT combustor cycle conditions and the candidate part-power operating schedule set the value of ØR and airflow split (S) for each condition. Table VI-9 displays these stoichiometries for the conditions defined in Table VI-1. The second portion of Fig. VI-18 graphically displays the variation of S over the engine cycle as represented by F/AOA.

Table VI-9 Part-Power Stoichiometries

Condition	F/AOA	ØR	S
Idle	0.0090	0.8	0.16
15 pct	0.0090	0.8	0.16
34 pct	0.0112	1.0	0.16
65 pct	0.0175	1.5	0.16
Sea-Level Takeoff (SLTO)	0.0373	1.8	0.30
Subsonic Climb (SuCl)	0.0402	1.8	0.33
Supersonic Cruise (SSC)	0.0300	1.8	0.24
Subsonic Cruise (SuC)	0.0139	1.2	0.16
Supersonic Climb (SSCl)	0.0318	1.8	0.26

Part-power tests conducted using the flametube-scale RQL combustor focused on four of these engine cycle conditions: Idle, 34 pct, 65 pct, and SuCl. Really these four conditions represented other conditions as well because of similarity in the values of F/AOA and UREF. That is, the paired conditions of Idle and 15 pct, 34 pct and SuC, and SuCl and SLTO were similar. For each of the four operating conditions, parametric variations in ØR for a constant F/AOA (i.e. ØR-Split parametric) were performed which spanned the nominal ØR values for the paired conditions, and provided data to define alternative control strategies which avoided the near-stoichiometric conditions. These studies were performed for combustor assemblies using either the eight slanted-slot quench or the eight circular-hole quench . This

section of the report presents the findings from these part-power studies. The results are organized according to the quench configuration.

Part-Power Emissions Using the Slanted-Slot Quench

Idle Operation

Combustion tests were performed at the Idle condition for values of ØR which were either less than unity (lean-lean combustion mode) or greater than unity (rich-lean combustion mode). The former range was consistent with the candidate control strategy defined above, while the latter was an attempt to assess a strategy which always kept the first combustion zone fuel-rich and thereby never experience stoichiometric conditions. The flametube-scale RQL combustor was configured to include an 8-in. long cylindrical rich combustor and a 3-in. long cylindrical lean combustor.

Figure VI-19 presents the NOx and CO emission indices for ganged-sample concentrations measured at the combustor exit when operating in the lean-lean mode. They are shown as functions of the rich combustor equivalence ratio as determined by a ØR-split parametric. As shown, both NOx and CO increased as the rich zone stoichiometry increased from ØR = 0.5 to 0.8. NOx values ranged from EINOx = 5 to 12, while CO increased from EICO =1.5 to nearly 10.

While operating at Idle, the lean combustor bulk temperature was approximately TL = 1050 F. This level was too low to significantly promote either CO oxidation or NOx formation; the quench mixer froze the rich combustor effluent. Hence, these results were representative of emissions levels generated in the rich combustor as diluted by the quench airflow. The dilution effect was automatically included in the data by using the emission index format.

The CO levels measured at Idle were marginally above the calculated equilibrium values shown on the figure and consequently the combustion efficiency was always greater than 99.9 pct. Such a high level of CO burnout was expected at the long residence time of 12 ms in the rich combustor at ØR = 0.6 because of the low value of S. In contrast, the NOx levels were higher than typical for a combustor at Idle because of this high residence time. Measured unburned hydrocarbon emissions were insignificant and the Smoke Number was less than unity throughout the lean-lean Idle tests.

An alternative control strategy considered was to always operate the RQL combustor in a rich-lean mode to avoid transitioning through ØR = 1. Figure VI-20 presents the NOx and CO emission indices for ganged-sample concentrations measured at the combustor exit when operating in the rich-lean mode. They are shown as functions of the rich combustor equivalence ratio as determined by a ØR-split parametric. The NOx values were lower

then those measured during the lean-lean mode and ranged from EINOx = 3 to 4 for ØR values between 1.28 and 1.45. The corresponding CO levels were very high and increased from EICO = 105 to 125.

As for the lean-lean Idle tests, the low value of TL promoted neither NOx formation nor CO oxidation in the lean combustor for a rich-lean operation. While the quench process attempted to freeze the rich combustor effluent, the non-ideal quench process did permit some oxidation. Therefore, the measured NOx levels were very low because the rich combustor was fuel-rich, but they were non-zero because of NOx formation in the non-ideal quench. If the quench froze the rich combustor CO at near-equilibrium levels, then EICO > 1000 would have been obtained. The oxidation processes occurring in the quench reduced the CO by approximately one order-of-magnitude. While this vigor may be adequate to achieve low CO at other operating conditions, it was not sufficient to achieve acceptable Idle emissions. The level of combustion efficiency associated with EICO = 125 was only 97.1 pct.

Based on these emissions results, and the Idle LBO ØR = 0.4 value discussed previously, lean-lean operation at Idle for ØR = 0.6 would ensure moderate emissions output and significant stability margin.

34 pct Operation

The operating schedule shown in Fig. VI-18 and detailed in Table VI-9 indicated that the value of ØR would be near unity for operation at 34 pct. The obvious undesirability of this condition led to RQL combustor tests for both lean-lean and rich-lean modes to avoid it. For the former mode, ØR ranged from 0.5 to 0.8, while for the latter mode, it ranged from 1.4 to 1.6. The flametube-scale RQL combustor was configured to include an 8-in. long cylindrical rich combustor and a 3-in. long cylindrical lean combustor.

Figure VI-21 presents the NOx and CO emission indices for ganged-sample concentrations measured at the combustor exit when operating in the lean-lean mode. They are shown as functions of the rich combustor equivalence ratio as determined by a ØR-split parametric. As shown, both NOx and CO increased as the rich zone stoichiometry increased from ØR = 0.5 to 0.8. NOx values ranged from about EINOx = 5 to 23, while CO increased from EICO =0.5 to 5.

The data corresponding to operation at 34 pct power were acquired for F/AOA = 0.0110 and 0.0124. The corresponding lean combustor bulk temperature was approximately 1400 F. As for the Idle condition, this level was too low to significantly promote either CO oxidation or NOx formation in the lean combustor. Unlike the lean-lean Idle results, however, the CO levels at 34 pct power indicated that oxidation did occur in the quench transition, particularly for ØR > 0.7. That is, the measured CO levels were less than the computed equilibrium levels corresponding to ØR as shown in the figure. For example,

the equilibrium level corresponding to ØR = 0.75 was EICO = 10 but the measured level was EICO = 5.

The oxidation of CO in the quench was a result of the degradation of the quench effectiveness for the lean-lean operation. The operating schedule described above would achieve S = 0.16. However, in setting ØR =0.7, the airflow split increased to S = 0.23, with a corresponding reduction of J from 38 to 15. The reduced vigor of the quench permitted local oxidation processes to continue. The combination of lean-lean operation and continued oxidation resulted in low CO emissions and a corresponding combustion efficiency of 99.9 pct. Unburned hydrocarbon emissions and exhaust Smoke Numbers were insignificant for all lean-lean operation at 34 pct power. Lean-lean operation near ØR = 0.65 achieved EINOx = 14.

Testing at 34 pct power was also conducted for rich-lean operation, consistent with a control strategy that would retain fuel-rich operation throughout the entire power curve. NOx and CO emissions data acquired for ØR =1.4 to 1.6 are presented in Fig. VI-22. The results were similar to those obtained at the rich-lean Idle condition; NOx levels were lower and CO much higher than for lean-lean operation. In particular, EINOx = 4 and EICO = 69 at ØR = 1.4. Again the CO level was high because of the partial quenching of the rich combustor concentrations, but well below the calculated equilibrium level for that combustor because of oxidation in the quench. The level of combustion efficiency associated with EICO = 69 was only 98.3 pct.

65 pct Operation

The candidate operating schedule specified a value of ØR = 1.5 for operation at 65 pct power. Tests were performed using a ØR-split parametric to document the effect of alternative ØR settings while retaining a rich-lean combustion mode. The flametube-scale RQL combustor was configured to include an 8-in. long cylindrical rich combustor and a 3-in. long cylindrical lean combustor.

NOx and CO emissions data were acquired over the range of ØR = 1.4 to 1.9. As described previously, significant variations of J and TAUR can be experienced in ØR-split parametrics. The calculated values for two ØR in the test range are tabulated in Table VI-10. As indicated, the momentum ratio nearly doubled with the increase in ØR by reduction of S.

Table VI-10 ØR-Split Variation at 65 pct

Parameter	Unit	ØR-1	ØR-2
P3	psia	120	120
T3	F	800	800
ØR	---	1.4	1.8
F/AOA	---	0.018	0.018
UREF	ft/s	78	78
S	---	0.182	0.142
TR	F	3690	3150
TAUR	msec	14	21
J	---	34	69
TL	F	1870	1870
TAUL	msec	2.8	2.8

The measured NOx and CO concentrations were relatively insensitive to changes in the rich zone equivalence ratio achieved in the ØR-split parametric (Fig. VI-23), with levels of EINOx = 5 and EICO = 13. The corresponding combustion efficiency was 99.7 pct.

As was the case with the data acquired at the SSC condition, the insensitivity of the exhaust emissions at 65-pct power indicated that competing processes were occurring in the quench. That is, while an increased quench vigor would be expected for the higher J values at higher ØR, the NOx was not lower. Among the possible explanations for not achieving lower NOx could be that the quench jets over-penetrated at the high J and no benefit resulted. Alternatively, while the quench was more vigorous, the range of stoichiometries to be spanned in reaching F/AOA was greater. While the fuel-air ratio range important for NOx production was likely restricted to values near stoichiometric, the probability of encountering it for a longer time was increased for the wider transition.

Similarly, the more vigorous quench did not significantly produce either higher or lower CO. The higher J achieved with higher ØR could be expected to produce greater CO in the rich combustor. A vigorous quench would promote CO oxidation by intimately mixing the quench airflow into the rich combustor products, assuming the mixture temperature did not retard the oxidation kinetics. Alternatively, a less vigorous quench could sustain local regions which promoted higher oxidation rates.

Neither the detail nor the trend of the NOx and CO data were sufficient to substantiate the dominant process. Detailed studies of the reacting, quench mixing process are required to clarify the trade-offs occurring in this component. Nevertheless, low emissions levels were achieved for this RQL

combustor configuration, and the insensitivity of the emissions to airflow split was a desirable feature to ease the precision of the combustor control.

Subsonic Climb Operation

NOx and CO emissions levels were studied at Subsonic Climb (SuCl), the condition with the highest values of F/AOA and combustor heat release. Data were obtained for a range of ØR = 1.8 to 2.5 during a ØR-split parametric to document the effect of alternative ØR settings while retaining a rich-lean combustion mode. The flametube-scale RQL combustor was configured to include an 8-in. long cylindrical rich combustor and a 3-in. long cylindrical lean combustor.

The measured NOx and CO emissions from ØR-split parametric tests are presented in Fig. VI-24. As shown, NOx emissions were constant at a nominal value of EINOx = 5, similar to the results at the 65 pct power condition. Again, the insensitivity to combined ØR and J variations suggested that competing processes were occurring in the quench.

Generally, the CO concentrations were very high with a range of EICO = 80 to 130. The CO data minimized near ØR = 2.2, with higher levels for either leaner or richer operation. This trend suggested that increasing vigor in the quench process benefited CO oxidation up to ØR = 2.2 by achieving a more intimate mixing of the rich products and the quench airflow. Beyond this value of ØR, the continuously increasing CO concentration from the rich combustor overwhelmed the oxidation process and the exhaust CO increased. The combustion efficiency at the minimum CO value was only 98 pct. At this condition, individual probe samples indicated that the exhaust CO profile was center-peaked; the concentrations on the centerline were 10 times greater than the average of the other five samples. Hence, improvements to the quench mixing process should achieve lower CO and higher efficiencies.

Unlike other operating conditions, the Smoke Number was significant at the Subsonic Climb condition (Fig. VI-24). Measurable smoke was detected for ØR = 1.8 and increased to SN = 15 at ØR = 2.4. This trend was consistent with the behavior of the CO emissions.

As described previously, the combustor experienced a rich blowout at ØR = 2.5. This result was consistent with values for a well mixed system.

Part-Power Emissions Using the Eight Circular-Hole Quench

Combustion tests were performed with the flametube-scale RQL combustor configured with an eight circular-hole quench at several part-power operating conditions. Primarily, data were acquired at the exit of the flametube-scale RQL combustor to compare the emissions control achieved with these quench designs to that achieved with the slanted-slot quench. Samples from

either the individual or ganged probes were analyzed. Limited data were also acquired from samples extracted during a traverse across a flow diameter in a plane 2.3 in. downstream of the quench-jet centerline. This plane was approximately in the middle of the conical transition to the lean combustor where the flow had expanded from the 3.0-in ID quench to a 3.25 in. diameter These two types of data are presented and discussed in the following sections.

Combustor Exit Emissions

Idle Operation

Combustion tests were performed at the Idle operating condition with flametube-scale RQL combustor containing the cooled, eight circular-hole quench to determine the effectiveness of this quench configuration at controlling emissions when operating with ØR greater than one (i.e. rich-lean combustion mode). For these tests ØR ranged from 1.25 to 1.6 during a ØR-split parametric to document the effect of alternative ØR settings while maintaining a constant FAOA. No lean-lean Idle combustion tests were performed with this configuration. The flametube-scale RQL combustor was configured to include a 4-in. long cylindrical rich combustor and a 3-in. long cylindrical lean combustor.

Ganged sample concentrations of NOx and CO emissions as measured at the combustor exit are shown in Fig. VI-25 as functions of the rich combustor equivalence ratio as determined by a ØR-split parametric. NOx levels were slightly lower than those obtained for the slanted-slot quench and ranged from EINOx = 1.7 to 2.7 for ØR values between 1.25 and 1.55. EICO levels increased from 150 to 190, approximately 50 pct higher than those measured for the slanted-slot quench. This increase was consistent with the enhanced quenching behavior displayed by this quench configuration during SSC testing.

As previously described for rich-lean Idle with the slanted slot quench, the emission levels obtained for the eight circular-hole quench during rich-lean Idle operation was attributed to an effective, but non-ideal, quench process. That is, the process limited NOx formation but did not completely freeze the rich combustor effluent; some NOx formation and CO oxidation did occur. Although the CO was reduced significantly below the rich combustor equilibrium value, an EICO = 190 corresponded to an unacceptable efficiency of only 95.6 pct. Based on tests with the slanted-slot quench, it appeared that a lean-lean Idle mode would be required to attain an acceptable efficiency level.

Subsonic Climb Operation

Emissions levels for combustion tests using the cooled, eight-circular hole quench at the Subsonic Climb (SuCl) condition were obtained for a range of ØR = 1.6 to 2.5 during a ØR-split parametric to document the effect of alternative ØR settings while retaining a rich-lean combustion mode. The

flametube-scale RQL combustor was configured to include a 4-in. long cylindrical rich combustor and a 3-in. long cylindrical lean combustor.

The changes in combustor parameters for a ØR-split variation at SuCl are depicted in Table VI-11. For this condition the lean combustor always operated with a high level of TL and high oxidation rates of CO were expected. Because of the high value of F/AOA, the flow split was high producing very low values of J. As ØR increased, J increased but always remained at a relatively low value.

Table VI-11 ØR-Split Variation at Subsonic Climb

Parameter	Unit	ØR-1	ØR-2	ØR-3
P3	psia	104	104	104
T3	F	660	660	660
ØR	---	1.6	2.0	2.2
F/AOA	---	0.040	0.040	0.040
UREF	ft/s	59	59	59
S	---	0.365	0.292	0.265
TR	F	3330	2800	2530
TAUR	msec	5	7	9
J	---	5	11	15
TL	F	2940	2940	2940
TAUL	msec	2.2	2.2	2.2

The NOx and CO levels obtained at this cycle condition are shown in Fig. VI-26. NOx concentrations were relatively constant at a nominal value of EINOx = 3.8, 30 percent lower than the levels obtained with the slanted slot quench at the SuCl condition. As with the slanted slot configuration, the constant NOx emissions obtained for various ØR-split parametrics indicated competing processes occurring in the quench as discussed earlier.

CO levels were significantly lower than those obtained with the slanted-slot quench and ranged from EICO = 10 to 55. The CO data maximized near ØR = 2.0, with lower levels for either leaner or richer operation. This trend was opposite that observed with use of the slanted-slot quench. In that case, a CO minima was observed which was interpreted as a competition of increasing rich combustor CO production but also increasing J with ØR, and the expected high CO oxidation in the lean combustor. In that case, CO ultimately rose because the lean combustor was overwhelmed by the rich combustor CO because the mixing was inefficient; if perfectly mixed, the high TL could oxidize it. The fall-off in CO for ØR > 2 with the eight circular-hole quench can only be explained by an increased mixing efficiency with the holes as compared to the slanted-slot, allowing the increase in J to compensate for the greater rich combustor CO. For he highest level, EICO = 55, the combustion

efficiency was 98.7 pct, but the efficiency increased to 99.7 pct for an EICO = 10. As compared to the slanted-slots, the eight circular-hole configuration provided better quench mixing, lower emissions, and higher efficiencies for this cycle condition.

Sea-Level Takeoff Operation

NOx and CO concentrations were acquired using the cooled, eight circular-hole quench at the Sea-Level Takeoff (SLTO) condition to determine the emissions control at this power setting. For these tests ØR ranged from 1.6 to 2.2 during a ØR-split parametric to document the effect of alternative ØR settings while retaining a rich-lean combustion mode. The flametube-scale RQL combustor was configured to include a 4-in. long cylindrical rich combustor and a 3-in. long cylindrical lean combustor.

Ganged sample concentrations of CO and NOx measured at the lean combustor exit are presented in Fig. VI-27. NOx emissions, constant at a nominal value of EINOx = 4 over the ØR span, nearly duplicated the concentration and trend observed at the SuCl condition. Again, the insensitivity of NOx to ØR reflected the competition between increased quench vigor associated with higher J values and the stoichiometry.

In the range from ØR = 1.6 to 2.0, CO concentrations showed little variation around a level of EICO = 10. However, at ØR = 2.2 the CO level increased to EICO = 26, twice the concentration recorded at ØR = 2. The trend indicated that the increased quench vigor promoted CO oxidation in the lean combustor up to a ØR = 2. Beyond this value, the increasing CO generated in the rich combustor overwhelmed the oxidation process and the exhaust CO increased. The efficiency corresponding to an EICO = 10 is 99.8 pct.

Smoke levels measured at the Sea-Level Takeoff condition were negligible at ØR = 1.8 but increased to SN = 10 at ØR = 2.2. This trend was consistent with the behavior of the CO emissions. These smoke numbers are comparable to those obtained for the slanted-slot quench configuration operating at Subsonic Climb, a condition with greater lean combustor oxidation.

Quench Exit Emissions

Quench exit emissions at part power conditions were acquired in the same manner detailed earlier for SSC. Samples, extracted following the procedures described in Section IV, were obtained in tests at Idle, SuCl and SLTO using the cooled, eight circular-hole quench. All data were acquired during a ØR-split parametric to document the effect of quench jet penetration while holding F/AOA constant. This was a different process than used for the quench traverse test conditions at SSC which held ØR, and hence the rich combustor composition, constant. For these part-power tests, the overall condition was held constant while the split was altered to achieve different

values of ØR and S. The combustor was configured to include the 4-in. long cylindrical rich combustor and the 3-in. long cylindrical lean combustor. For each of these three part power conditions, the sample compositions were fuel-lean as denoted by always containing greater than 4 pct oxygen. The measured oxygen levels were consistent with F/AOA and with the locally-determined emissions-based fuel-air ratio.

Idle

Data from a flow traverse during rich-lean Idle tests with ØR = 1.3 and 1.6 are shown in Fig. VI-28; the flow centerline is at the 1.6-in. location. Corresponding to these conditions were values of J = 105 and 150, respectively, which were very high because of airflow split S < 0.1. The centerline emissions-based fuel-air ratio was highly depressed below the nominal F/AOA = 0.009 for both ØR conditions. These profiles reflected the expected over-penetration of the quench jets for the very high values of J.

CO concentrations were not symmetric about the flow centerline with levels 12 to 20 percent lower on one side of the combustor. On either side of the flow centerline, the values were insensitive to the sampling location. CO levels were suppressed at the lower J (higher S) condition, but this was attributed to reduced CO generation at the lower ØR. Again, the CO values for either ØR condition were significantly below the rich combustor equilibrium levels but comparable to those measured at the combustor exit (Fig. VI-25). This indicated that CO was substantially oxidized in the quench up to the traverse location, but TL was too low for the lean combustor to achieve further oxidation.

NOx emission levels at Idle were insensitive to sampling location and had values of EINOx = 1.5 and 2.3 for ØR = 1.6 and 1.3, respectively. The slightly lower NOx concentration at ØR = 1.55 was attributed to a more vigorous quench at this condition. The NOx values for either ØR condition were comparable to those measured at the combustor exit (Fig. VI-25), indicating that the NOx was formed in the quench with no additional formation in the lean combustor.

Subsonic Climb Operation

Data recorded from a quench exit traverse at the SuCl condition for a range of ØR from 1.6 to 2.5 are illustrated in Fig. VI-29. Representative conditions for this span were indicated in Table VI-10 which illustrated the low values of J and high value of TL for these test conditions. Despite being at low J levels, increased quench-jet penetration suppressed the emissions-based fuel-air ratio and EICO near the flow centerline; the CO reduction occurred despite an increasing rich combustor concentration with the higher ØR. This trend was consistent with the increased mixing efficiency hypothesis presented with combustor exit emissions data. At the nominal SuCl condition defined in

Table VI-9, the fuel-air profile was center-peaked and it was depressed at the higher J condition. The CO was center-peaked for all conditions except that with the highest J; some non-symmetry was evident in the data.

The NOx profile was slightly center-depressed for all ØR-split parametrics. Levels ranged from EINOx = 0.5 to 2.5; approximately 40 pct of the levels measured at the combustor exit. This indicated that the lean combustor also contributed to NOx formation, a plausible occurrence because of the high level of TL.

As with the SSC quench traverse results explained earlier, the center-peaked CO and center-depressed NOx emissions profiles at this condition could not simply be explained by under-penetrating quench jets.

Sea-Level Takeoff Operation

Figure VI-30 shows quench exit emission data from traverses during ØR-split tests at the SLTO condition for values ØR = 1.6 to 2.5. The results were similar to those acquired at SuCl where increased jet penetration suppressed the emissions-based fuel-air ratio and EICO, even though CO generation was increasing. At the nominal SLTO condition the fuel-air profile peaked near the flow centerline, but it was slightly center-depressed at the maximum J. CO was center-peaked throughout the span of ØR-split variations and centerline values ranged from EICO = 200 to 900. These levels were significantly greater than those measured at the combustor exit indicating that the majority of CO oxidation occurred in the lean zone. This could be the result of a low J (J = 10 for ØR = 1.8) and lower mixture temperature in the quench than for the SuCl condition. However, quench exit CO concentrations did respond to increased quench vigor, and were 4.5 times lower for the highest J condition than for the nominal J.

As with the SuCl condition, the NOx profile at SLTO was slightly center-depressed with values ranging from EINOx = 1.5 to 3; 60 pct of the concentration obtained at the combustor exit.

Again, the quench exit emissions profiles obtained at SLTO did not conform with a simple under-penetrating jet representation and further studies which focus on the quench process should be performed.

RQL Combustion Test Summary

Combustion tests were performed using the flametube-scale RQL combustor described in Section IV to assess its performance and emissions control characteristics. Tests were performed at HSCT engine cycle operating conditions and at parametric variations from them. The test variables also included geometrical variations to achieve different residence times in the rich and lean combustors, and variations in the quench-jet configuration.

The primary data were analyses of emissions samples extracted from the exit of the lean combustor; limited analyses of samples from the exit of the rich combustor or the quench section were also performed.

Extensive combustor testing was performed at the Supersonic Cruise (SSC) condition of a HSCT engine cycle. Data obtained with a slanted-slot quench configuration were correlated to described the NOx emission response to changes in inlet air pressure or temperature, and lean-combustor equivalence ratio and residence time. The dependence determined for pressure was typical for thermal NOx, while the dependence on stoichiometry was best represented by a combination of the inlet temperature and lean equivalence ratio; this combination was not equal to the lean combustor temperature. This hybrid representation was interpreted to reflect a combination of diffusion combustion during the transition from fuel-rich to fuel-lean conditions in the quench, and premixed combustion in the high-temperature lean combustor downstream of the quench. The residence time in the lean combustor influenced the NOx emissions, but the effectiveness of the quench process was the dominant influence on the level of NOx at the combustor exit. Neither the rich-combustor equivalence ratio (ØR) nor its residence time was a direct contributor to the exit NOx; near-equilibrium specie concentrations exit the rich combustor. The CO and smoke emissions were very low at SSC, even for a short lean-combustor residence time, with combustor efficiencies typically exceeding 99.9 pct.

Test results with alternative quench configurations demonstrated the importance of the quench-jet penetration in controlling the combustor emissions. Circular-hole quench configurations, which produced rapidly-, highly-penetrating jets, were more effective at limiting NOx. NOx data acquired near, and corrected to, the SSC condition with an eight, circular-hole quench were at the HSCT program goal of EINOx = 5.

Data obtained from probe traverses near the quench exit confirmed that the quench section was the critical component in controlling combustor emissions. At the SSC condition, 60 to 70 pct of the exit NOx was formed in the quench; 99 pct of the CO entering the quench was oxidized by its exit. The spatial profiles of NOx and CO at the quench exit were not directly interpretable using a simple flow model based on quench-jet penetration, and a greater understanding of the flow and chemical processes in this section are required to optimize it.

Combustion tests were performed at selected part-power operating conditions of a HSCT engine cycle following a candidate schedule to control ØR. In particular, data were acquired to assess the performance and emissions for this candidate schedule and alternatives to it which imposed ØR values more favorable for emissions control, combustor durability, and combustor air redistribution. At lower power conditions, it was determined that the desirable combustor mode was lean-lean, with a rich-lean mode at higher power. The lean-lean mode was required because the lean combustor was

ineffective at oxidizing CO frozen in the quench section; unacceptable combustion inefficiencies were achieved at low power in the rich-lean mode. Quench configurations which demonstrated enhanced emissions control at SSC also performed better at part-power conditions. Data from quench exit traverses reflected the expected quench-jet behavior for off-design quench-jet to crossflow momentum ratios.

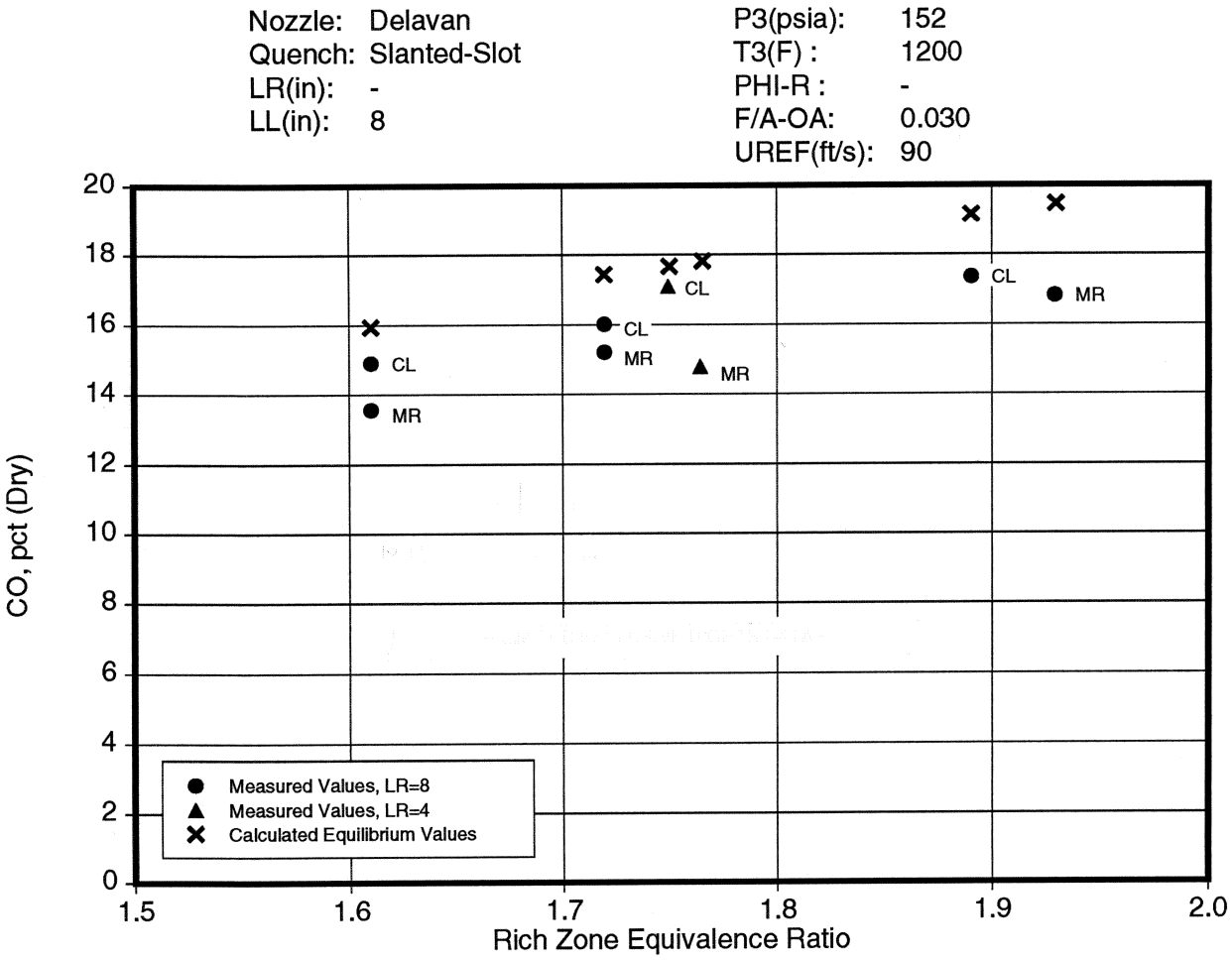

Figure VI-1 -- Rich Combustor CO

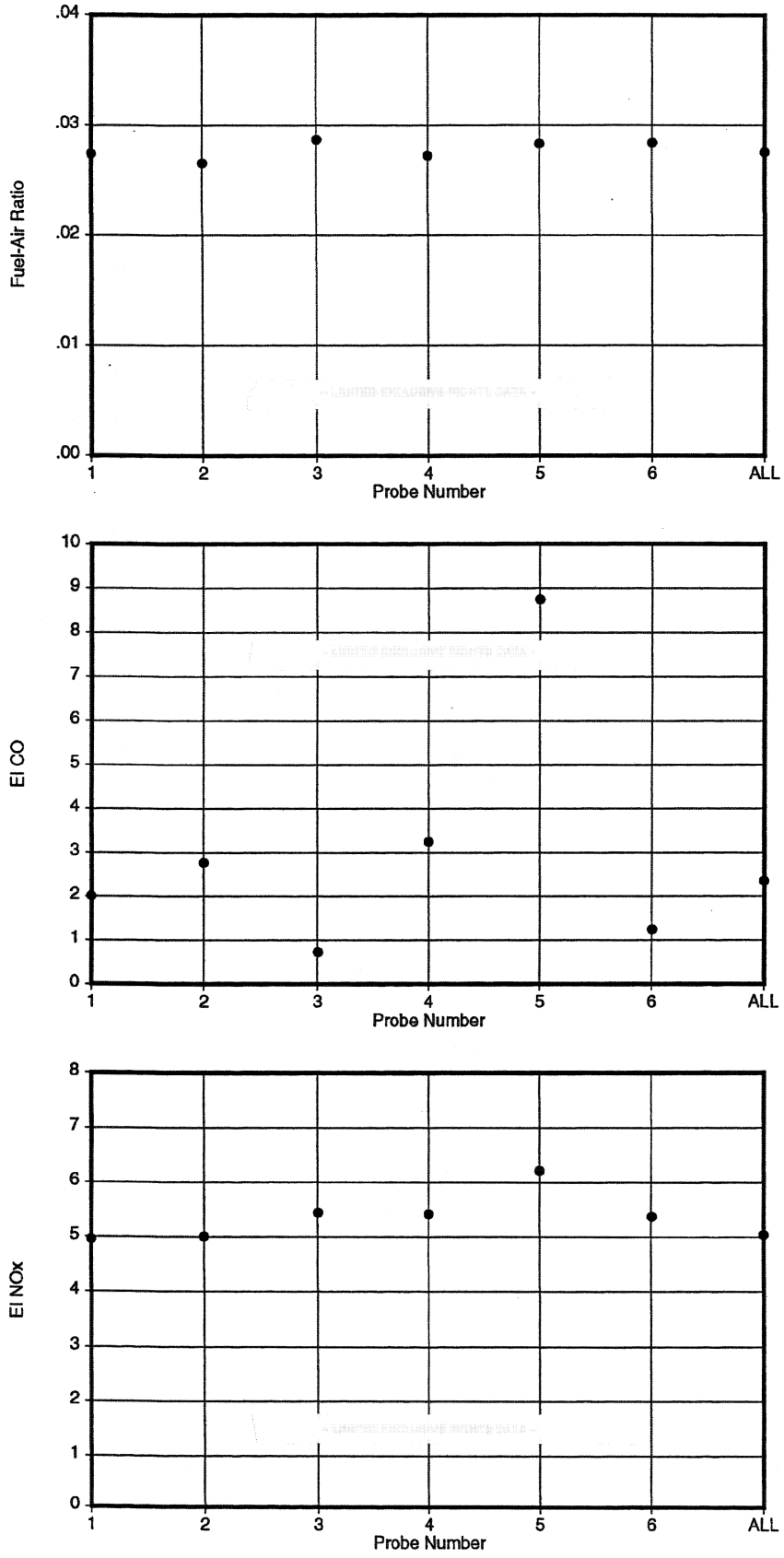

Nozzle: Delavan
Quench: Slanted-Slot
LR(in): 8
LL(in): 8

P3(psia): 118
T3(F) : 900
PHI-R : 1.8
F/A-OA: 0.028
UREF(ft/s): 90

Figure VI-2 -- Emission Profiles at Scaled SSC with Slanted-Slot Quench

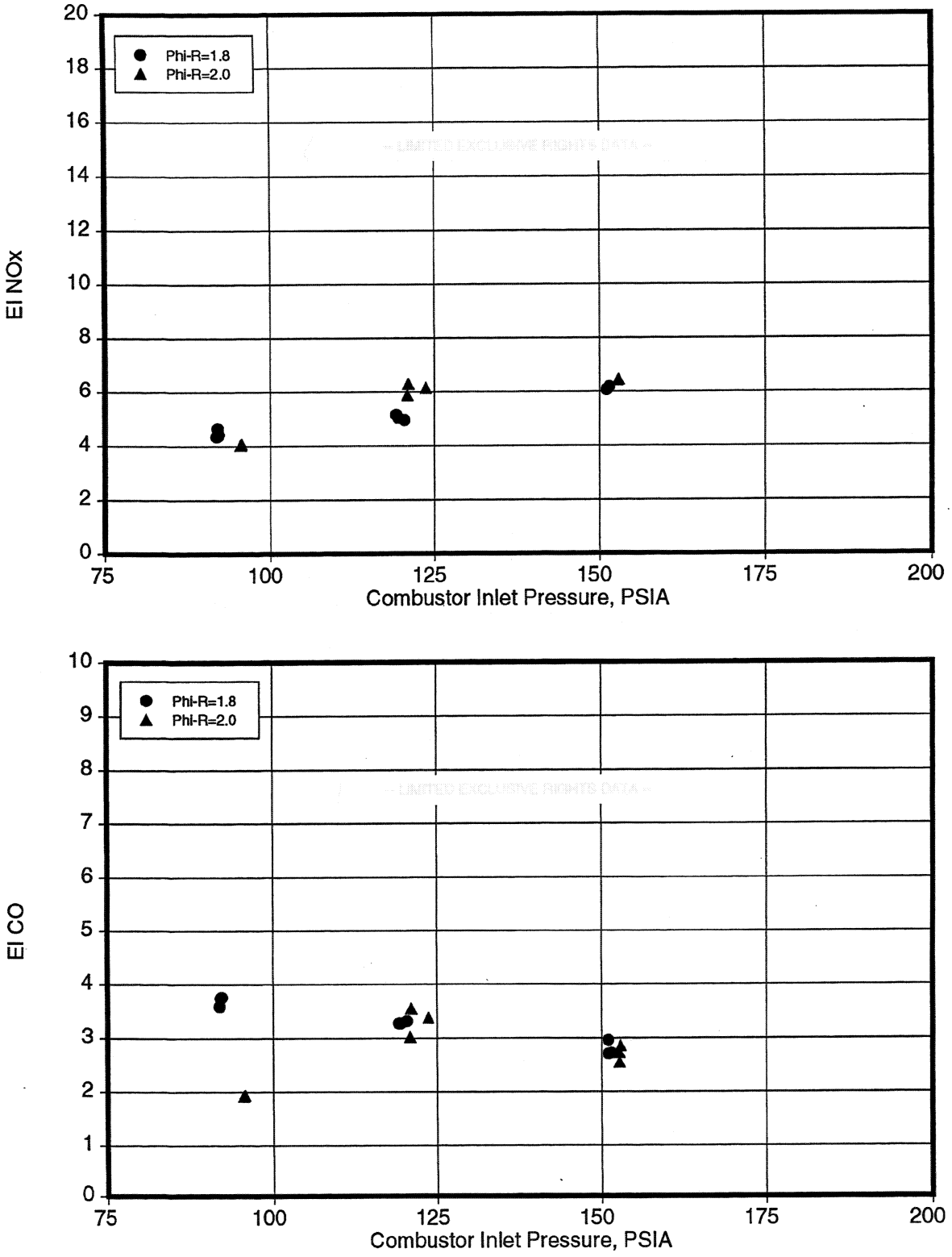

Figure VI-3 -- NOx and CO Responses to Pressure with Slanted-Slot Quench

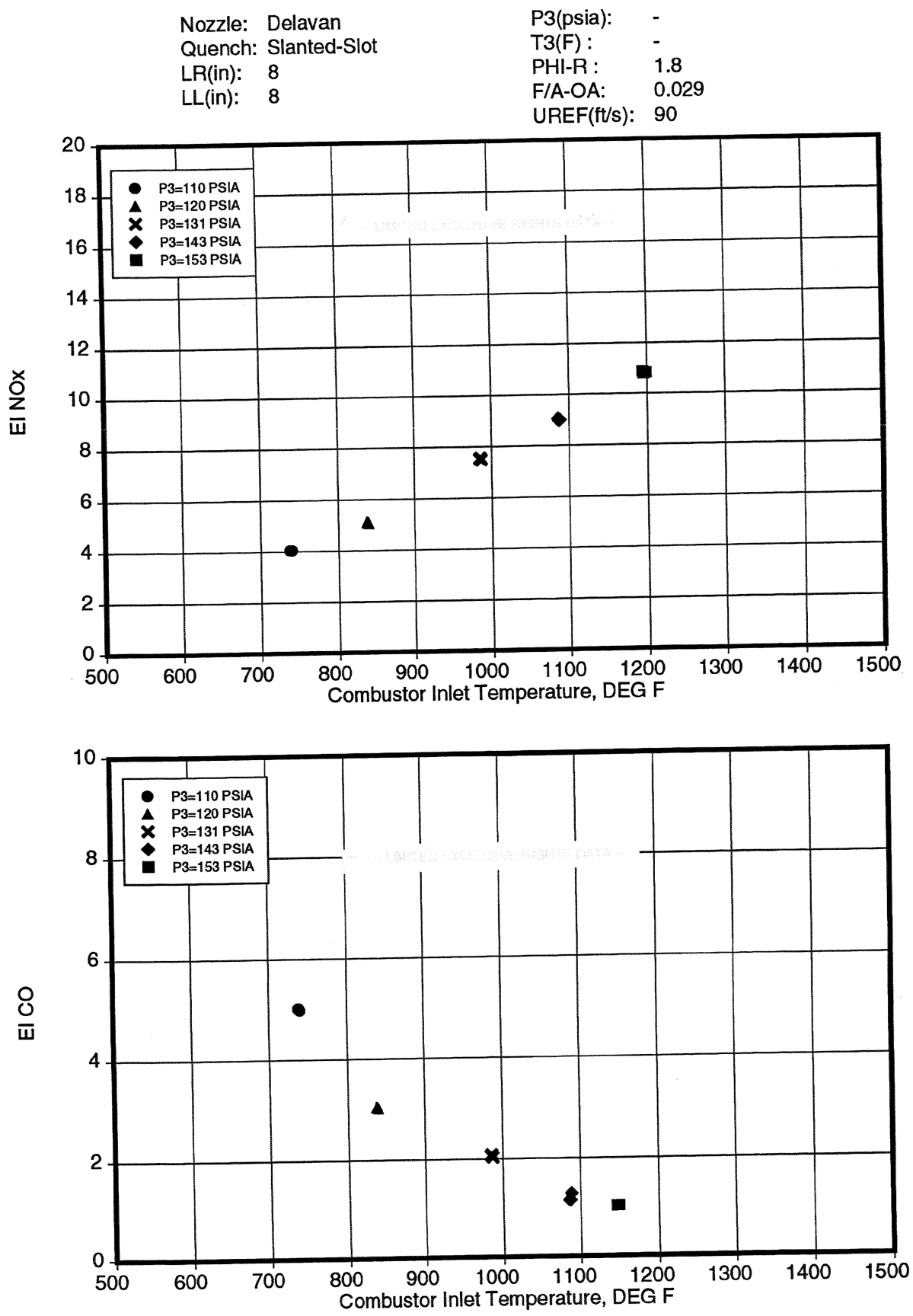

Figure VI-4 -- NOx and CO Responses to Inlet Temperature with Slanted-Slot Quench

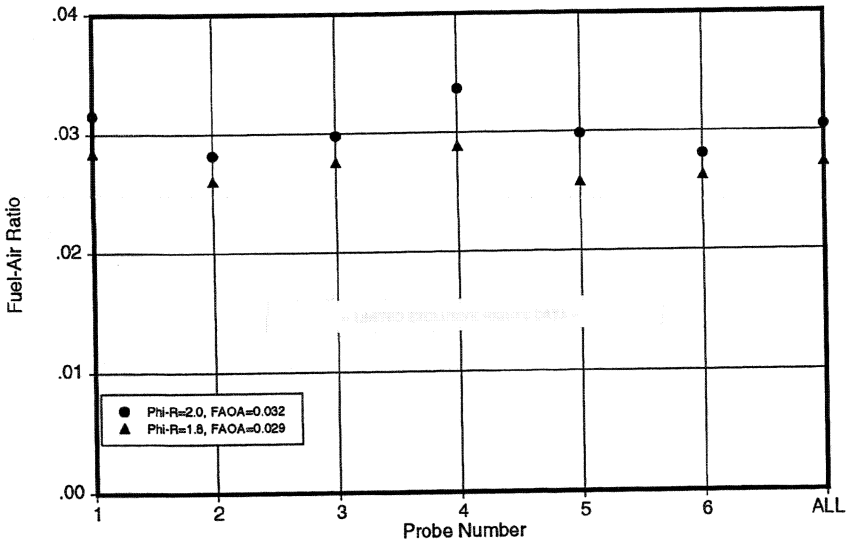

Nozzle:	Delavan
Quench:	Slanted-Slot
LR(in):	8
LL(in):	8
P3(psia):	150
T3(F) :	1183
PHI-R :	-
F/A-OA:	-
UREF(ft/s):	90

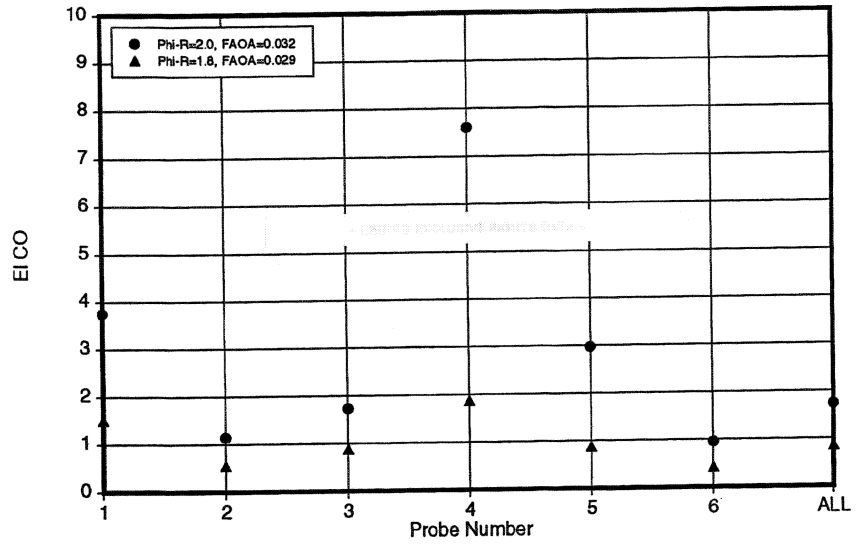

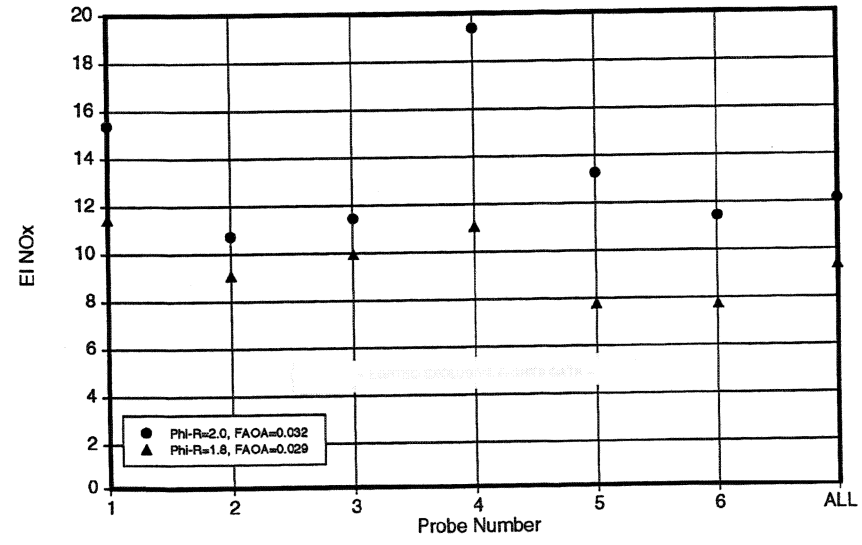

VI-5 -- Emission Profiles with Slanted-Slot Quench at SSC

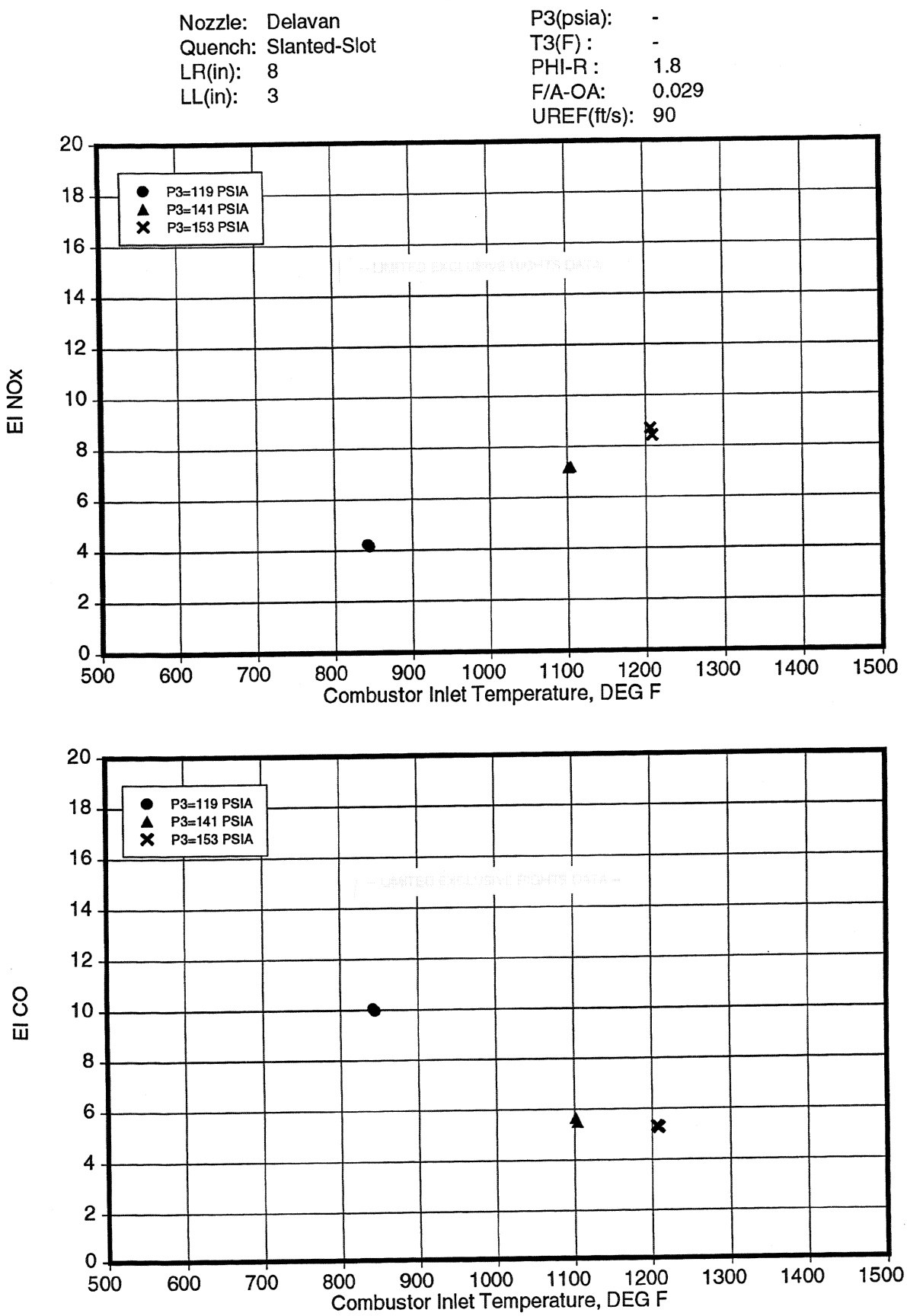

Figure VI-6 -- NOx and CO Responses to Inlet Temperature for Shortened Lean Combustor with Slanted-Slot Quench

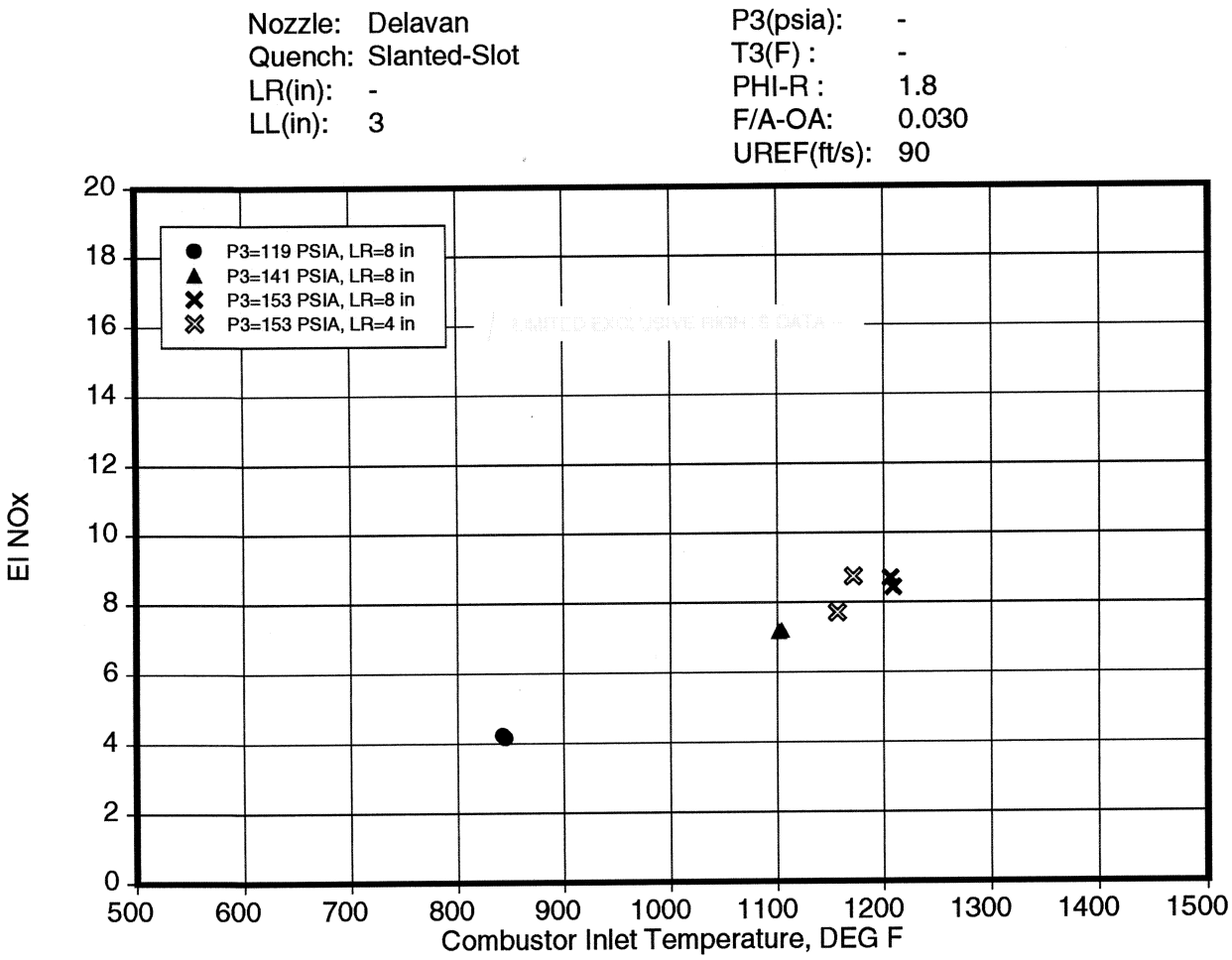

Figure VI-7 -- NOx Response to Rich Combustor Length at SSC with Slanted-Slot Quench

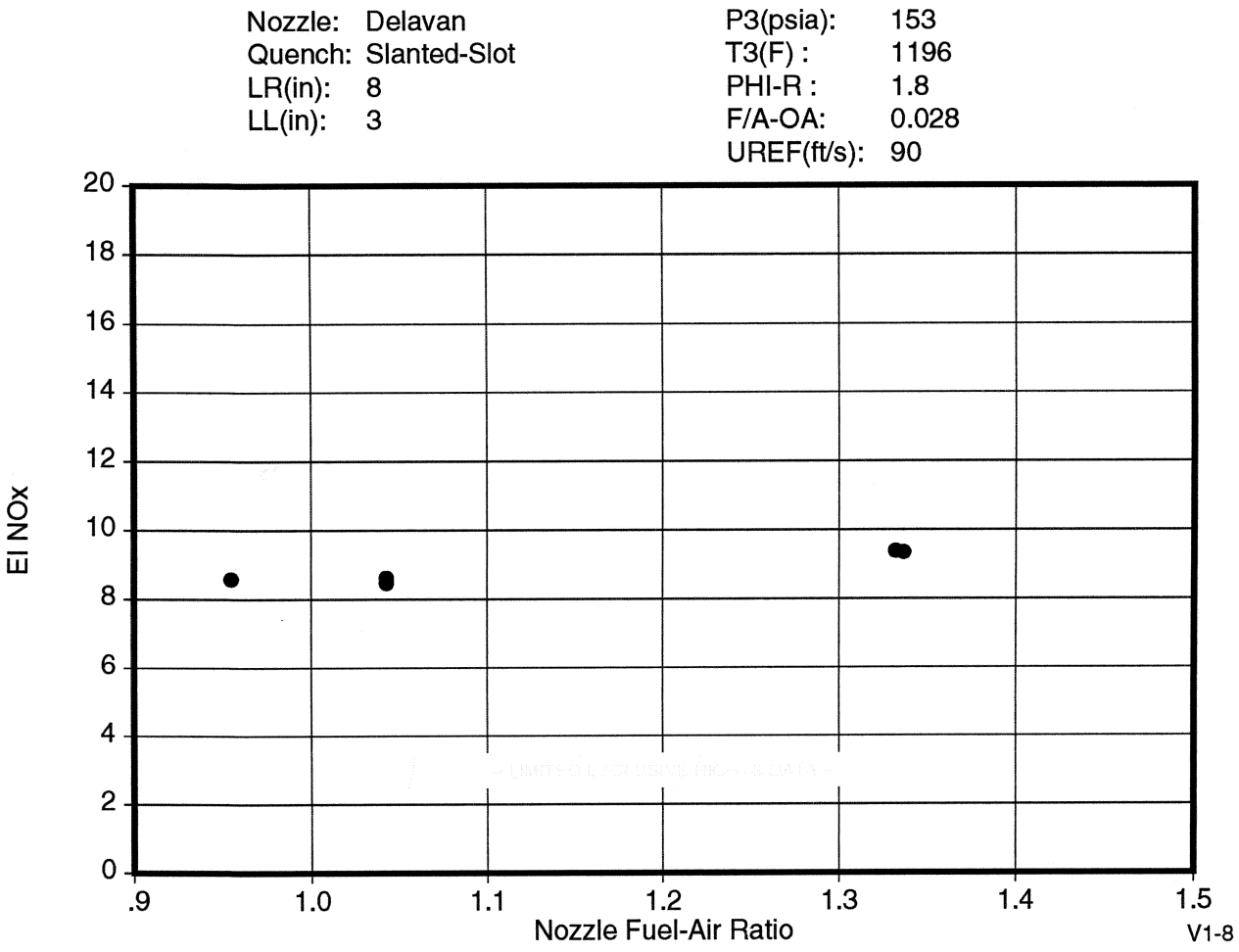

Figure VI-8 -- NOx Response to Fuel Nozzle Air Assist

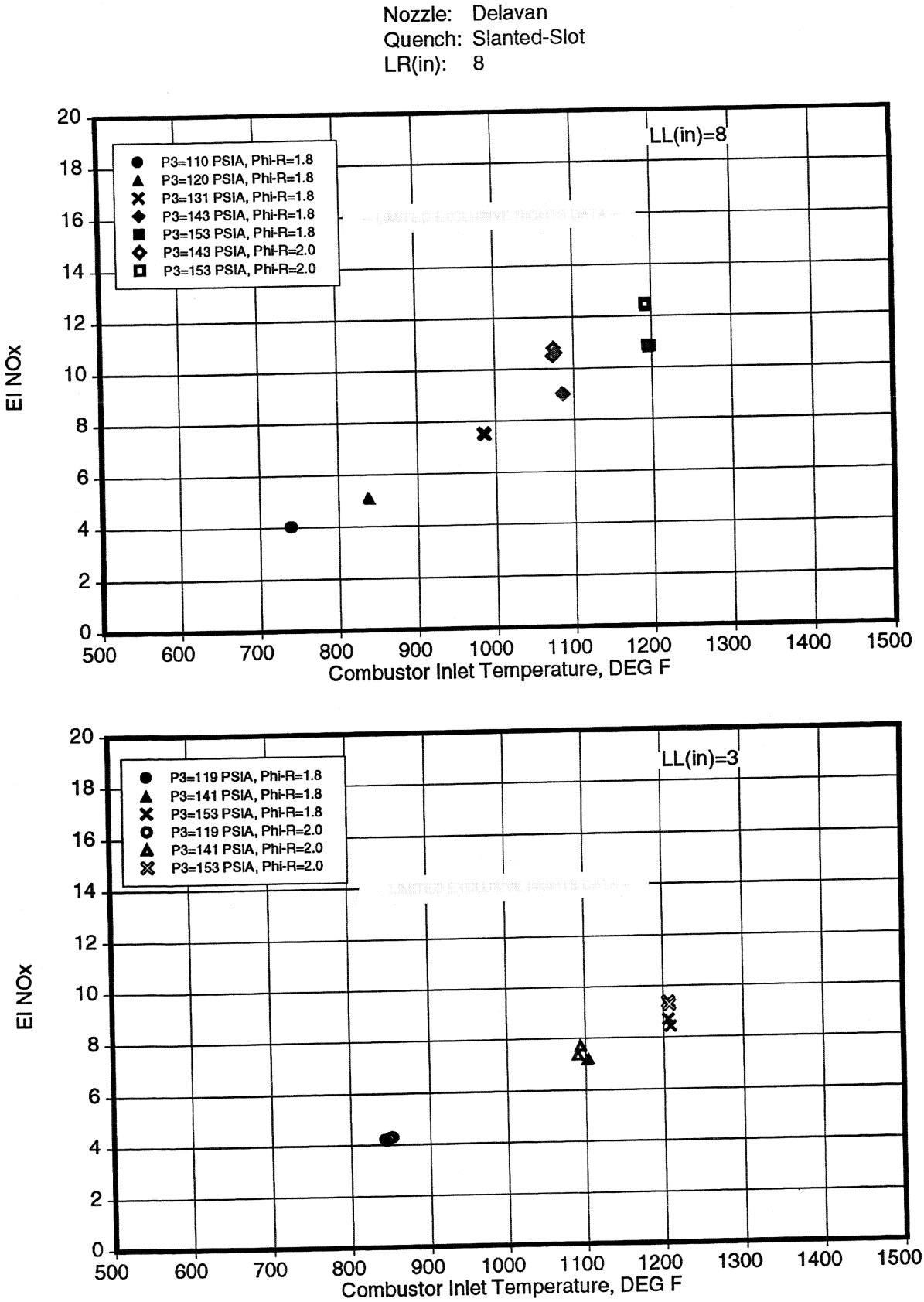

Figure VI-9 -- NOx Response to Inlet Temperature and Equivalence Ratio for Long and Short Lean Combustor with Slanted-Slot Quench

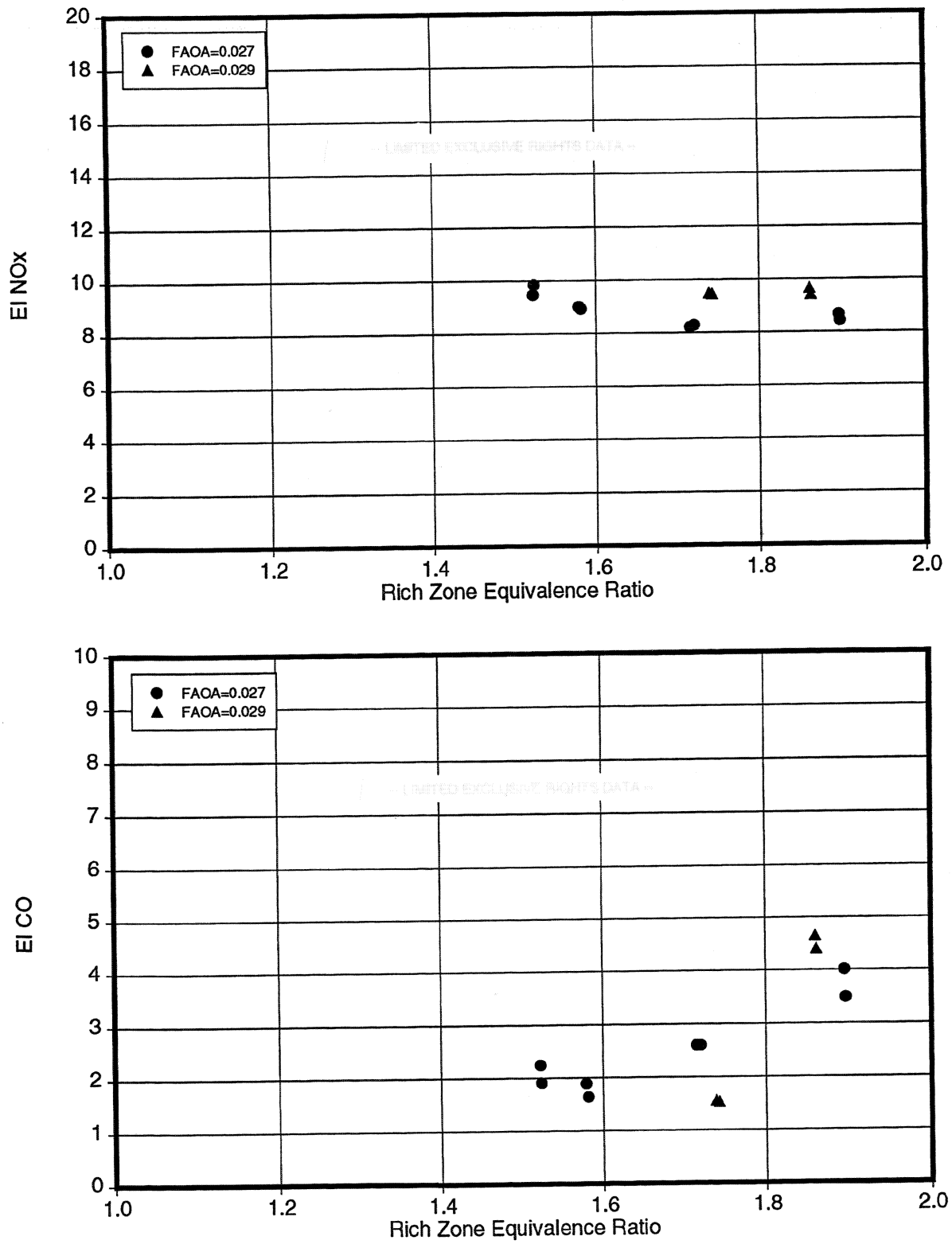

Figure VI-10 -- NOx and CO Responses to Airflow Split at SSC

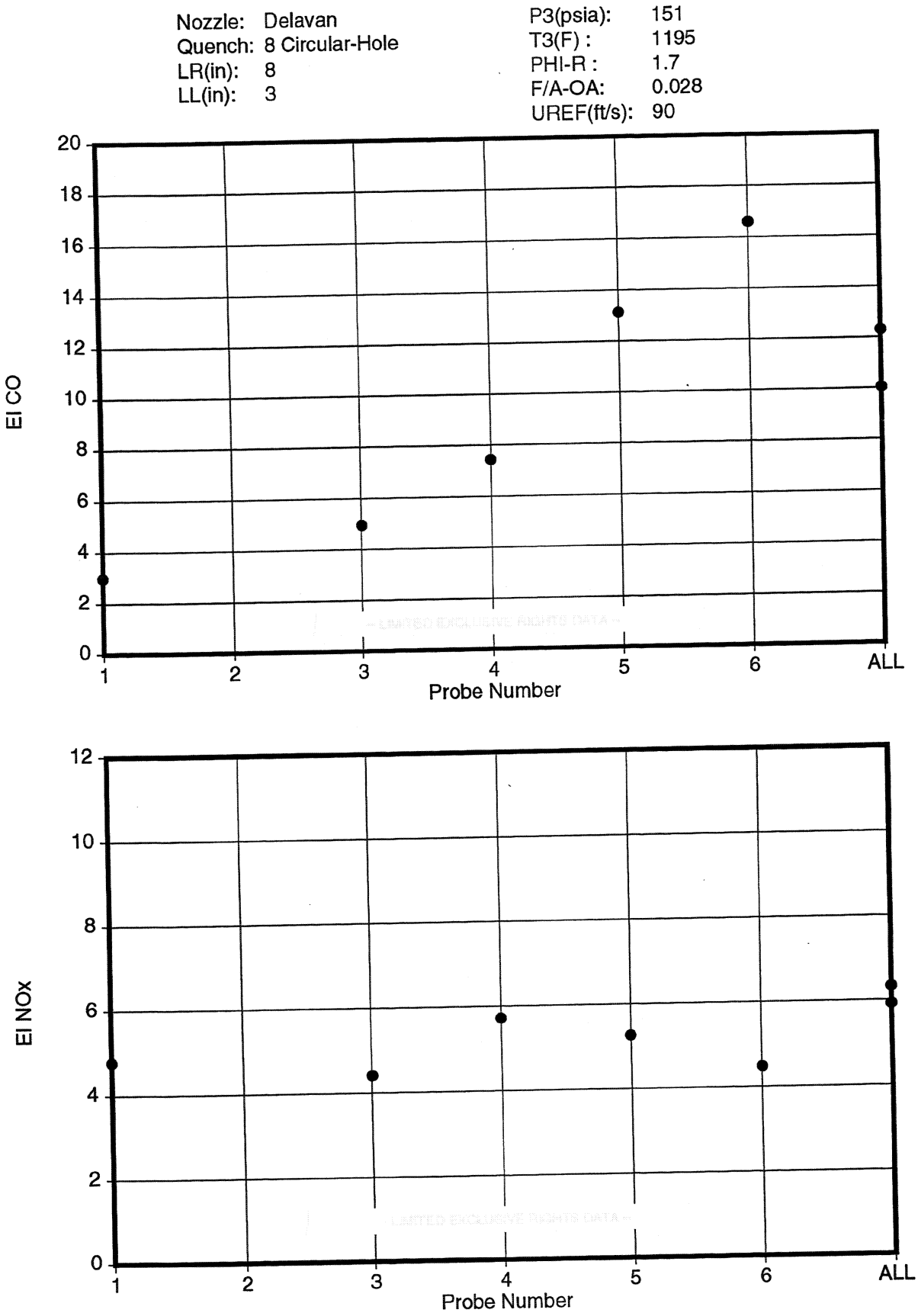

Figure VI-11 -- Emission Profiles with Eight Circular-Hole Quench at SSC

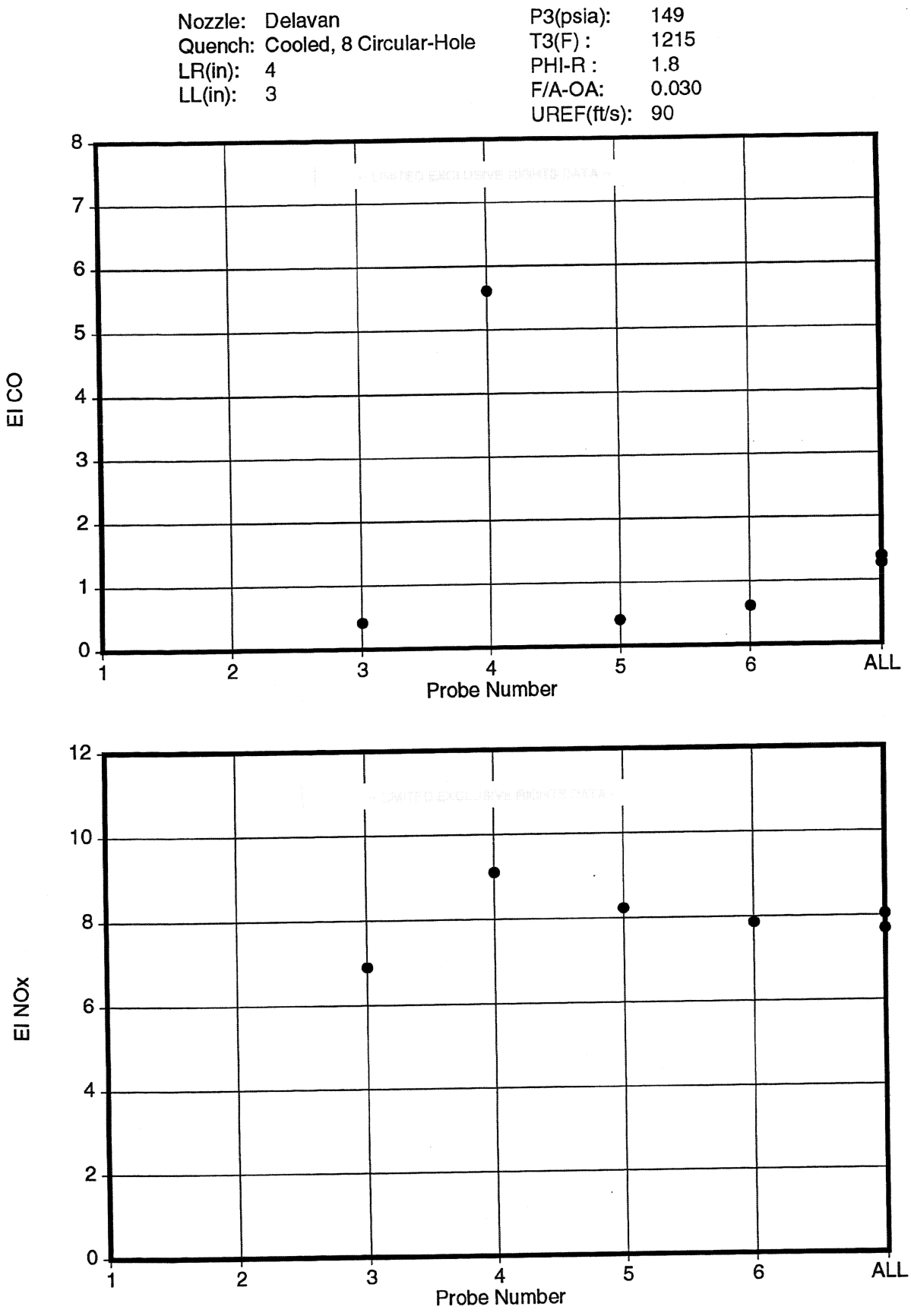

Figure VI-12 -- Emission Profiles with Cooled, Eight Circular-Hole Quench at SSC

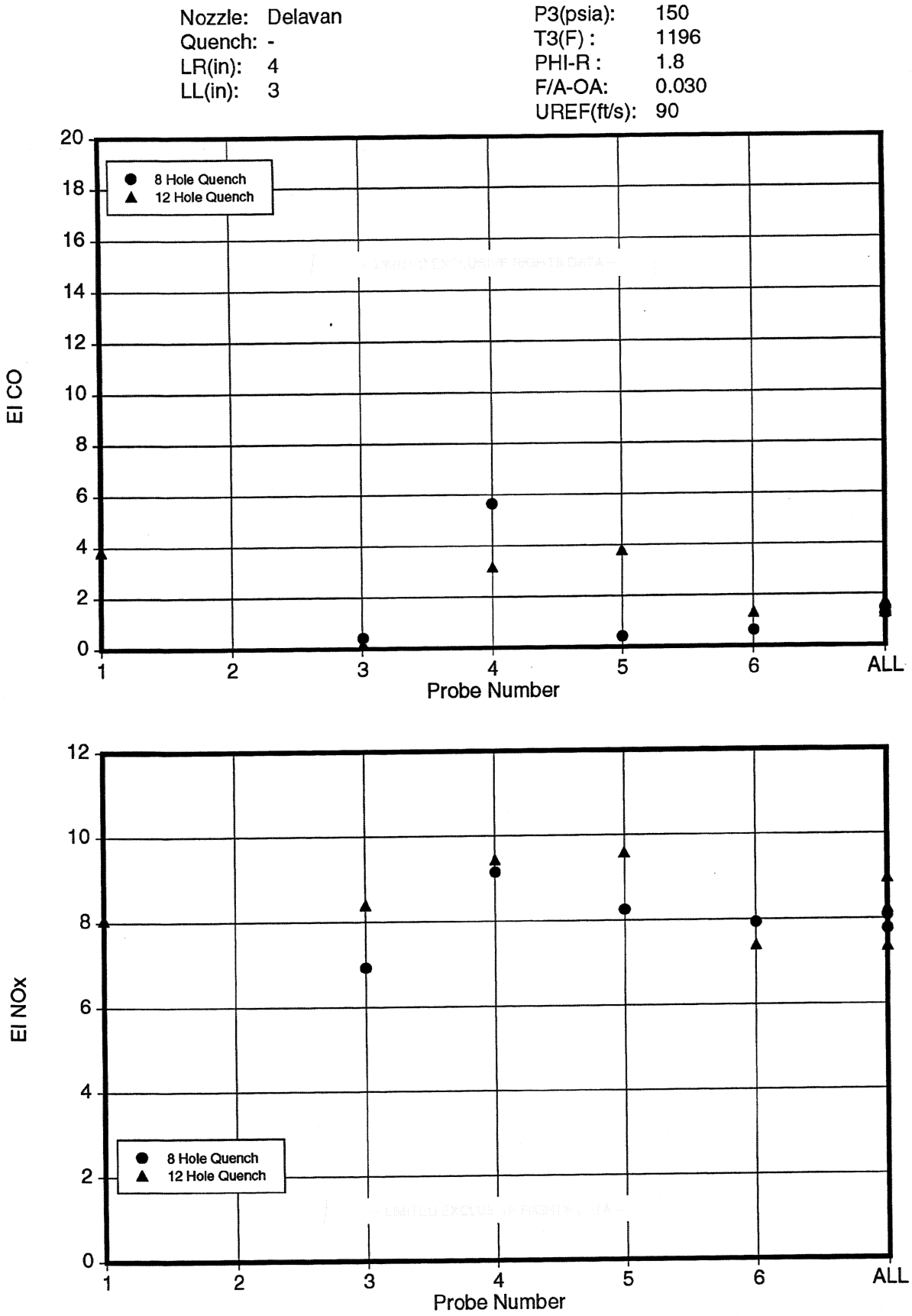

Figure VI-13 -- Comparison of NOx and CO Profiles for Circular-Hole Quench at SSC

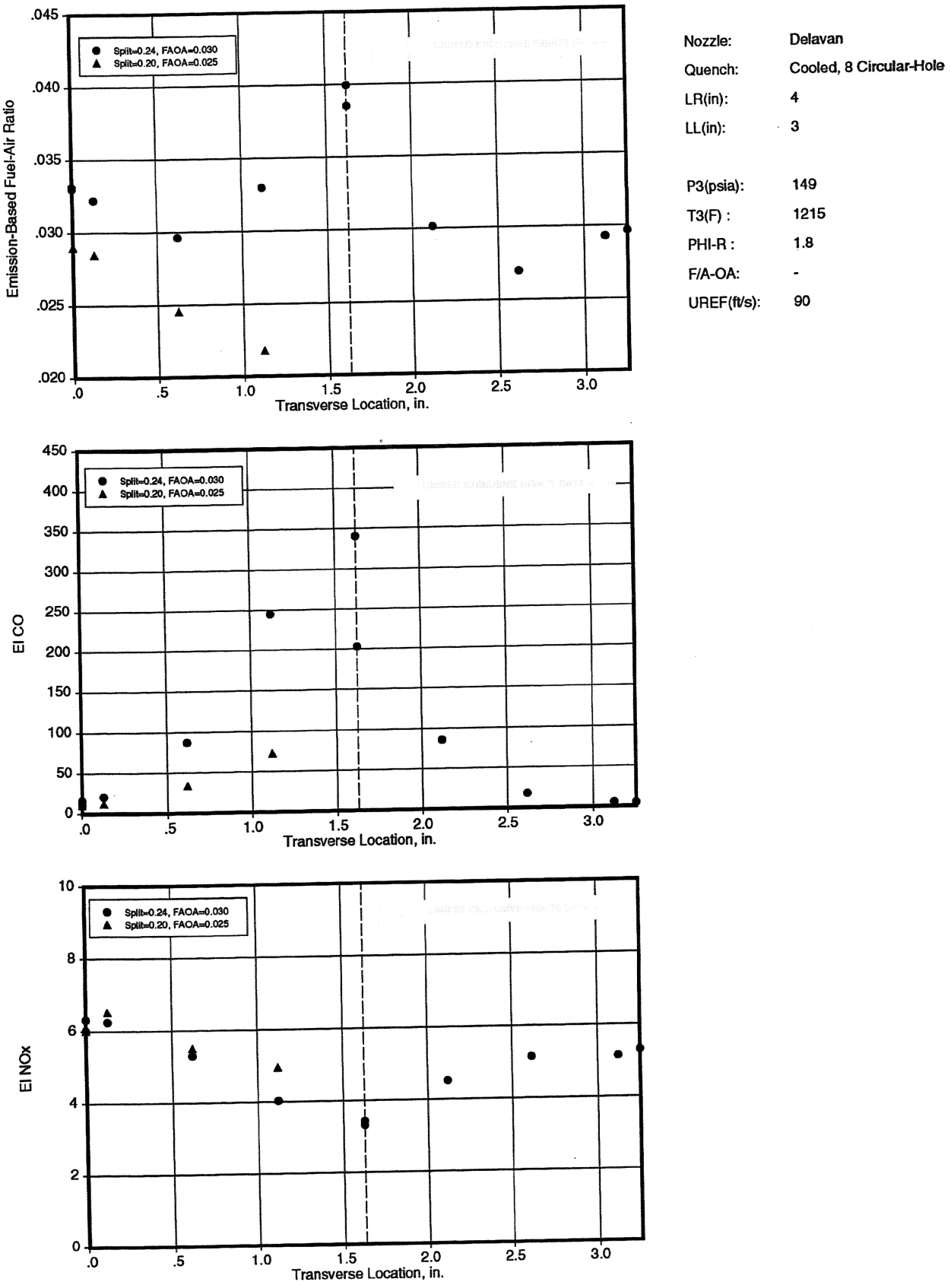

Figure VI-14 -- Emission Profiles at Eight Circular-Hole Quench Exit

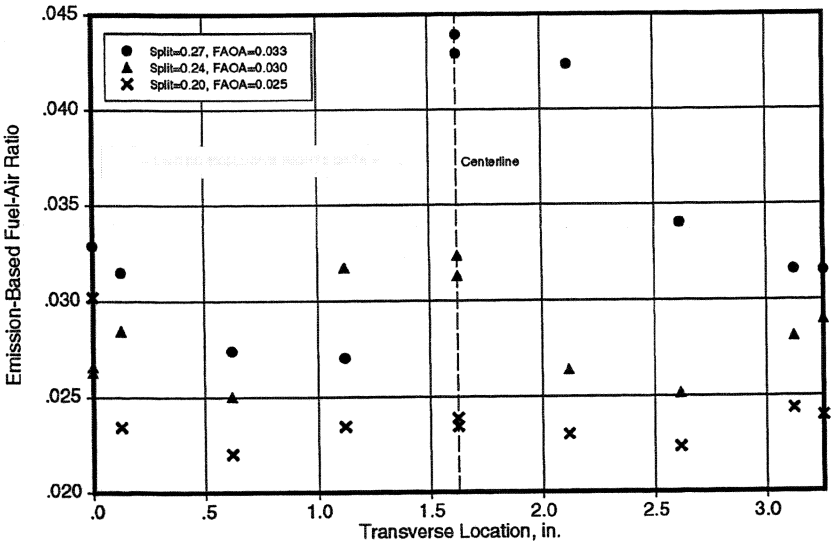

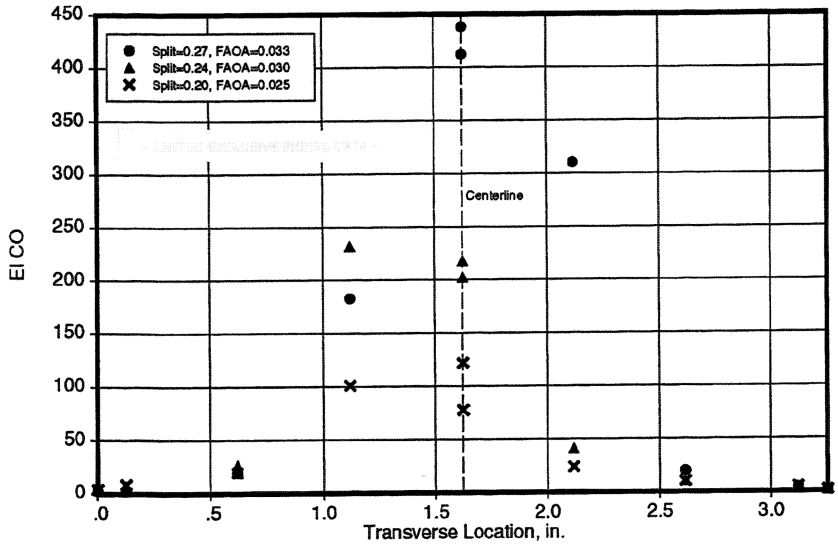

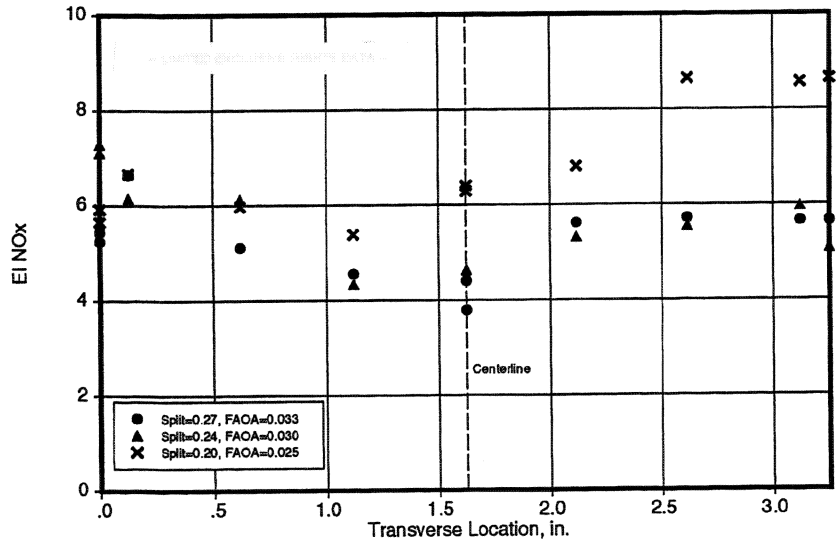

Nozzle:	Delavan
Quench:	Cooled, 12 Circular-Hole
LR(in):	4
LL(in):	3
P3(psia):	150
T3(F) :	1180
PHI-R :	1.8
F/A-OA:	-
UREF(ft/s):	90

Figure VI-15 -- Emission Profiles at Twelve Circular-Hole Quench Exit

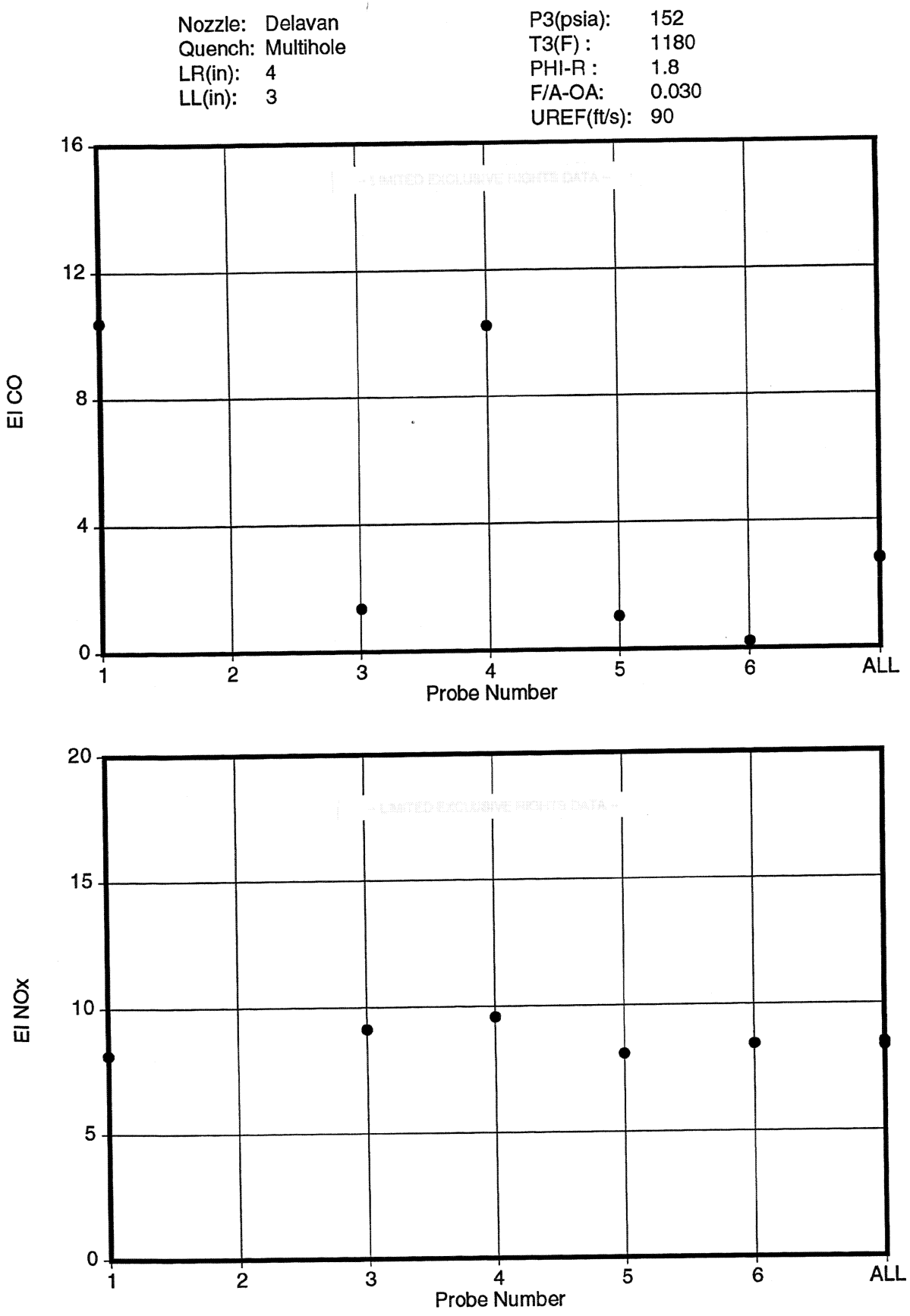

Figure VI-16 -- Emission Profiles for Multihole Quench at SSC

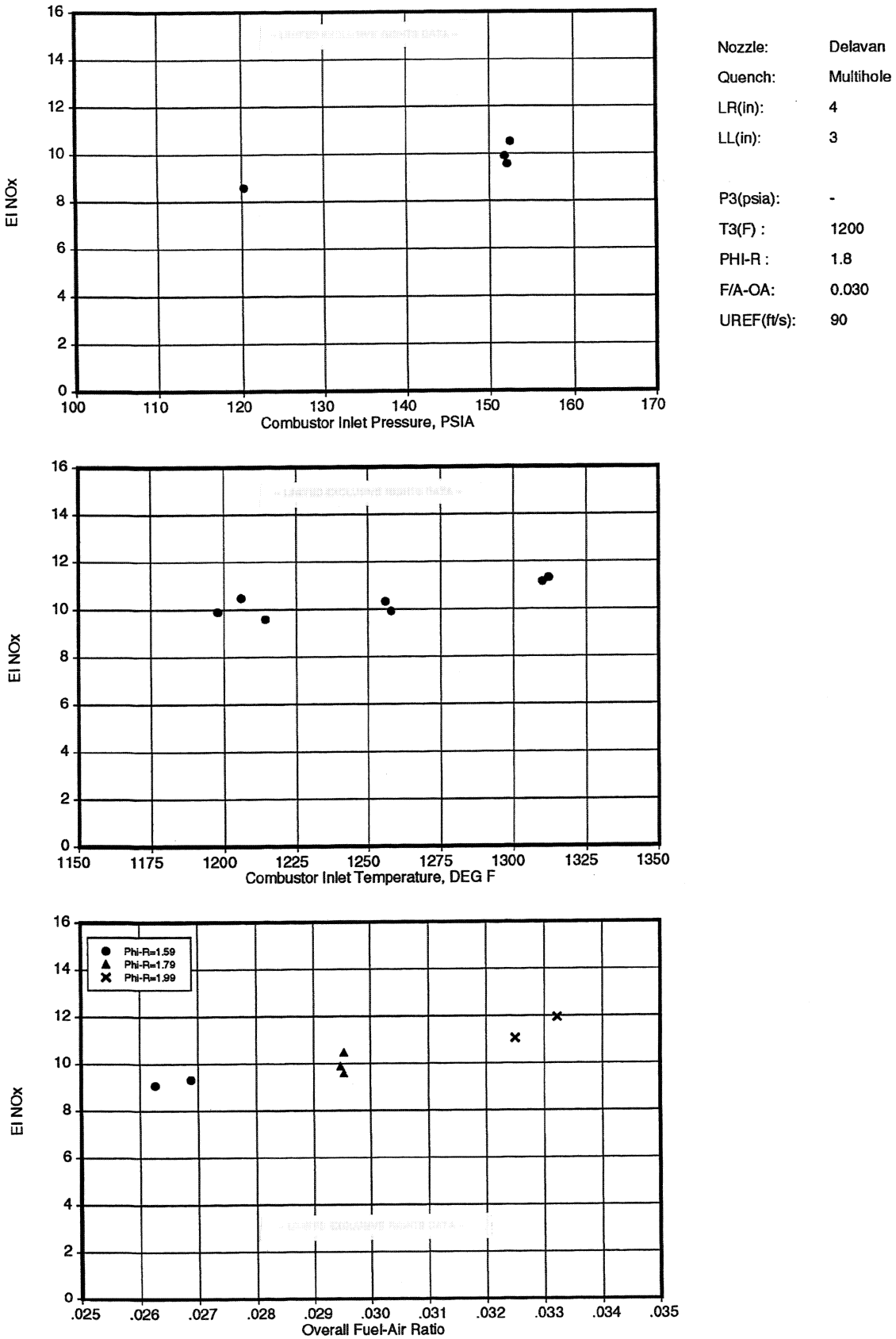

Figure VI-17 -- NOx Response to P3, T3, and F/AOA Parametrics with Multihole Quench

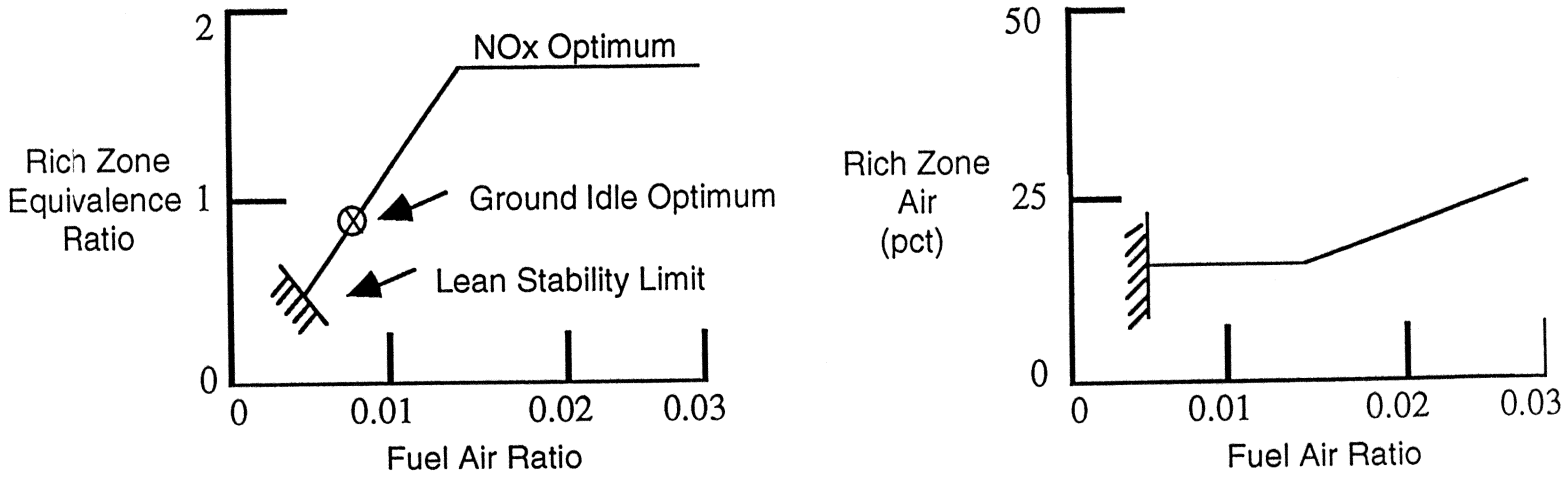

Figure VI-18 - Candidate RQL Operating Schedule

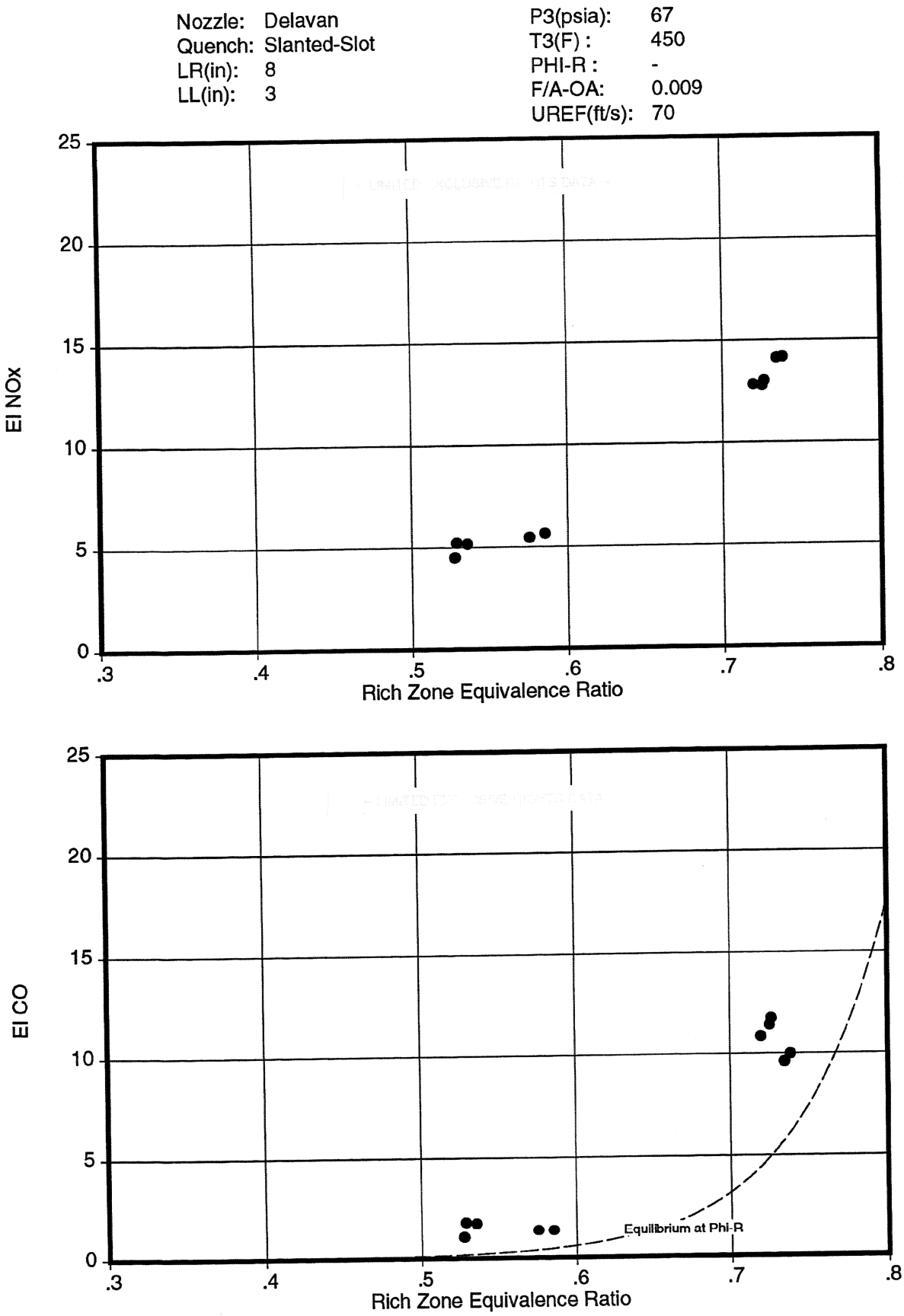

Figure VI-19 -- NOx and CO Responses at Lean-Lean Idle with Slanted-Slot Quench

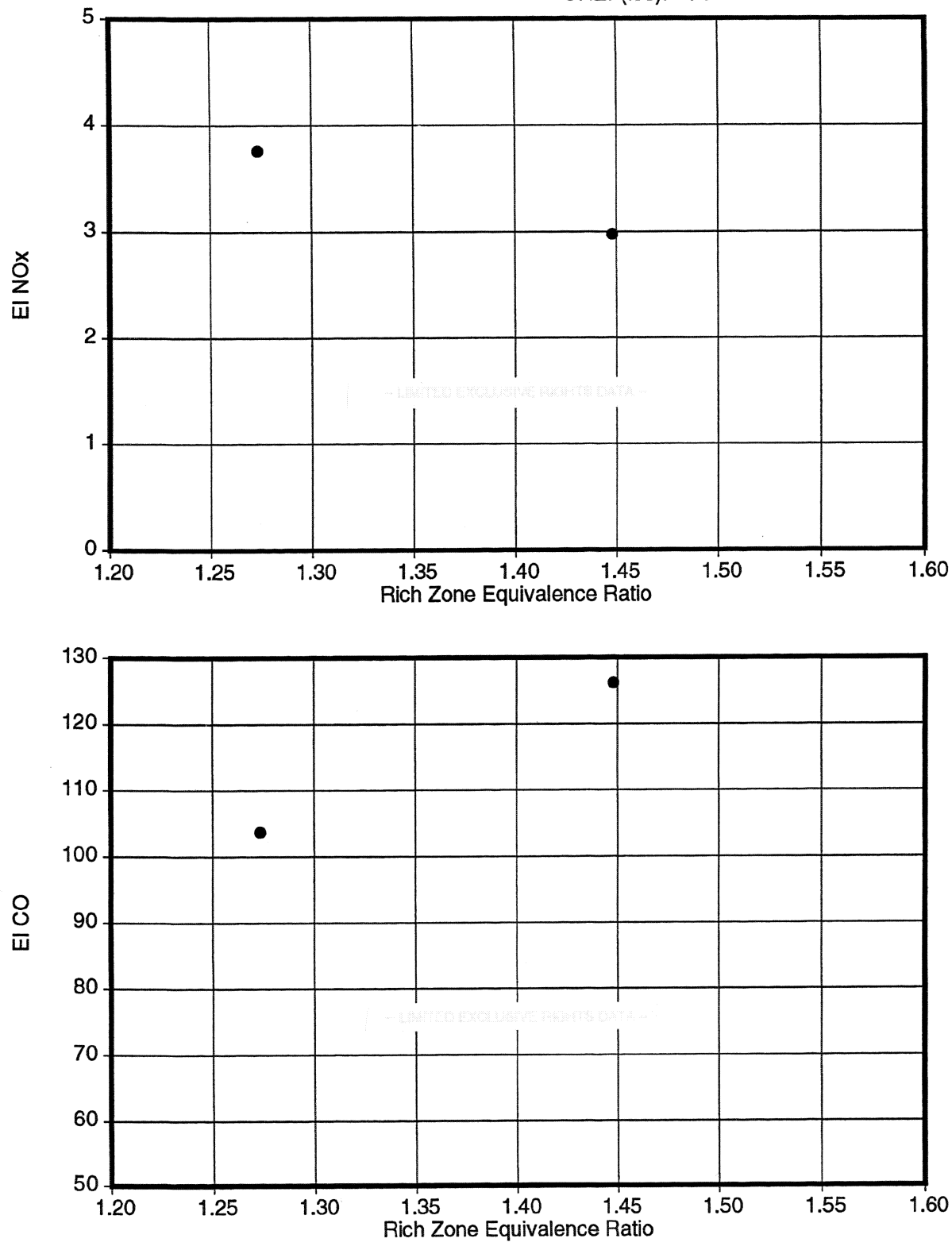

Figure VI-20 -- NOx and CO Responses at Rich-Lean Idle with Slanted-Slot Quench

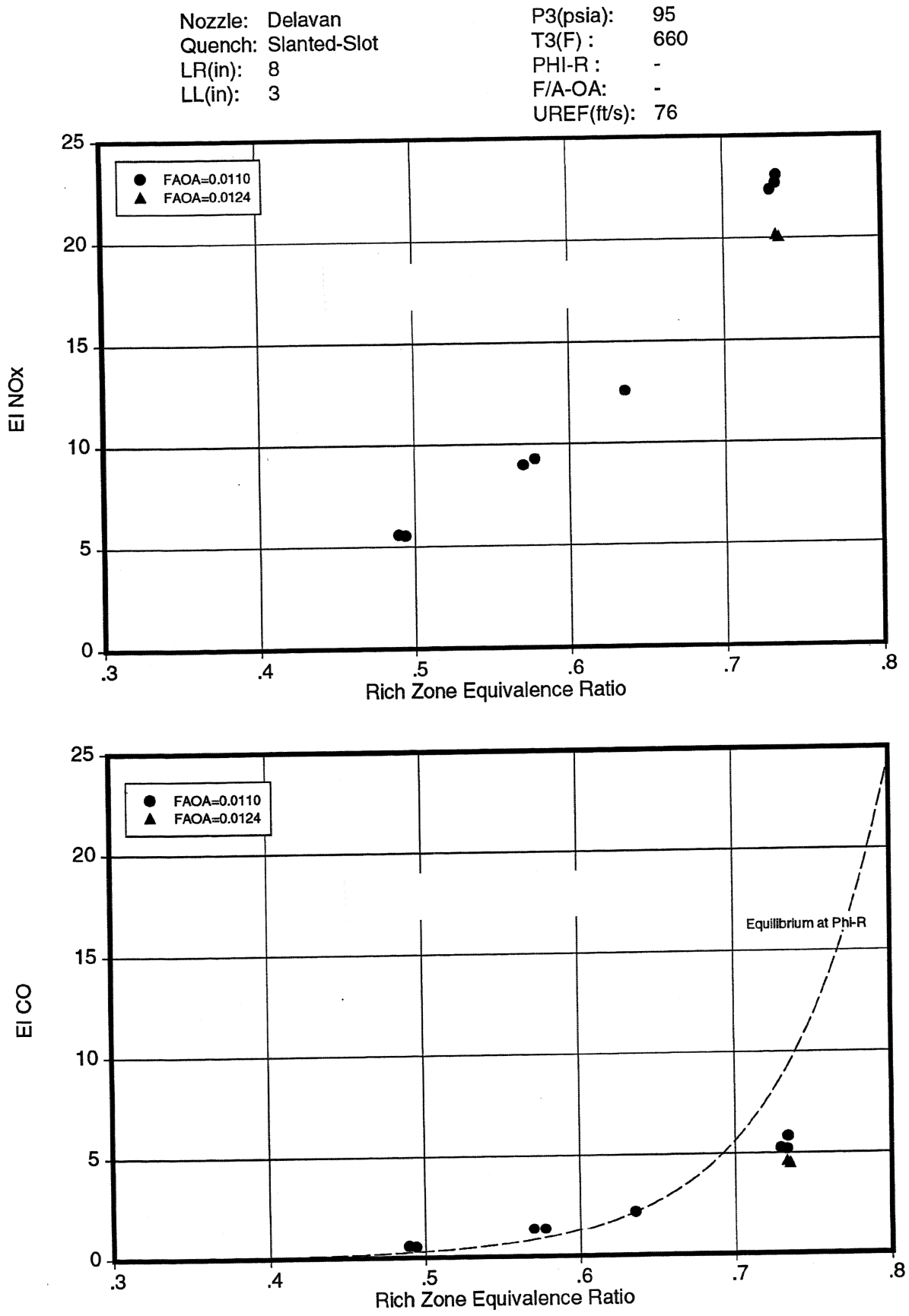

Figure VI-21 -- NOx and CO Responses at Lean-Lean 34-Pct Power with Slanted-Slot Quench

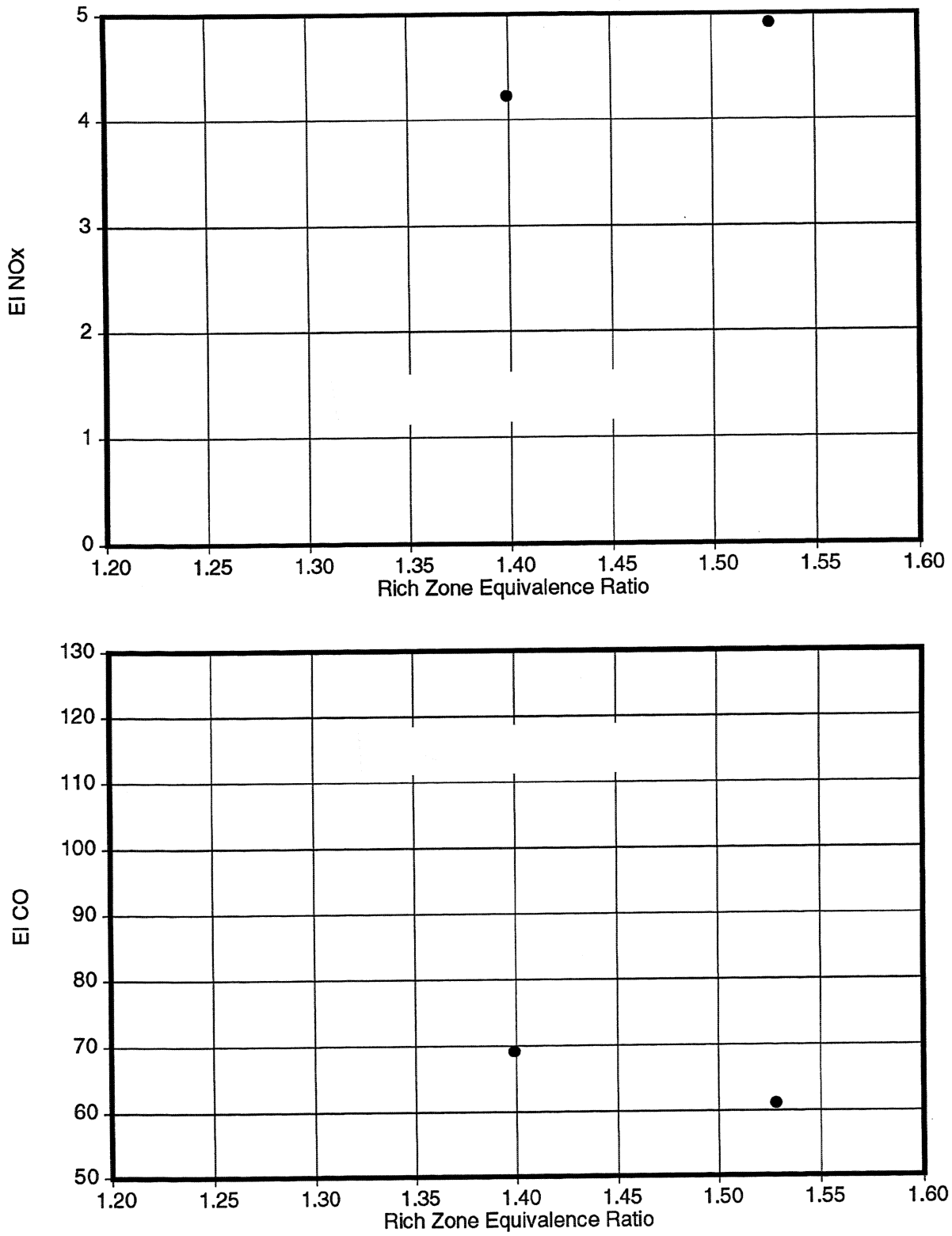

Figure VI-22 -- NOx and CO Responses at Rich-Lean 34-Pct Power with Slanted-Slot Quench

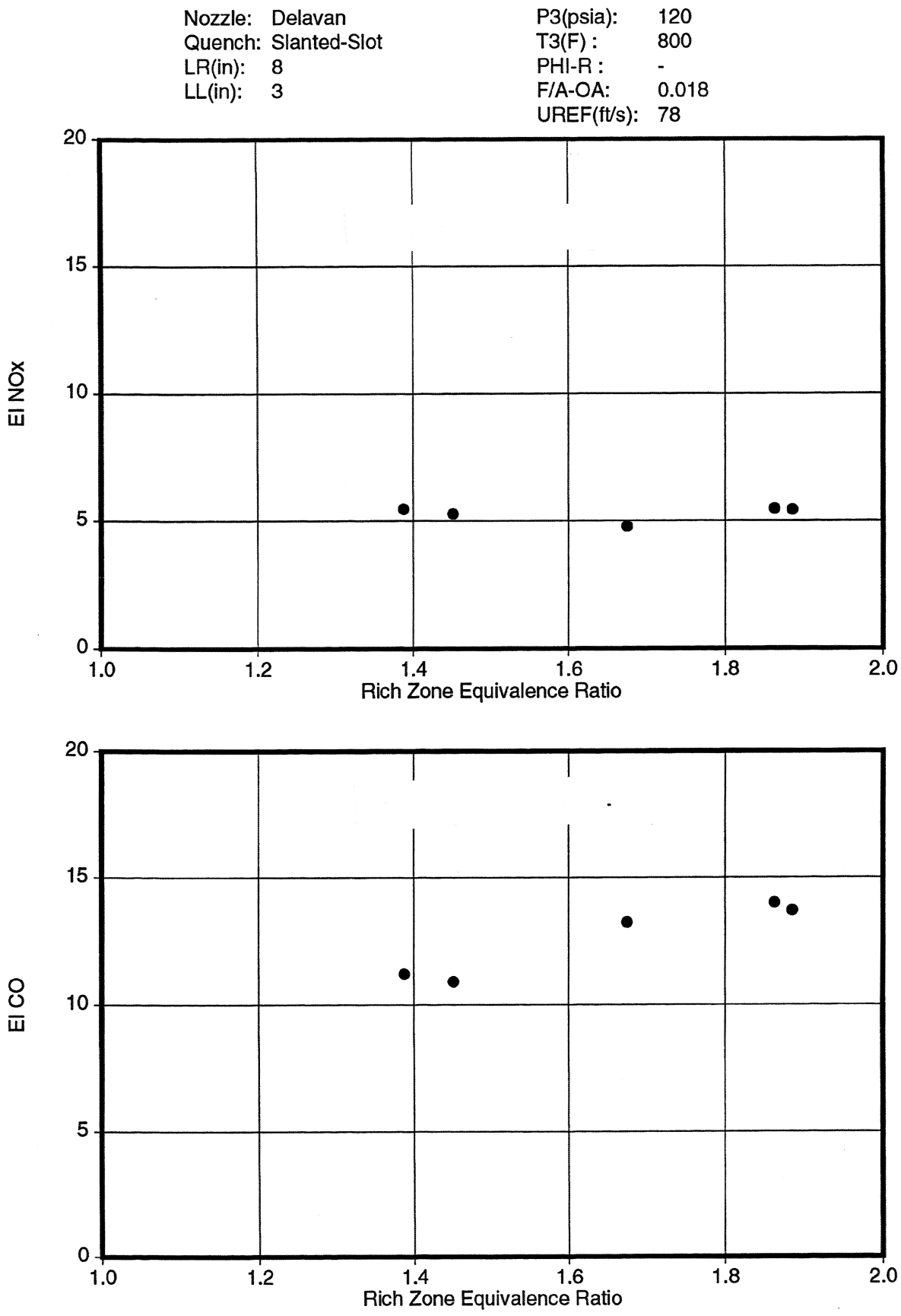

Figure VI-23 -- NOx and CO Responses at 65-Pct Power with Slanted-Slot Quench

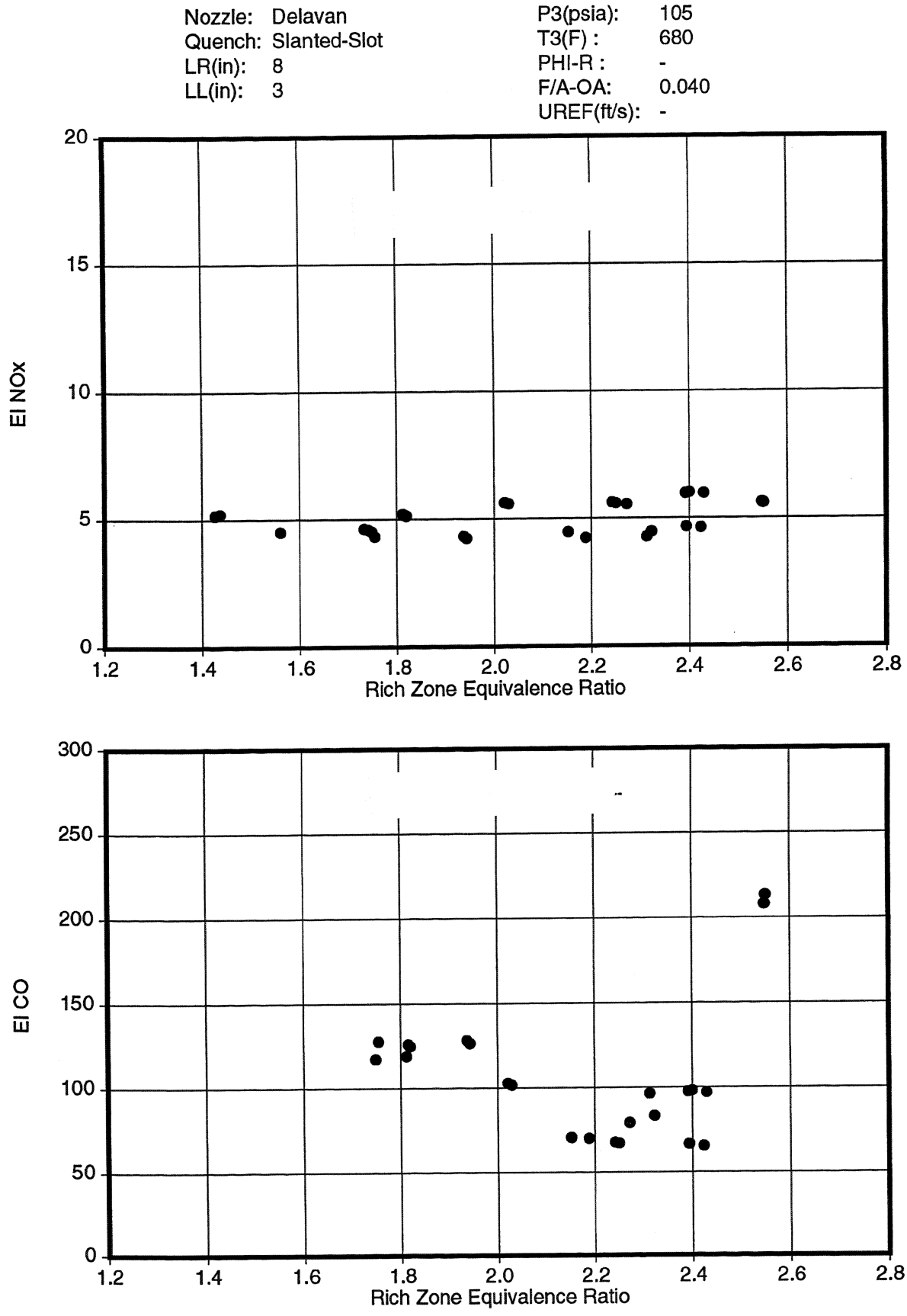

Figure VI-24 -- NOx and CO Responses at Subsonic Climb with Slanted-Slot Quench

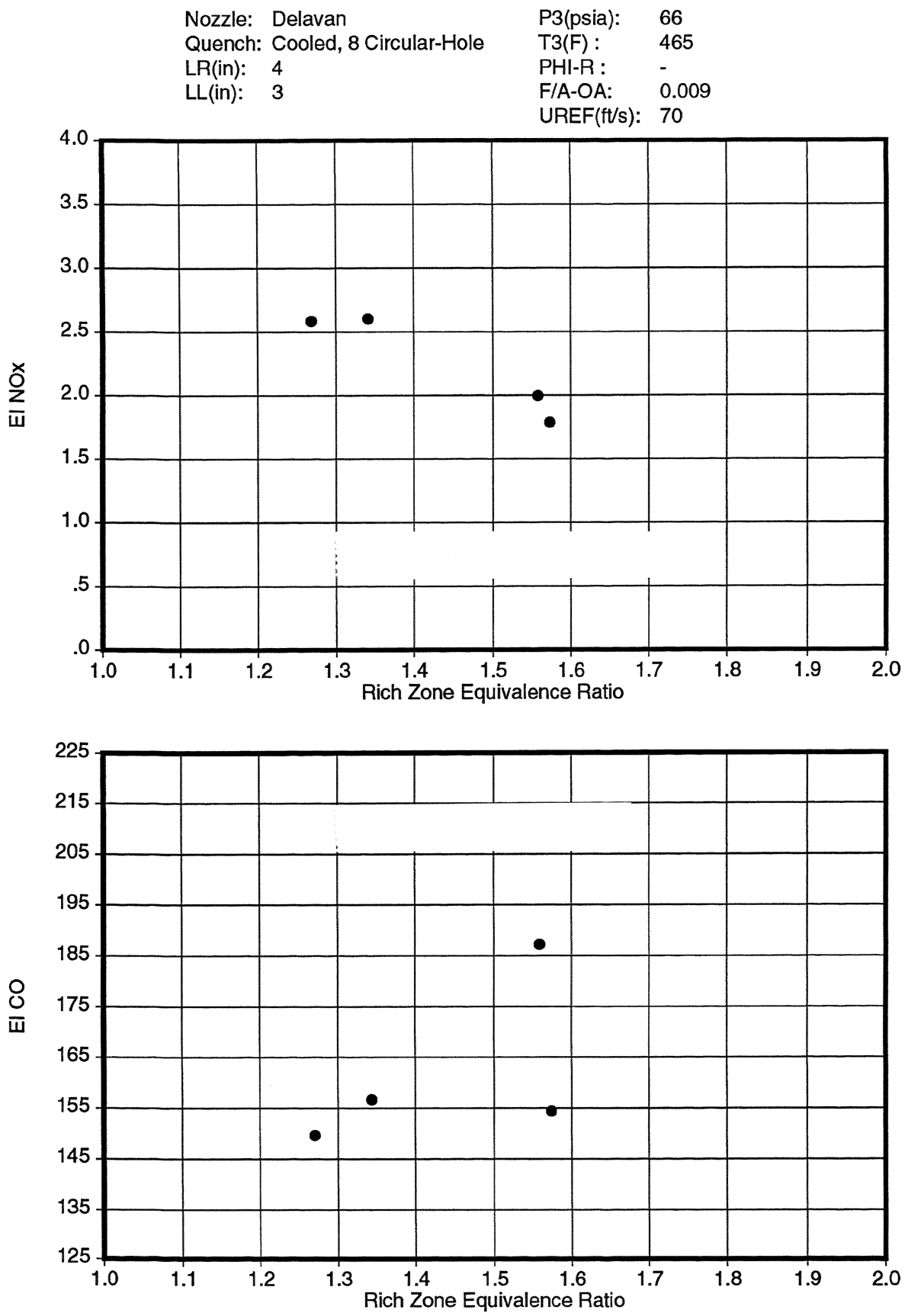

Figure VI-25 -- NOx and CO Responses at Rich-Lean Idle with Eight Circular-Hole Quench

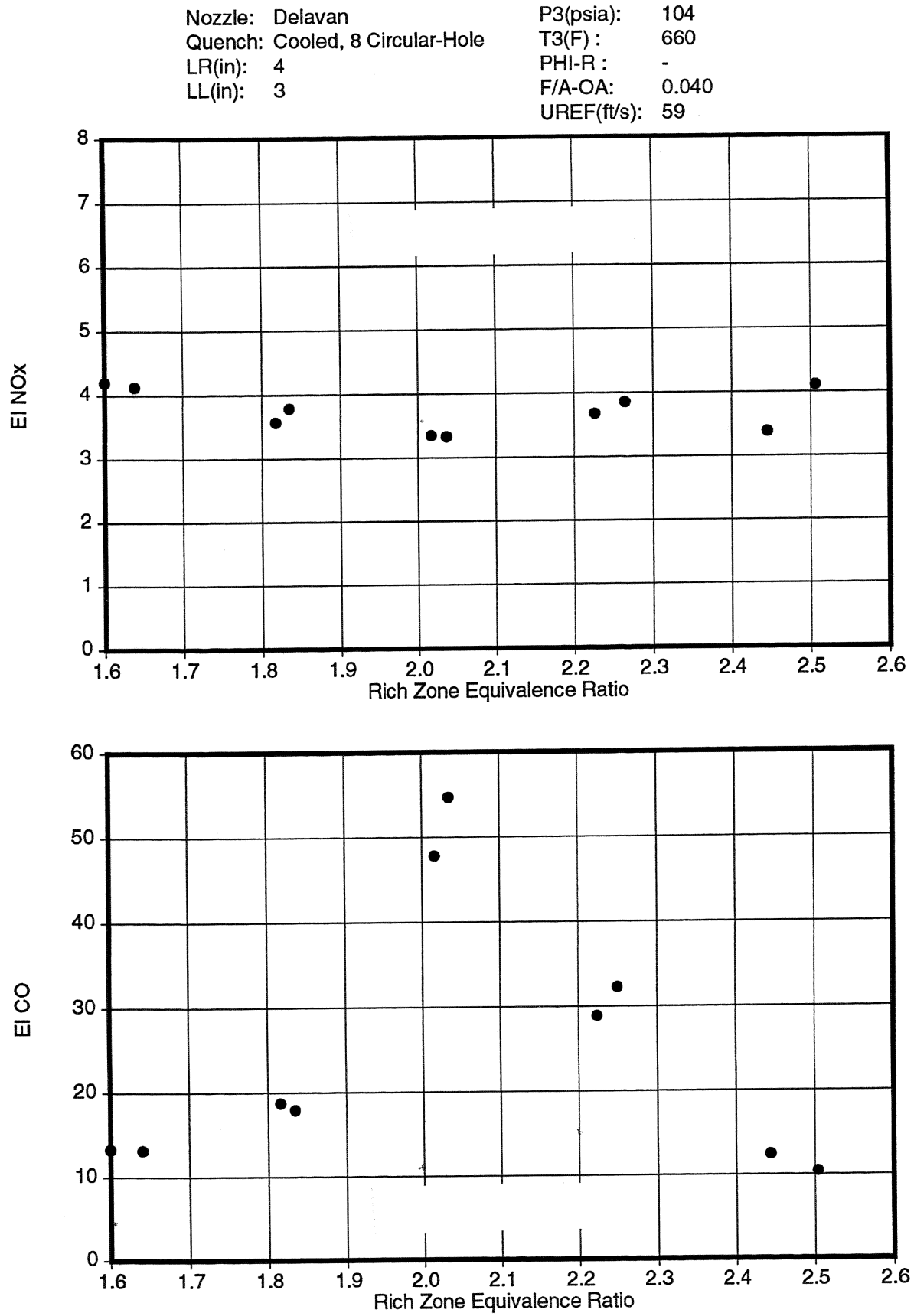

Figure VI-26 -- NOx and CO Responses at Subsonic Climb with Eight Circular-Hole Quench

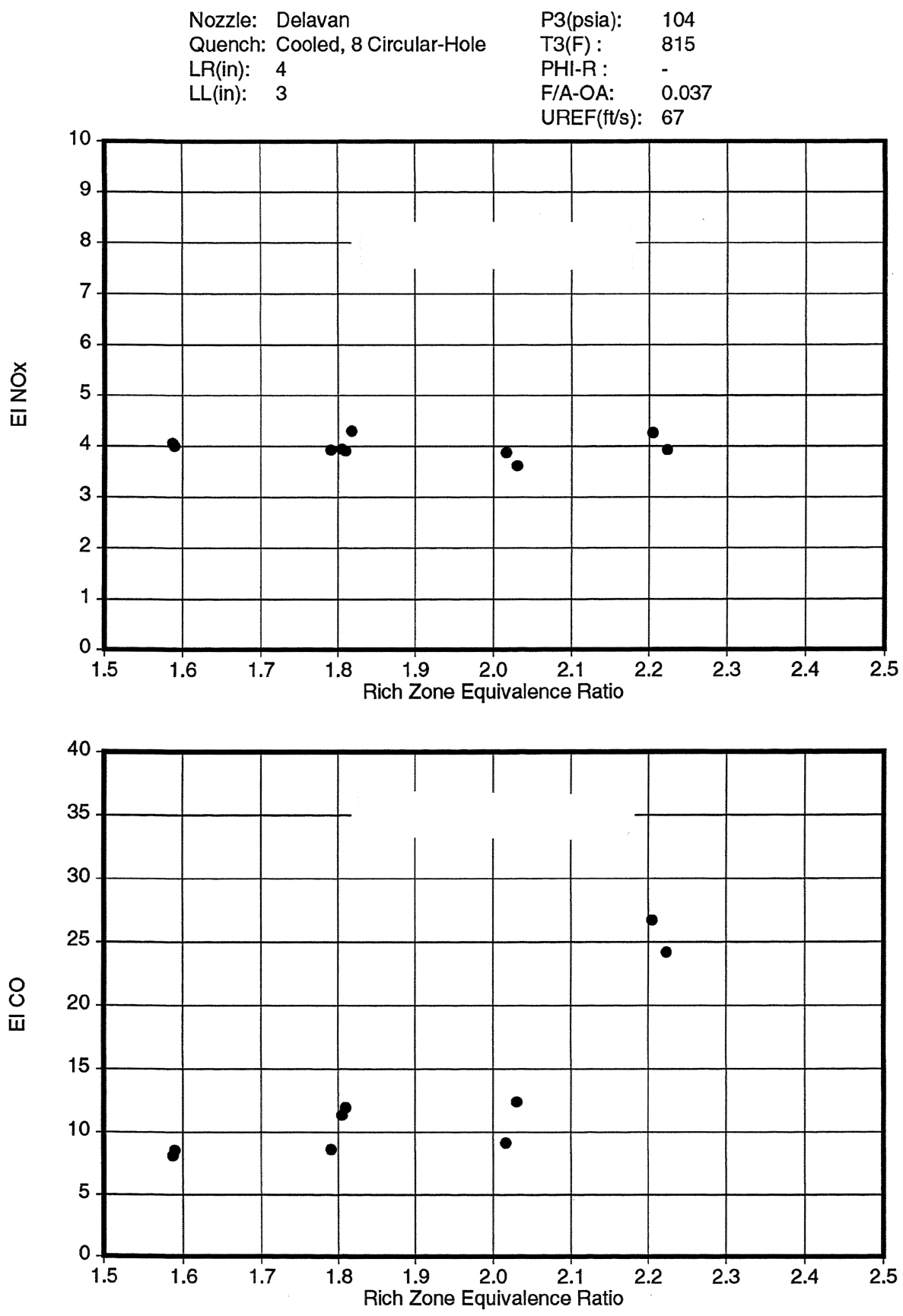

Figure VI-27 -- NOx and CO Responses at SLTO with Eight Circular-Hole Quench

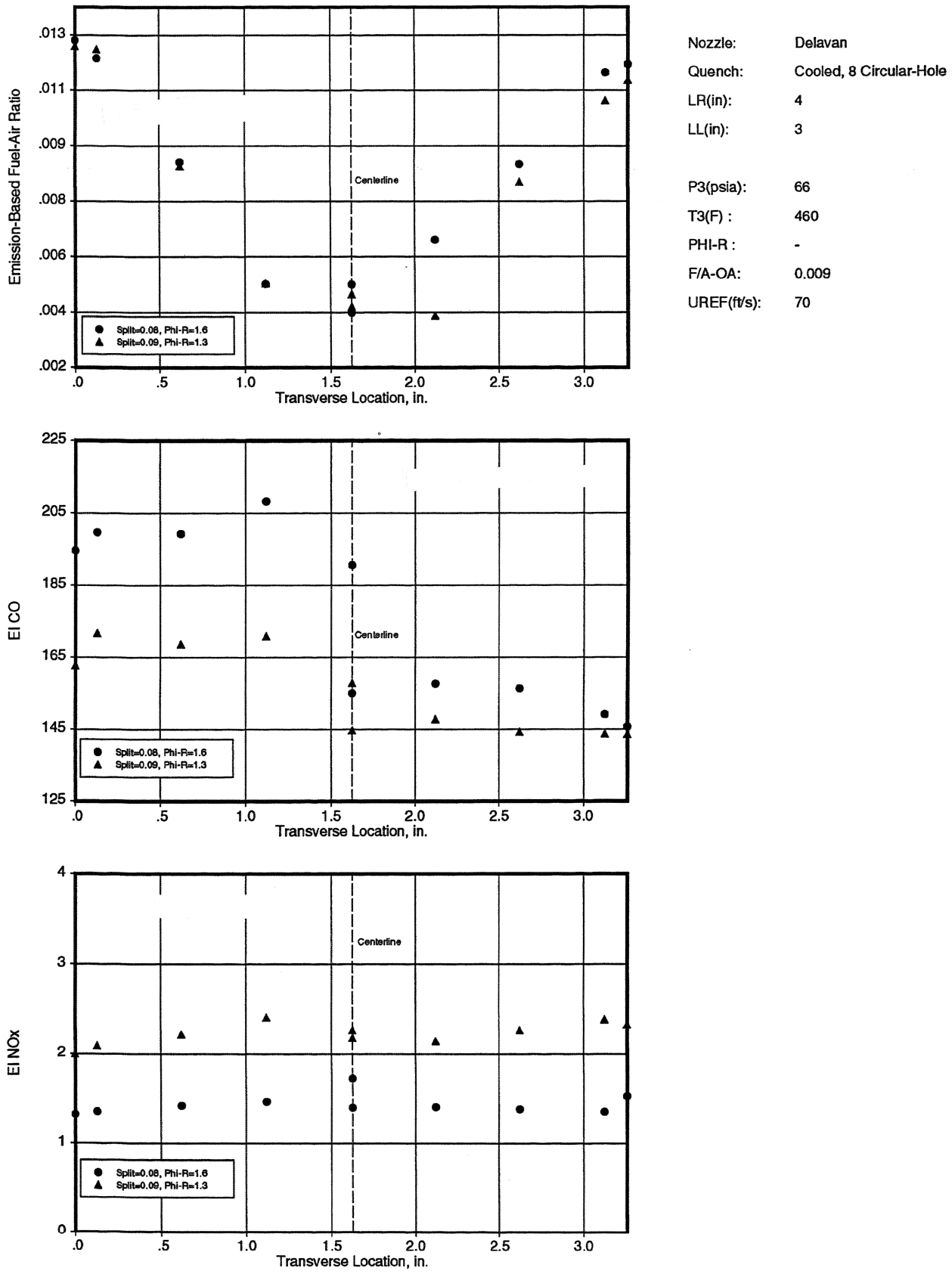

Figure VI-28 -- Quench Exit Emission Profiles at Rich-Lean Idle with Eight Circular-Hole Quench

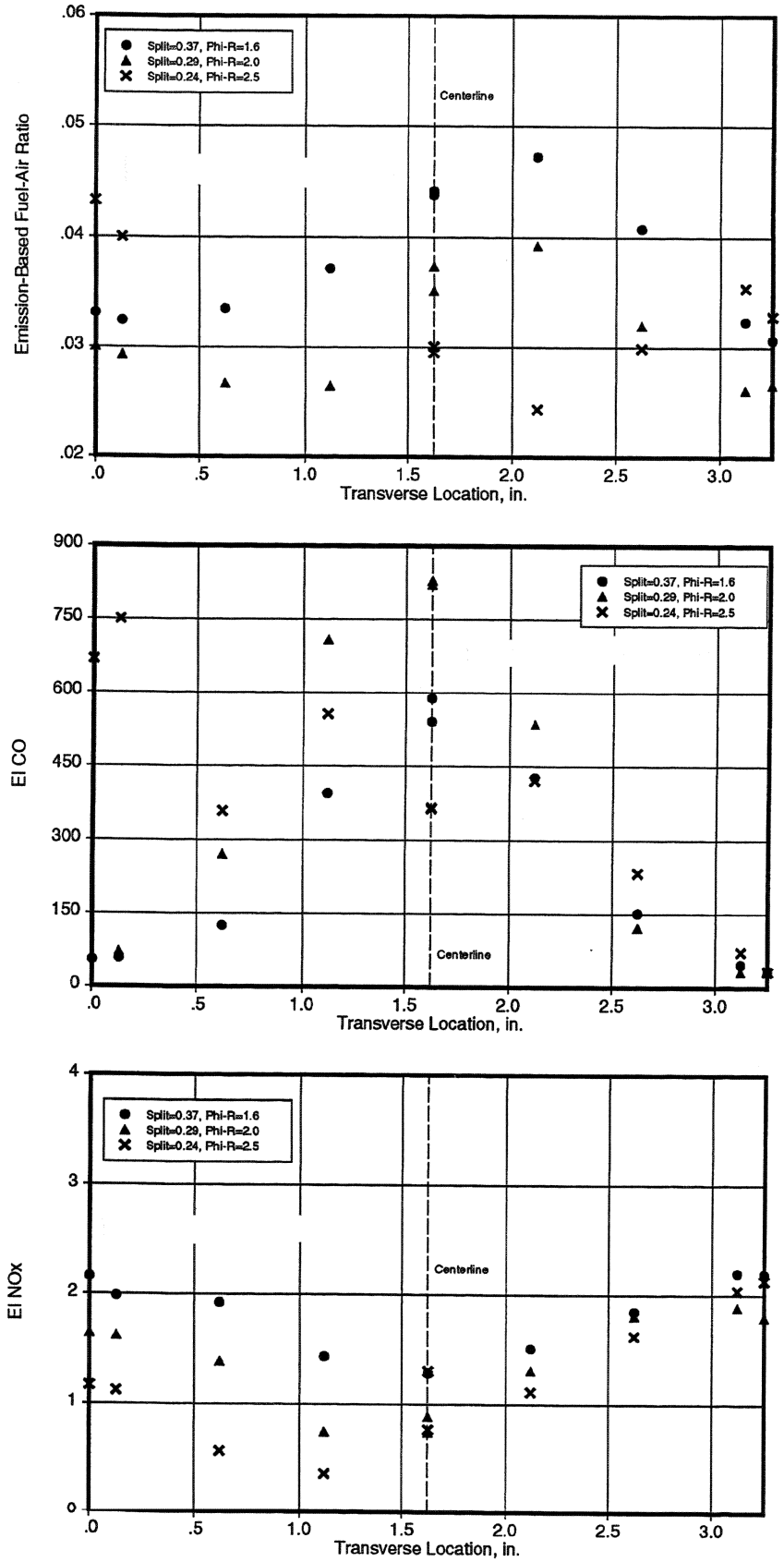

Nozzle:	Delavan
Quench:	Cooled, 8 Circular-Hole
LR(in):	4
LL(in):	3
P3(psia):	103
T3(F) :	665
PHI-R :	-
F/A-OA:	0.040
UREF(ft/s):	59

Figure VI-29 -- Quench Exit Emission Profiles at Subsonic Climb with Eight Circular-Hole Quench

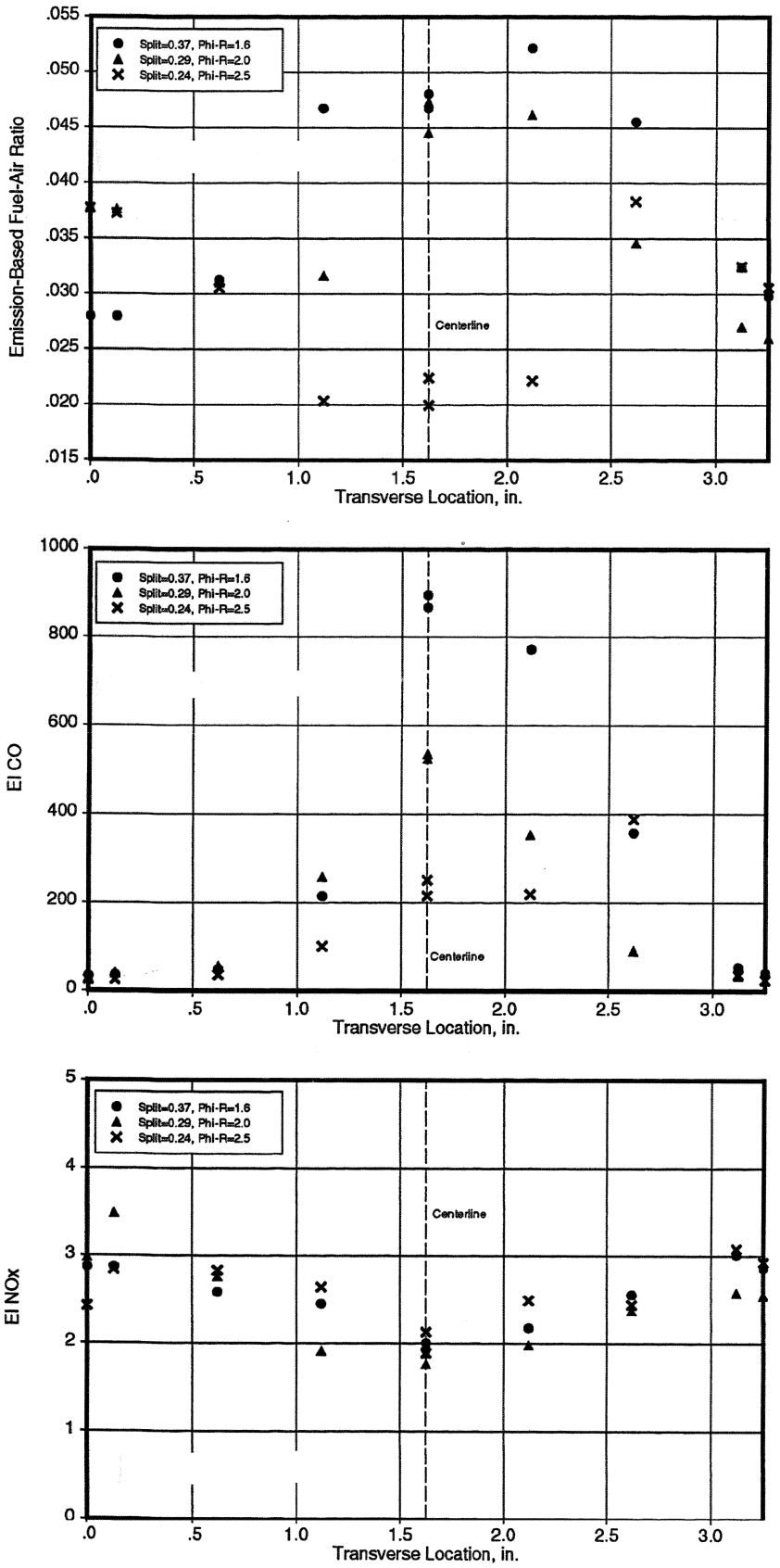

Nozzle:	Delavan
Quench:	Cooled, 8 Circular-Hole
LR(in):	4
LL(in):	3
P3(psia):	104
T3(F) :	815
PHI-R :	-
F/A-OA:	0.037
UREF(ft/s):	67

Figure VI-30 -- Quench Exit Emission Profiles at SLTO with Eight Circular-Hole Quench

SECTION VII CONCLUSIONS

In support of Pratt & Whitney efforts to define a RQL combustor for the HSCT aircraft engine, the United Technologies Research Center conducted a flametube-scale study of the RQL concept at HSCT cycle conditions. The overall objective of this study was to evaluate the suitability of applying the RQL combustor concept to the HSCT cycle. Specific technical objectives were to:

- determine whether the RQL combustor concept offered sufficient emissions control to achieve a nitric oxides emission index (EINOx) of 5 while retaining high combustion efficiency at the Supersonic Cruise (SSC) operating condition; and

- assess the sensitivities of the combustor performance and emissions to variations in the RQL design or operating condition.

On the basis of the studies performed in this program, the following conclusions are stated:

1. A RQL combustor can achieve the emissions goal of EINOx = 5 at the Supersonic Cruise operating condition for a HSCT engine as defined in Table IV-1, namely:

Table IV-1 RQL SSC Test Condition

Parameter	Symbol	Units	Value
Combustor Inlet Air Pressure	P3	psia	150
Combustor Inlet Air Temperature	T3	F	1200
Combustor Overall Fuel-air Ratio	F/AOA	---	0.030
Combustor Reference Velocity	UREF	ft/s	90
Rich Combustor Equivalence Ratio	ØR	---	1.8

2. While NOx formation in both the quench section and the lean combustor contribute to the overall emission, the NOx formation in the quench section dominates. Negligible NOx exits the rich combustor.

3. Quench section designs based on discrete quench jets are more effective at controlling NOx formation when rapidly-, highly-penetrating jets are produced.

4. A stable rich combustor flowfield structure, consisting of an axial vortex core surrounded by larger recirculation zones as produced by the swirling inlet flow, exists for combustor length-to-diameter ratios as low as 0.8. The ability of CFD to predict this structure strongly depends on the turbulence model.

5. The gas composition exiting the rich combustor can be reasonably represented by the equilibrium composition corresponding to the rich combustor operating condition defined by P3, T3, and ØR.

6. At the SSC condition, the oxidation processes occurring in the quench section consume 99 pct of the CO exiting the rich combustor. Soot formed in the rich combustor is also highly oxidized, with combustor exit SAE Smoke Number < 3.

7. A RQL combustor can achieve stable, robust, and efficient combustion at all operating conditions of a representative HSCT engine cycle.

8. Low power operating conditions require that the RQL combustor operate as a lean-lean combustor to achieve low CO and high efficiency.

SECTION VIII RECOMMENDATIONS

Studies performed to assess the suitability of applying the RQL combustor concept to the HSCT cycle identified the following recommended areas of further study:

1. Quench section flow and kinetic processes

The quench section is the critical component of the RQL combustor. It is primarily responsible for attaining low NOx emissions and high combustion efficiency. All of the quench designs evaluated promoted high levels of CO oxidation, but different degrees of NOx control were experienced. The quench contains coupled fluid dynamic and chemical kinetic processes. Information is required to describe these processes and their interaction to permit the design of devices with improved performance. Among the issues requiring clarification are:

a. How does mixing performance reflect the NOx quenching performance?

b. What are suitable methods to model the fluid dynamic and kinetic processes?

c. What are the preferred experimental techniques and diagnostics to characterize the processes in the quench section?

d. How do the quench inlet flow and composition profiles affect quenching effectiveness?

e. How do the quench-jet geometry, and flow and turbulence profiles affect quenching effectiveness?

f. How do temporal variations affect quenching effectiveness?

g. How are experiences from cylindrical geometries translated to two-dimensional geometries?

2. The RQL combustor must perform in a rich-lean mode at high power to control NOx formation and in a lean-lean mode at low power to consume CO and attain high efficiency. These limits suggest that the RQL design permit either:

- fuel injection into both combustion zones (e.g. inject fuel into the rich zone only for rich-lean operation, and into both zones, or lean zone only, for lean-lean operation); or

- airflow redistribution between the rich and lean zones (e.g. low airflow split for rich-lean operation, and high airflow split for lean-lean operation).

Each of these represents a family of RQL control strategies which should be considered to select a preferred one. Additional required technologies will likely be identified as a consequence of this selection. For example, if airflow redistribution is preferred, the mechanism to alter it must be developed, and both its performance and the consequence of the alteration must be assessed. Currently, the two primary air passages are through the fuel preparation device and the quench jets. Development and assessment of mechanisms for one or both of these paths would be required.

3. Two components not studied in this program require development: the fuel nozzle and the combustor liners.

The fuel preparation used in the current program was idealized by use of an air-assist fuel nozzle. A high airflow capacity fuel nozzle which is compatible with the preferred RQL control strategy must be developed and evaluated.

The combustor liners used in this program were not meant to represent engine design practice. Since cooling airflow may not be admitted into the rich combustor, a liner design and material is required to tolerate the rich combustor heat loads without the use of cooling films. Since the combustor exit temperature at SSC approaches the level at which thermal NOx formation rates increase rapidly, and the lean combustor cooling budget increases this temperature by increasing the bulk flow fuel-air ratio, a lean combustor liner design and material is required which minimizes the required coolant flowrate.

4. The development of a RQL combustor will be aided by the effective application of modeling. The flow within this combustor is complex and the chemistry spans both rich and lean mixtures. Among the modeling issues requiring consideration are:

a. What are alternative modeling approaches? What are the trade-offs of technical rigor and computational efficiency? Can submodels be developed for components of the RQL combustor?

b. How well do the models predict the non-reacting flowfield features?

c. Are kinetic mechanisms available that can predict the NOx formation and destruction with the rich, quench, and lean components?

d. Can suitable kinetic mechanisms be used with complex flowfield models?

e. Can combusting flow models predict the emissions data?

f. Can combusting flow models predict the liner heat loads?

REFERENCES

II -1 "Pratt & Whitney, GE Team to Study HSCT Propulsion," Aviation Week and Space Technology, Oct 15, 1990.

III -1 Roffe, G. and Venkataramani, K. S.: Effect of Cycle Pressure on Emissions and Performance of a Lean Premixied Combustor. AIAA Paper 78-1039, July 1978.

-2 Tacina, R.R.: Low NOx Potential of Gas Turbine Engines. AIAA Paper 90-0550, Jan 1990.

-3 Spadaccini, L. J. and J. A. TeVelde: Autoignition Characteristics of Aircraft-Type Fuels. NASA CR-159886, June 1980.

4 Holdeman, J. D.: Mixing of Multiple Jets with a Confined Subsonic Crossflow. AIAA Paper 91-2458, Jun 1991.

-5 Vranos, A. et al: Experimental Study of Cross-Stream Mixing in a Cylindrical Duct. AIAA Paper 91-2459, Jun 1991.

-6 Smith, C. E. et al: A CFD Study of Jet Mixing in Reduced Flow Areas for Lower Combustor Emissions. AIAA Paper 91-2460, Jun 1991.

-7 Talpallikar, M. V. et al: CFD Analysis of Jet Mixing in Low NOx Flametube Combustors. ASME Paper 91-GT-217, Jun 1991.

-8 Bain, D. B. et al: CFD Mixing Analysis of Jets Injected from Straight and Slanted Slots into Confined Crossflow in Rectangular Ducts. AIAA Paper 92-3087, July 1992.

-9 Hatch, M. S. et al: Influence of Geometry and flow Variations on NOx Formation in the Quick Mixer of a Staged Combustor. NASA TM 105639, Jul 1992.

-10 Liscinsky, D. S. et al: Experimental Study of Cross Flow Mixing in Cylindrical and Rectangular Ducts. NASA CR 187141, Jan 1993.

-11 Kroll, J. T. et al: Optimization of Circular Orifice Jets Mixing into a Heated Cross Flow in a Cylindrical Duct. AIAA Paper 93-249, Jan 1993.

-12 Liscinsky, D. S. et al: Experimental Investigation of Crossflow Jet Mixing in a Rectangular Duct. AIAA Paper 93-2037, Jun 1993.

-13 Oechsle, V. L. et al: An Analytical Study of Dilution Jet Mixing in a Cylindrical Duct. AIAA Paper 93-2043, Jun 1993.

-14 Bain, D. B. et al: CFD Mixing Analysis of Axially Opposed Rows of Jets Injected into Confined Crossflow. AIAA Paper 93-2044, Jun 1993.

-15 Liscinsky, D. S. et al: Mixing characteristics of Directly Opposed Rows of Jets Injected Normal to a Crossflow in a Rectangular Duct. AIAA Paper 94-217, Jan 1994.

-16 Bain, D. B. et al: CFD Assessment of Orifice Aspect Ratio nad Mass Flow Ratio on Jet Mixing in Rectangular Ducts. AIAA Paper 94-218, Jan 1994.

-17 Sowa, W. A. et al: Optimization of Orifice Geometry for Cross-Flow Mixing in a Cylindrical Duct. AIAA Paper 94-219, Jan 1994.

-18 Oechsle, V. L. et al: Comparison of Mixing Calculations for Reacting and Non-reacting Flows in a Cylindrical Duct. AIAA Paper 94-865, Jan 1994.

-19 Cutrone, M. B.: Low NOx Heavy Fuel Combustor Concept Program. NASA CR 165449, Oct 1981.

-20 Beal, G. et al: Low NOx Heavy Fuel Combustor Concept Program. NASA CR 165512, Oct 1981.

-21 Novick, A. S. and D. L. Troth: Low NOx Heavy Fuel Combustor Concept Program. NASA CR 165367, Oct 1981.

-22 White, D. J. et al: Low NOx Heavy Fuel Combustor Concept Program. NASA CR 165481, Nov 1981.

-23 Rosfjord, T. J. et al: Fuel Tolerance of Staged Combustors. ASME Paper 82-GT-195, Apr 1982.

IV -1 Hautman, D. et al: Transverse Gaseous Injection Into Subsonic Air Flows. AIAA Paper 91-576, Jan 1991.

-2 Novick, A. S. and D. L. Troth: Low NOx Heavy Fuel Combustor Concept Program. NASA CR 165367, Oct 1981.

-3 Vranos, A. et al: Experimental Study of Cross-Stream Mixing in a Cylindrical Duct. AIAA Paper 91-2459, Jun 1991.

-4 Holdeman, J. D.: Mixing of Multiple Jets with a Confined Subsonic Crossflow. AIAA Paper 91-2458, Jun 1991.

-5 Rosfjord, T. J. et al: Fuel Tolerance of Staged Combustors. ASME Paper 82-GT-195, Apr 1982.

-6 Chiappetta, L. and M. B. Colket, III: Design Considerations for Aerodynamically Quenching Gas Sampling Probes. ASME Journal of Heat Transfer, Vol 106, pp460-466, May 1984.

-7 Spindt, R. S.: Air-Fuel Ratios from Exhaust Gas Analysis. SAE Paper 650507, Jan 1965.

REPORT DOCUMENTATION PAGE

Form Approved
OMB No. 0704-0188

1. AGENCY USE ONLY (*Leave blank*)	2. REPORT DATE	3. REPORT TYPE AND DATES COVERED
	January 2001	Final Contractor Report

4. TITLE AND SUBTITLE

Experimental Assessment of the Emissions Control Potential of a Rich/Quench/Lean Combustor for High Speed Civil Transport Aircraft Engines

5. FUNDING NUMBERS

WU–714–01–4A–00

6. AUTHOR(S)

T.J. Rosfjord and F.C. Padget

7. PERFORMING ORGANIZATION NAME(S) AND ADDRESS(ES)

United Technologies Research Center
411 Silver Lane
East Hartford, Connecticut 06108

8. PERFORMING ORGANIZATION REPORT NUMBER

E–12572

9. SPONSORING/MONITORING AGENCY NAME(S) AND ADDRESS(ES)

National Aeronautics and Space Administration
Washington, DC 20546–0001

10. SPONSORING/MONITORING AGENCY REPORT NUMBER

NASA CR—2001-210613

11. SUPPLEMENTARY NOTES

Note: This work was performed in 1992. Project Manager, Robert R. Tacina, Turbomachinery and Propulsion Systems Division, NASA Glenn Research Center, organization code 5830, 216–433–3588.

12a. DISTRIBUTION/AVAILABILITY STATEMENT

Document Availability Change Notice

This document was published in January 2001 with an EAR restriction. It was changed April 2003 to Unclassified/Unlimited per DAA modified February 11, 2003.

Export Administration Regulations (EAR) Notice

This document contains information within the purview of the Export Administration Regulations (EAR), 15 CFR 730–774, and is export controlled. It may not be transferred to foreign nationals in the U.S. or abroad without specific approval of a knowledgeable NASA export control official, and/or unless an export license/license exception is obtained/available from the Bureau of Industry and Security, United States Department of Commerce. Violations of these regulations are punishable by fine, imprisonment, or both.

Unclassified - Unlimited
Subject Category: 07 Distribution: Nonstandard

Available electronically at http://gltrs.grc.nasa.gov

This publication is available from the NASA Center for AeroSpace Information, 301–621–0390.

12b. DISTRIBUTION CODE

13. ABSTRACT ***(Maximum 200 words)***

In support of Pratt & Whitney efforts to define the Rich burn/Quick mix/Lean burn (RQL) combustor for the High Speed Civil Transport (HSCT) aircraft engine, UTRC conducted a flametube-scale study of the RQL concept. Extensive combustor testing was performed at the Supersonic Cruise (SSC) condition of an HSCT engine cycle. Data obtained from probe traverses near the exit of the mixing section confirmed that the mixing section was the critical component in controlling combustor emissions. Circular-hole configurations, which produced rapidly-, highly-penetrating jets, were most effective in limiting NOx. The spatial profiles of NOx and CO at the mixer exit were not directly interpretable using a simple flow model based on jet penetration, and a greater understanding of the flow and chemical processes in this section are required to optimize it. Neither the rich-combustor equivalence ratio nor its residence time was a direct contributor to the exit NOx. Based on this study, it was also concluded that: (1) While NOx formation in both the mixing section and the lean combustor contribute to the overall emission, the NOx formation in the mixing section dominates. The gas composition exiting the rich combustor can be reasonably represented by the equilibrium composition corresponding to the rich combustor operating condition. Negligible NOx exits the rich combustor. (2) At the SSC condition, the oxidation processes occurring in the mixing section consume 99 percent of the CO exiting the rich combustor. Soot formed in the rich combustor is also highly oxidized, with combustor exit SAE Smoke Number <3. (3) Mixing section configurations which demonstrated enhanced emissions control at SSC also performed better at part-power conditions. Data from mixer exit traverses reflected the expected mixing behavior for off-design jet to crossflow momentum-flux ratios. (4) Low power operating conditions require that the RQL combustor operate as a lean-lean combustor to achieve low CO and high efficiency. (5) An RQL combustor can achieve the emissions goal of EINOx = 5 at the Supersonic Cruise operating condition for an HSCT engine.

14. SUBJECT TERMS	15. NUMBER OF PAGES
Combustor; RQL; Gas turbines	171
	16. PRICE CODE: A08

17. SECURITY CLASSIFICATION OF REPORT	18. SECURITY CLASSIFICATION OF THIS PAGE	19. SECURITY CLASSIFICATION OF ABSTRACT	20. LIMITATION OF ABSTRACT
Unclassified	Unclassified	Unclassified	